C. elegans as A Genetics Model to Study Paternal Mitochondria Elimination and Apoptosis Kinetics Regulation

by

Hanzeng Li

B.S., Shandong University, 2010

A thesis submitted to the

Faculty of the Graduate School of the

University of Colorado in partial fulfillment

of the requirements for the degree of

Doctor of Philosophy Department of Chemistry and Biochemistry

2016

This thesis entitled:

C. elegans as A Genetics Model to Study Paternal Mitochondria Elimination and Apoptosis Kinetics Regulation

written by Hanzeng Li

has been approved for the Department of Chemistry and Biochemistry

_____

Prof. Ding Xue

_____

Prof. Dylan Taatjes

Date _____

The final copy of this thesis has been examined by the signatories, and we find that both the content and the form meet acceptable presentation standards of scholarly work in the above mentioned discipline.

Li, Hanzeng (Ph.D., Biochemistry)

C. elegans as A Genetics Model to Study Paternal Mitochondria Elimination and Apoptosis Kinetics Regulation

Thesis directed by Prof. Ding Xue.

The round worm, *Caenorhabditis elegans*, provides a simple system to study complex questions. The philosophy behind it is that a single cell contains almost all of the components that make up life, even as complex as a human. I studied two conserved and fundamental biological topics over the span of the past 6 years: programmed cell death, and paternal mitochondrial elimination (PME). Programmed cell death (apoptosis) is the process by which individual cells sacrifice themselves for the good of the organism. Cells undergo apoptosis in a finely regulated fashion. Using *C. elegans*, I investigated the regulatory mechanism of CED-8, an apoptotic executor that not only mediates PS exposure, but also regulates the kinetics of apoptosis. A cis-acting motif within the N-terminal inhibitory domain of CED-8, as well as a transacting protein, CEI-1, (CED-8 Interaction protein) are both identified, and characterized. A further part of my Ph.D research aimed to decipher the mechanisms underlying the conserved process of paternal mitochondrial elimination (PME). In PME paternally derived mitochondria sacrifice themselves for the good of future progeny. Maternal inheritance of mitochondria is guaranteed through PME. Specifically, two pathways are characterized: first, the mitochondria localized nuclease, CPS-6 is activated to degrade the mitochondrial DNA during the process of PME; next, Parkin, a gene closely associated with familial Parkinson's disease, plays a conserved role in regulating autophagy, which serves to quarantine paternal mitochondria. In my research, the Parkin homolog, PDR-1, was shown to flag paternal mitochondria for selective autophagic degradation. Loss of Parkin leads to non-selective enclosing of maternal organelles, obviously excluding paternal mitochondria. Moreover, the ubiquitination E3 ligase of Parkin is essential for Parkin's role in PME. This novel physiological role of Parkin thus provides novel and critical mechanistic insights into how Parkin deficiency may cause Parkinson's disease.

Dedications

Dedicated to my grandfather, Li, Wenzhi, for his spiritual support throughout this endeavor.

Acknowledgements

First of all, I need to thank Dr. Ding Xue. He is always supportive when I suffered from emergencies. I would like to thank Dr. Dylan Taatjes for being my in-department thesis advisor, as well as other members in my committee: Dr. Amy Palmer, Dr. Xuedong Liu, and Dr. Hubert Yin. They have continuously provided me with many valuable suggestions to my projects as well as my dissertation. I would like to thank Dr. Jolien Tyler for the help in MCDB light microscopy core facility. During my Ph.D, the time I feel so proud of myself is when I got the SIM images of maternal autophagosome with paternal mitochondria inside. This is not possible without Jolien and Thor. This is the turning point I was salvaged from interiority. I also need to thank the worms that have sacrificed for the research. I would also like to thank Adam Hall, my buddy, for supporting me through my miserable times and provide help with proofreading this thesis. My wife and my grandma always make me feel strengthened. I love you and love to be loved by you. You are the only reason I persevere. Last but not the least, I owe so much to the church fellows. Without cares from all the people from the church, I cannot make it. Thank God for bringing all those wonderful people to me.

Contents

Tables

Figures

Chapter 1

Uni-parental inheritance of mitochondria during animal development

Maternal inheritance of mitochondria is highly conserved in almost all animals. It has been a major mystery in developmental biology why and how this unique event happens. Sperm derived mitochondria enter the oocyte after fertilization, but their mtDNAs are never transmitted to their offspring. Recently, multiple studies in several different model organisms have revealed a substantial amount of knowledge addressing the molecular mechanisms underlying active paternal mitochondria elimination, which will be referred to as PME. From the evolutionary point of view, I will review the current mechanisms underlying the prevention of paternal mitochondria transmission, including transmission of the mtDNA and its structure.

1.1 Where do mitochondria come from?

Mitochondria, well known as the hub of energy production in the cell are semi-autonomous organelles with their own genomic DNA, known as mtDNA (*1*). The current understanding of mitochondrial evolution is that mitochondria are derived from a monophyletic origin of endosymbiosis and resemble microbes in size (typically 1μm in length) as well as their dividing property (*2*). After endosymbiosis, the inner membrane underwent extensive infolding to form specialized compartmentalization called cristae, which allow for efficient oxidative phosphorylation. Mitochondrial presence in eukaryotes provides the energy to meet the need of energy costs for the vast expansion of genomic capacity and enables multicellular complexity (*3*). Besides the major role of producing ATP for cells, mitochondria are well known for their critical roles in metabolism as well as signaling regulation (*4*). Therefore, endosymbiosis results in intertwined reciprocal interactions between the eukaryotic cell host and mitochondria.

1.2 Mitochondria genome and proteasome

Harkening back to the bacterial origins of mitochondria, the mtDNA in most animals exist in circular forms, except cnidarians, which often contain linear mtDNA (*5, 6*). Mitochondria are referred to as semi-autonomous organelles, however, a majority of their genes have been transferred to the nuclear genome following long term evolution. For example, human mtDNA only encodes for 13 proteins, as well as 22 tRNA and 2 ribosomal RNA genes that are required for their translation (Fig. 1.1). This differs slightly from *C. elegans* mtDNA, which only encodes for 12 proteins, but produces the same number of tRNAs and ribosomal RNAs (*7*). A near complete inventory of the mitochondrial proteome contains more than 1,100 proteins (*8*). Nearly two thirds of these proteins have bacterial origins, while the rest represents eukaryotic innovations. The mixed composition of the mitochondrial proteome is evidence of interplay between the eukaryotic host and proteobacterial endosymbionts, during the course of evolution (*2*).

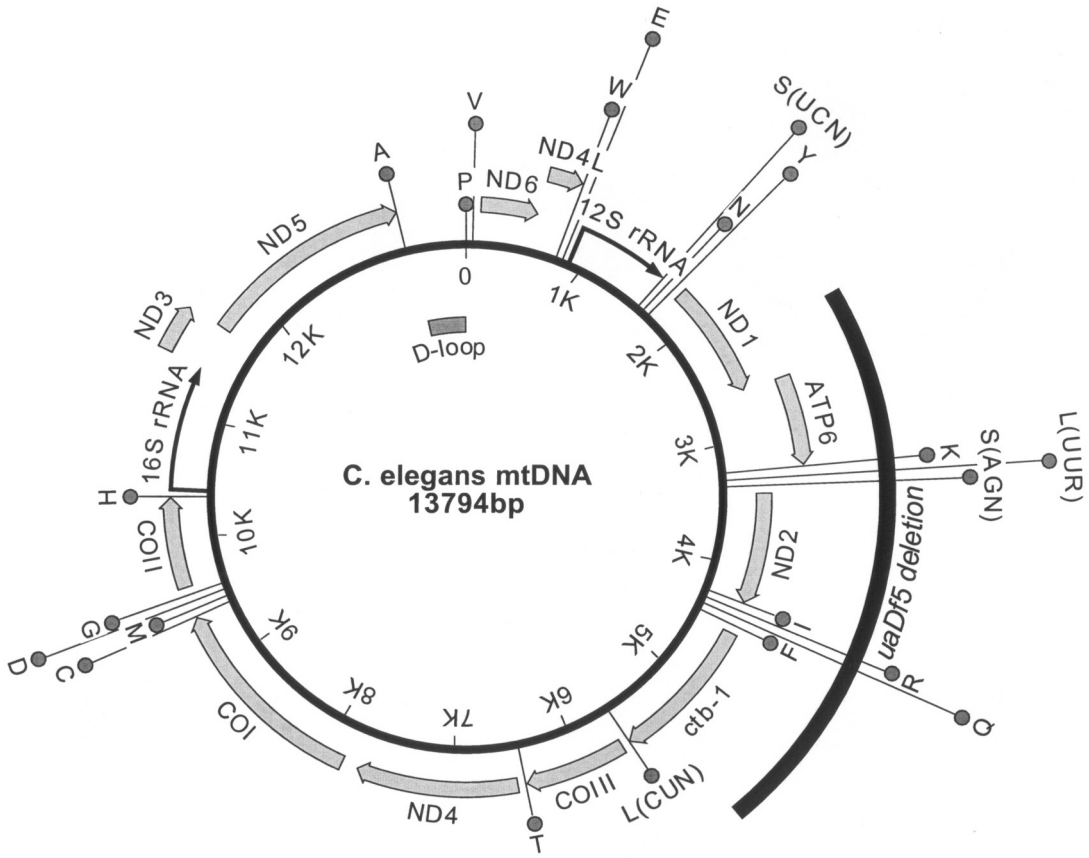

Fig. 1. 1. Gene map of the *C. elegans* mtDNA. The molecule contains the genes for twelve proteins (thick grey arrows), two rRNAs (black arrows), and 22 tRNAs (circles labeled with one-letter amino acid code). The serine and leucine tRNAs are also identified by the codon family recognized. The positions of the putative D-loop and of the *uaDf5* deletion mutation are indicated inside and outside the circle, respectively (*7*).

1.3 Current mechanisms of paternal mitochondrial elimination (PME)

Uniparental inheritance of organelles is prevalent in eukaryotes. Specifically, genetic materials are only inherited from one parent instead of both. For example, the sperm contributes the initial centrioles, whereas the maternal centrioles disappear in most species (*9-11*). Mitochondria are the sole organelle with their own genome (mtDNA) in animals. The maternal mode of inheritance for mitochondria and mtDNA is nearly absolute, suggesting an adaptive advantage pertaining to uniparental inheritance (*6*). How and why paternal mitochondria are selectively eliminated from the cytoplasm of zygotes after fertilization remains an enigma. Recently, several mechanisms including the autophagy-lysosome pathway, the mitochondrial

endonuclease pathway, and the proteasome pathway, have been shown to act independently or cooperatively to limit the presence of paternal mitochondria.

1.4 Shutdown of respiratory chain and loss of membrane potential during PME

The primary function of mitochondria is energy production through oxidative phosphorylation. Specifically, pyruvate produced by glycolysis in cytosol is imported into mitochondria and further converted to acetyl-CoA, which fuels the citric acid cycle. The net products of the citric acid cycle are the reducing equivalents, NADH or FADH2. Electrons deposited in the reducing equivalents are next transported through the respiratory chain (also called the electron transport chain) and eventually react with oxygen (*2, 12*). The respiratory chain is comprised of four mitochondrial inner membrane associated macromolecular complexes: complex I (for catalyzing NADH), II (for catalyzing FADH2), III and IV. Free energy is conserved by coupling electron transport to the formation of a proton gradient, which is then utilized by F1F0-ATPase to catalyze ATP synthesis. The proton gradient or membrane potential across the inner membrane of mitochondria is a hallmark of mitochondria healthiness and serve to signal the autophagy machinery in the cell (*12, 13*). Interestingly, the membrane potential of paternal mitochondria is lost immediately after fertilization in *C. elegans* (*14*). The key question that needs to be addressed is, if the loss of membrane potential in paternal mitochondria also signals to the autophagy machinery during the PME process. In addition, whether loss of membrane potential in paternal mitochondria is the sole cause of discrimination between the two forms of mitochondria (paternal and maternal) remains to be determined.

There is growing evidence to support a solid-state model for the organization of respiratory chain complexes (*15*), instead of a random-collision model (*16*). For example, physical interactions between complexes I, III and IV has been demonstrated (*17-19*). In mammalian cells, it has also been shown that the cristae structure of mitochondria can collapse

by disrupting the integrity of the respiratory chain (*20, 21*). Upon entry into the oocyte, paternal mitochondria display discontinuities and apertures on their surface, as well as a collapsed cristae structure. These abnormalities are visualized through the use of high-resolution electron microscopy and three-dimensional electron tomography (*14, 22*). Interestingly, *cps-6*, encoding the mitochondrial endonuclease G in *C. elegans,* is important but not essential for cristae collapse in paternal mitochondria after fertilization (*14*). CPS-6-mediated degradation of mtDNA appears to contribute to the internal breakdown of the inner-membrane of paternal mitochondria, although the mechanisms behind this phenomenon have yet to be elucidated. The initial inner membrane breakdown of paternal mitochondria is probably triggered by an unknown mechanism; CPS-6 can then relocate to the matrix to digest mtDNA. The degradation of mtDNA by CPS-6 may impair transcription and translation of the thirteen mitochondrial proteins encoded by mtDNA, which are crucial components of the respiratory chain complexes. This would exacerbate membrane depolarization of paternal mitochondria and facilitate the structural collapse of paternal mitochondria. Alternatively, degradation of mtDNA by CPS-6 might trigger a mtDNA-damage response and the activation of some mitochondrial proteases or lipases that leads to breakdown of the inner membrane of paternal mitochondria.

It has been reported that the mitochondrial respiration rate correlates with the amount of mtDNA in the cell (*23-25*). The rate-limiting step in the assembly of new respiratory complexes is the rate of transcription of the ND5 subunit of NADH dehydrogenase, which is encoded by mtDNA (*26, 27*). Furthermore, the expression of several complex I genes, which are encoded by mtDNA, is sensitive to changes in oxygen concentrations. Within thirty minutes of moderate hypoxia, down-regulation of the ND4 and ND5 transcripts is observed (*3, 28*). Therefore, it is disruptive to normal mitochondrial functions and integrity when paternal mitochondria are insulated by autophagosomes and deprived of O_2 inputs and when mtDNA is degraded. Studies in *C. elegans* have described a mitochondrial unfolded protein response (UPRmt) that is

activated by disturbed protein homeostasis. This perturbation results from insults to the respiratory chain (*29*). From these studies, it is clear that loss of membrane potential in paternal mitochondria can be attributed to multiple mechanisms, and is likely the primary sign that signals the difference between paternal and maternal mitochondria.

1.5 The conserved role of allophagy in PME.

1.5.1 Allophagy is sequestering and degrading paternal mitochondria in *C. elegans.*

Autophagy, an ubiquitous cellular process responsible for the orderly degradation of bulk cytoplasmic components or organelles, is executed through double-membrane compartments called autophagosomes. These autophagosomes are often used to usher damaged or surplus organelles to lysosomes for complete degradation (*30, 31*). Although the term autophagy literally means “self-eating”, in the case of paternal mitochondrial elimination, the term “allophagy”, which means “eating non-self ” is better suited and proposed to use in the field (*32, 33*). Allophagy pertains to the process of the maternal autophagosome encapsulating and delivering the paternal mitochondria to the lysosome for degradation.

In *C. elegans*, several reports have shown allophagy is involved in sequestering paternal mitochondria shortly after fertilization (*34-37*). Different from mammalian sperm, *C. elegans* spermatozoe have no flagellum, and contain nematode-specific membranous organelles (MOs) underneath their plasma membrane (*34, 35*). Along with the sperm nucleus, cytosolic components, such as mitochondria and the MOs enter ooplasm. When paternal mitochondria are degraded by allophagy, the panoply of autophagy related proteins (ATG) are employed. Critical to the function of the autophagy are members of the Atg8p family. These are ubiquitin-like proteins that mediate the formation and expansion of the autophagosome. There are two subfamilies of Atg8p, LC3, (full name is MAP1LC3, short for microtubule-associated protein 1 light chain 3) and the GABARAP proteins. In *C. elegans*, there are two homologs for Atg8p:

LGG-1 (the homolog of GABARAP) and LGG-2 (the homolog of LC3) (*38*). When imaged with the Structured Illumination Microscopy (SIM) using antibodies that specifically recognize LGG-1, paternal mitochondria are enclosed in ring-like autophagosomes (*14*). Electron microscopy also shows that paternal mitochondria are wrapped in autophagosomes featuring double delimiting membranes in zygotes (*14, 34, 35*). RNAi treatment or deletion mutations of genes in the canonical autophagy pathway, such as LGG-1, LGG-2, ATG-7, and RAB-7, lead to persistence of paternal mitochondria as well as the mtDNA (*34, 35*). In addition, treatment with the lysosomal inhibiting agent, ammonium chloride, or inactivation of lysosome biogenesis gene *glo-1*, both result in delay of paternal mitochondrial degradation (*36*). Thus, the role of allophagy is functionally verified.

1.5.2 Role of LGG-2 and the endosome pathway in allophagosome migration

In allophagy, the step following the closure of the autophagic vesicle is fusion with and acidification by the lysosome. Lysosomes are the major digestive organelles in the cell that contain a variety of internal degradation enzymes such as hydrolases. Degradation of paternal organelles in allophagosomes occurs after acidification enabled by their fusion with lysosomes. The mature allophagosome contains the hydrolases along with a low PH environment and completes degradation of the paternal organelles inside. The fusion (between the allophagosome and the lysosome) step is facilitated by LGG-2 through direct interaction with VPS-39, a subunit of the HOPS complex that is attached to the lysosome (*38*). In the absence of LGG-2, dispersion of allophagosome is not as pronounced as when LGG-2 is present. It is also documented as a clustering of allophagic substrates in the inner region of the zygote cortex, away from the centrosomes, around which are rich in lysosome. The LGG-2-mediated migration of the allophagosomes is also dependent on the microtubule architecture and the minus end-directed motor, dynein (*39*). Thus, these studies support a model where LGG-1 is necessary for

the formation of allophagic autophagosomes around paternal mitochondria, which is an upstream event of the LGG-2 recruitment. LGG-2 is dispensable for allophagosome formation, but mediates their microtubule-dependent retrograde transport towards pericentrosomal region by participation in tethering and fusion with lysosomes. The consequence of defective migration and lysosome acidification is clustering of paternal mitochondria and failure of efficient degradation of paternal mitochondria and MOs.

The mechanism behind how LGG-1 and LGG-2 have different functions in allophagy can be analyzed from a structural standpoint despite their sequence similarity (Fig. 1.2). LGG-1 and LGG-2 interact differently with autophagy substrates and ATG proteins. For example, the adaptor P62 is recruited to autophagosomes by LC3 but not GABARAP (*40*). The crystal structure has revealed that LGG-1 and LGG-2 possess 2 hydrophobic pockets, the W-site and the L-site, which recognize the LIR motif in Atg8-binding proteins. The plasticity of the W-site and the size as well as the shape of the L-site differ between LGG-1 and LGG-2, thus determining their preferences for distinct LIR motifs. Although LGG-1 and LGG-2 are both conjugated with phosphatidylethanolamine (PE), the N-terminal tails of LGG-1 and LGG-2 adopt unique closed and open conformations, respectively (*41, 42*). These structural differences result in distinct membrane tethering and fusion activities. Therefore, the structural insights into the non-redundant activities of LGG-1 and LGG-2 provide a good way to appreciate the functional differences of two related proteins originating from the same Atg8 ancestor during evolution.

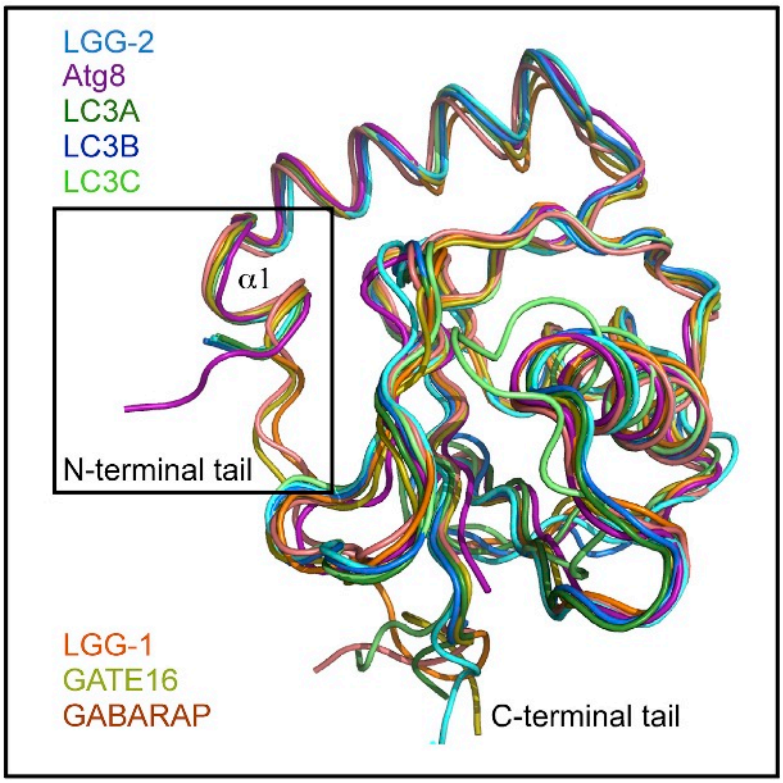

Fig. 1. 2. Structure superimposing of the two ATG8 subfamily proteins. LGG-2, Atg8, LC3A, LC3B and LC3C belong to the LC3 subfamily; LGG-1, GATE16 and GABARAP belong to the GABARAP subfamily. Adapted from *Wu et al., 2015, Molecular Cell 60, 914–929 (41).*

1.5.3 Conservation of allophagic degradation of paternal mitochondria

In *Drosophila*, at the end of meiosis, spermatogenesis occurs and spermatid mitochondria fuse into two larger mitochondria that wrap around each other to form a spherical aggregate, called mitochondrial derivative (*43, 44*). During spermatid elongation, the mitochondrial derivative unfolds and extends in parallel with the axoneme along the length of the entire tail. Mature sperm in the fruit fly, *Drosophila Melanogaster*, lack mtDNA (*45, 46*). Currently, the primary mechanism that prevents paternal mtDNA transmission is hypothesized as the interplay between cellular remodeling and endonuclease activity. Both of these cellular processes are thought to play a role in the removal of the vast majority of mtDNA before fertilization. In other species of *Drosophila*, such as *D. simulans*, mature sperms do contain

mtDNA, which reflects a discrepancy across taxa (*46*). In *Drosophila Melanogaster,* although the mitochondrial derivatives are deprived of mtDNA, the whole sperm tail along with the mitochondrial derivative still enter the oocyte. A process, dubbed Paternal Mitochondrial Destruction (PMD), occurs rapidly in which the sperm tail and mitochondrial derivative are degraded (*47*). As a phenomenon unique to the fruit flies, the sperm cell completely penetrates the egg through micropyle. The plasma membrane of sperm cell is disintegrated by microvesicles that were already present in unfertilized eggs prior to the interaction. The mitochondrial derivative then separates from the axoneme and breaks into oval fragments, which are then enveloped by the autophagosome. Finally, the lysosome fuses with these autophagosomes and completes the degradation of the paternally derived mitochondria (*47*). Thus, it is clear that the destruction process of paternal mitochondria is mediated by the endocytic and autophagic machinery found throughout the egg. Due to the need for the long tubule paternal mitochondria to be fragmented before engulfment by the allophagic vesicles, the role of mitochondrial fission in this process is an interesting aspect to test. The importance of autophagy in paternal mitochondrial destruction is also verified as defects in the autophagy pathway indeed delay the kinetics of PMD in *Drosophila*. However, inactivation of several important autophagy genes did not completely block PMD, suggesting that redundant pathways are present for removal of the mitochondria derivative.

There are conflicting reports regarding the role of autophagy in mammalian PME. Several independent studies in mice have shown that the autophagy receptor p62 and the ubiquitin-like modifier LC3 colocalize to the sperm tail after fertilization (*34, 48, 49*). A recent report suggests that the sperm mitochondria in mice are not degraded by autophagy. Rather, the maternal inheritance may be a passive outcome that results from uneven distribution of paternal mitochondria in the early embryo along with the elimination of sperm mtDNA before fertilization (*49-51*). Several lines of evidence also suggest that allophagy is not present in

mammalian PME. First, the entire sperm tail is associated with both K48 and K63 polyubiquitination, which rapidly disappears following fertilization around 1-cell stage. Next, the autophagy receptors p62/sqstm1 and GFP-LC3 both disappear prior to the clearance of labeled sperm mitochondria, suggesting that LC3 was not involved in their autophagy degradation. Further, no sperm-derived mitochondria are ingested by lysosomes in mice. Sperm-derived paternal mitochondria occasionally leak into a few newborn mice even in wild type animals, suggesting that there is not a regimented system of PME in mice. Finally, the conditional knockout of Atg5 (required for the coupling of LC3 proteins to the PE anchor) did not dramatically affect the fate and distribution of sperm mitochondria in the embryos studied (*50*). According to a parallel study in mice, PME is not affected by the autophagy inhibitor, 3-methyladenine (3-MA), but the process can be accelerated by the autophagy inducer, rapamycin (*48*). *In vitro* fertilization via intracytoplasmic spermatozoon injection causes LC3 and ubiquitin to be recruited onto the midpiece of sperm; however, some remnants of sperm mitochondrial sheath may persist until the morula stage (*48*). Thus, in mouse embryos, the major mechanism behind PME is probably the pre-elimination of mtDNA before fertilization, along with the separation of paternal mitochondria to a limited number of daughter cells, with a bias towards the blastomeres that form the future extra-embryonic tissue.

It has been reported that porcine and rhesus monkey utilize another strategy to remove paternal mitochondria. A SQSTM1 mediated, unconventional ubiquitin-recognizing mitophagy pathway acts in concert with the ubiquitin-proteasome pathway, along with the ubiquitin-binding protein, valosin-containing protein (VCP) (*52*). Three ubiquitinated mitochondrial outer membrane proteins are identified through their copurification with the ubiquitin-associated domain of SQSTM1 (*52*). Most importantly, the role of this unconventional mitophagy is functionally verified by the pharmacological inhibition of VCP, which significantly delays the process of sperm removal. Furthermore, sperm removal is completely prevented when the

inhibition is combined with microinjection of autophagy targeting antibodies that are specific to SQSTM1 and/or GABARAP (*52*). Overall, the roles of autophagy and ubiquitination in paternal mitochondrial elimination in mammals need to be investigated more rigorously.

1.5.4 What signals the autophagy machinery?

In *C. elegans*, the initiation of allophagy is dependent on the occurrence of fertilization. When the oocyte exhibits polyspermy in the spe-11 mutant or with egg-4 RNAi or egg-5 RNAi treatment, autophagosomes surround both of the paternal pronuclei (*34, 35*). These results suggest that allophagy is triggered locally and correlates temporally with the entry of sperm components. K63 polyubiquitination has been shown to induce autophagy in mammalian neuronal cells. While membrane organelles (MOs) are associated with K63 or K48 polyubiquitination modifications, neither of the modifications has been observed on paternal mitochondria in *C. elegans* (*34, 35*). The question remains, could it be other types of tagging, such as mono-ubiquitination or poly-ubiquitination of novel branching pattern that is responsible for triggering autophagy? Using a GFP-tagged ubiquitin transgene, paternal MOs, but not paternal mitochondria are shown to be associated with ubiquitin-GFP. This observation makes it less likely that novel ubiquitination forms on paternal mitochondria (*34*). It has been speculated that ubiquitination of MOs could provide signals to nearby paternal mitochondria (*37*). The paternally derived mitochondria may be brought into allophagosomes via their close association with ubiquitinated MOs (*37*). This hypothesis is not supported by the high-resolution EM analysis, which instead show that autophagosomes are encapsulating tightly spherical paternal mitochondria de novo. This EM observation is also in contrast to the model where the autophagosomes expand from nearby MOs (*14, 34, 35*). There remains a major gap in our understanding of the signals responsible for triggering the degradation of mitochondria in *C. elegans*. Studies in mammals, however, indicate that the degradation of sperm mitochondria

could be inhibited by microinjection of anti-ubiquitin antibodies into zygotes or treatment of zygotes with the lysosomotropic agent ammonium chloride (*53*). The target of ubiquitination in this case is the mitochondrial membrane protein, prohibitin (*54*). In parallel, the K63 polyubiquitination modification has also been associated with paternal mitochondria derivative shortly after fertilization in *Drosophila* (*47*). The autophagy receptor/adaptor proteins, p62/SQSTM1, and NBR1 serve to bridge the K63 polyubiquitination signal on paternal mitochondria derivative to the autophagosomes in *Drosophila* (*47*). Although the role of allophagy in PME is conserved in a variety of species, their recruitment signals are diverse and need to be identified and analyzed further.

1.5.5 Insulating effect of autophagosome

Besides the fact that an allophagosome with a paternal mitochondrion inside will fuse with a lysosome for complete degradation, paternal mitochondria should no longer be functional to produce energy for two more reasons. First, in order to gain the requisite materials to maintain a functional respiratory chain, mitochondria need to exchange ingredients and products with cytosol. This includes, but is not limited to the importation of NAD^+, pyruvates, O_2 and ADP, as well as exportation of NADH, ATP and others to the cytosol. Once insulated by the allophagosome, paternal mitochondrion quickly consumes the limited amount of remaining ingredients. As a result, membrane potential of paternal mitochondria will be lost due to the action of the ATP synthase that decimates H^+ gradient for ATP synthesis. The other event that disrupts paternal mitochondria behavior is the continued dissociation from the ER; it has been shown mitochondrial fission requires ER tubule to mark and facilitate mitochondrial division (*55*). Moreover, mitochondrial DNA replication is coupled with ER-mitochondria contact sites (*56*). Paternal mitochondrion should not be able to replicate since being encapsulated in an autophagosome and kept separated from ER. Thus, allophagy not only actively degrades

paternal mitochondria, but also quarantines paternal mitochondria to prevent its fission and fusion with maternal mitochondria.

1.5.6 Dynamics of mitochondria is determining the kinetics of PME.

Mitochondria fission and fusion are coordinated in normal cells to control appropriate mitochondrial morphology and dynamics. Dnm1/DRP1 is the central gene that mediates mitochondrial fission, while fzo1/MFNs and Mgm1/OPA1 are two major genes that mediate mitochondrial fusion of outer membrane and inner membrane, respectively (*57-61*). There are reports that reduced mitochondrial fission or increased mitochondrial fusion can protect against mitophagy (*62-65*). For example, during nutrient starvation, normal cells with elongated mitochondria are protected from autophagy elimination, while fusion-deficient cells, in which mitochondria become fragmented, do not survive (*64, 65*). In wild-type (N2) *C. elegans* embryos, mitochondria display different shapes and sizes, broadly distributed in the cytoplasm of each blastomere. In *drp-1* loss-of-function embryos that are defective in mitochondrial fission, long and highly connected mitochondria are observed, which often exist as asymmetric, concentrated clusters in the blastomeres. In contrast, mitochondria are highly fragmented in *fzo-1* loss-of-function embryos that are defective in mitochondrial fusion. The mitochondrial fusion defect caused by loss of *fzo-1* can be completely suppressed by the mitochondrial fission defect mediated by loss of *drp-1* (*22*). This line of data suggests that there is a counteracting, reciprocal role between mitochondrial fission and fusion; the two must have a synergistic balance if normal function is to be maintained.

Recently, the mitochondrial fission and fusion processes in both sperm and oocytes have been shown to play important roles in regulating the kinetics and specificity of PME (*22*). Specifically, a defect in paternal mitochondrial fission and a defect in maternal mitochondrial fusion synergize to greatly delay PME, whereas a defect in paternal mitochondrial fusion

accelerates PME. In agreement with the role of mitochondrial fusion in mitochondria quality maintenance, mitochondria in the animals defective in *fzo-1* often display reduced membrane potential, as they are stained poorly by TMRE, a membrane-potential sensitive mitochondrial dye (*22*). Consequently, selective targeting of paternal mitochondria by the allophagic machinery seems to be crippled when maternal mitochondria are compromised and compete with damaged paternal mitochondria for the allophagy machinery. The PME defect in *fzo-1* loss-of-function animals can be rescued by treatment of oligomycin, an inhibitor of ATP synthase, to increase the membrane potential of mitochondria, indicating that the membrane potential decrease of maternal mitochondria in *fzo-1* defective animals is the root reason that interferes with the proper function of autophagy and that impairs PME. The mitochondrial fission and fusion machineries thus impose critical regulation of the kinetics and specificity of PME in *C. elegans*.

1.5.7 Comparison between allophagy and xenophagy

Reminiscent of their bacteria ancestors, allophagy of paternal mitochondria that enter into the oocyte exhibits similarity to elimination of pathological bacteria (xenophagy) that invade into the eukaryotic cell (Fig. 1.3). Both processes utilize the autophagy arsenal (*34-36, 66, 67*). A number of microbial pathogens can be targeted by autophagy during innate immune responses. Free bacteria in the cytosol can be captured by macroautophagy and pathogen-conditioned phagosome can fuse with or get engulfed by autophagosomes. Several recent studies have shown autophagy is crucial for removal of invading pathological bacteria or parasites. This process is termed as xenophagy. For example, Group A Streptococci are enveloped by autophagosomes and delivered for lysosomal degradation, while autophagy defective mice are more susceptible to Group A Streptococci infection (*68*). Pathological bacteria, such as *Listeria monocytogenes, Salmonella enterica, Francisella tularensis and*

Toxoplasma gondii, are targeted and captured by autophagosomes (*69-78*). These processes can be blocked by pharmacological autophagy inhibitors and accelerated by starvation treatment, which stimulates macroautophagy (*79*). Pathological bacteria also developed counteractive mechanisms to fight against hosts. For example, *Shigella flexneri* inhibits autophagy in host by expressing a protein, IcsB, that disrupts the binding of Atg5 to VirG, which serves as the ligand for host recognition (*80*). Other pathogenic bacteria, such as *Brucella* and *Legionella*, establish their replication niche in the autophagosome by preventing autophagosome from fusion with lysosome (*81, 82*). It has been shown that Parkin is responsible for polyubiquitination modification on the invading bacteria. For example, *Mycobacterium leprae* and *Salmonella*, are marked by polyubiquitination on their surface proteins and therefore targeted by the host autophagy machinery (*75*). An alternative “eat-me” signal that has been hypothesized is the reactive oxygen intermediates produced by invading bacteria, which are often associated with the induction of autophagy in the host cell (*74, 78*). The reactive oxygen species (ROS) are also thought to be the hallmark that signals the difference between paternal mitochondria and maternal mitochondria. However, solid evidence is still lacking to validate the role of ROS in PME. Thus, similar to the penetrating paternal mitochondria in the oocyte, the invading bacterial pathogens are also substrates of autophagy as innate defense response. Mechanistic comparison between xenophagy and allophagy can shed light into how the ancient autophagic machinery is multitasked to recognize and defend against foreign bacteria or bacteria derivative, such as paternal mitochondria, during evolution. In addition, the process of xenophagy and paternal mitochondria elimination may exhibit clues pertaining to how early eukaryotic cell captured the first mitochondrion.

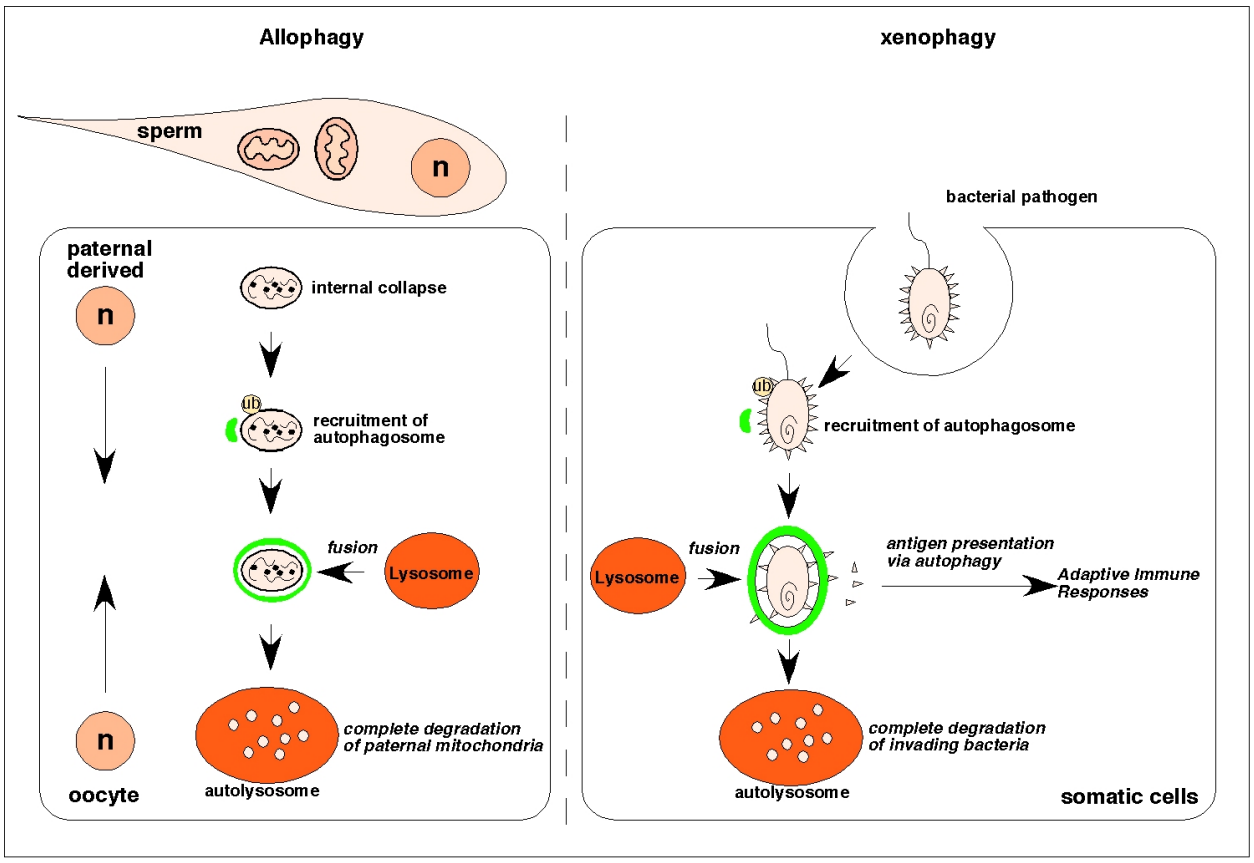

Fig. 1. 3. Comparison between allophagy and xenophagy. The ubiquitination modifications on the paternal mitochondria that signal to recruit allophagosome act in a specie-specific manner. The fates of bacterial pathogens in autophagosome also vary depending on if the invading bacteria evolve counteractive mechanisms.

1.6 Ubiquitination-Proteasome pathway are involved in PME

The ubiquitination-proteasome pathway, as the major proteolysis mechanism for degradation of unneeded proteins, has been shown to be involved in PME in several organisms. In *C. elegans*, the K48 polyubiquitination, which usually signals proteasome degradation, is associated with sperm-derived MOs, but not paternal mitochondria after fertilization (*34, 35*). Besides, the 19S proteasome also colocalizes with paternal-derived MOs in mature sperm before and after fertilization. The presence of the K48-linked ubiquitin chains and the 19*S* regulatory subunit of the proteasome around MOs suggests that some proteasome activity could be crucial for degradation of paternally derive proteins on MOs. Moreover, RNAi

knockdown of genes encoding proteasomal ubiquitin receptors, such as *rpn-10, rpn-13* and *rad-23,* caused significant delay in removal of paternal mitochondria, suggesting that the ubiquitin-proteasome degradation pathway functionally contribute to elimination of paternal mitochondria (*36*).

The proteolytic ubiquitin–proteasome system (UPS) for substrate-specific, regulated protein recycling has also been implicated in the targeted degradation of paternal mitochondria in mammals. Mammalian sperm mitochondria are already modified with ubiquitin during spermatogenesis and ultimately degraded by proteasome-mediated proteolysis (*53*). Specific cell-permeable proteasome inhibitors, MG132 and lactacystin, block the progression of sperm mitophagy after porcine fertilization, and the resumption of sperm mitochondrial degradation was observed once the MG132 (a reversible inhibitor) was removed from the zygotes (*83*). Although the proteasome holoenzyme is limited to its capability of degrading only one protein molecule at a time, the degradation of mitochondrial surface proteins may still be important for priming destruction of the whole organelle or critical to induce the exposure of the unknown “eat-me” signals that recruit the allophagic machinery.

1.7 Endonuclease G plays an important role in PME.

The disappearance of mtDNA in PME implies participation of nucleases. It is plausible that the nucleases in lysosome are coupled to the digestion of mtDNA downstream of complete breakdown of mitochondrial structures in the allophagy pathway. However, the degradation of mtDNA, which resides in the mitochondrial matrix, seems to start earlier, evident from the fact that the self-mediated internal mitochondrial breakdown occurs prior to the allophagic membrane recruitment. In the well-studied genetic models, *Drosophila* and *C. elegans*, endonuclease G, originally residing in the intermembrane space of mitochondria, has been identified to play a role in degrading mtDNA before and after fertilization, respectively (*14, 45*).

The mitochondrial endonuclease G was first characterized as a nuclease involved in chromosomal DNA fragmentation during programmed cell death (*84-87*). In *C. elegans*, disruption of mitochondrial integrity during apoptosis leads to release of CPS-6, the *C. elegans* homologue of endonuclease G, along with its binding partner and activator, WAH-1 (worm apoptosis-inducing-factor homologue), from the intermembrane space of mitochondria and relocation to the nucleus to promote chromosomal DNA fragmentation (*84, 86, 88*). Through the RNAi screen of 217 genes encoding mitochondrial protein, CPS-6 is identified unexpectedly as the mitochondrial nuclease that mediates PME (*14*). Loss of *cps-6* in males results in persistence of paternal mitochondria to around 550-cell stage and persistence of paternal mtDNA to the latest embryonic stage, whereas both paternal mitochondria and mtDNA disappear before 64-cell stage in wild type animals (*14*). Another unexpected observation is that the allophagy pathway is partially defective in *cps-6* mutant embryos, indicating that CPS-6-mediatd self-destruction process is important for efficient recruitment of autophagosomes to paternal mitochondria (*14*). In *Drosophila*, spermatogenesis includes sequential morphologic transformation, where mitochondria fuse with each other to form two long mitochondria (over 1800μm) aligning with the axoneme (*43, 44*). The mtDNA within the two elongated mitochondria are gradually degraded before the sperm fertilize the oocyte. In the EndoG mutant fly, the degradation of mtDNA nucleoids in the apical tail is significantly delayed (*45*). Since endonuclease G normally resides in the mitochondrial intermembrane space, how endonuclease G is released to the matrix and acquires access to mtDNA remains enigmatic. In *Drosophila*, endoG inhibitor, endoGI, does not seem to regulate the activation of endonuclease G during spermatogenesis (*45*). Using immuno-electron microscopy (EM) with an antibody against CPS-6, the translocation of CPS-6 from the mitochondrial peripheral to the mitochondrial matrix is clearly observed in *C. elegans* (*14*). The loss of membrane potential and internal breakdown of paternal mitochondria coincide with this CPS-6 translocation event and may

account for the activation of mtDNA degradation by CPS-6 (*14*). Mitochondrial endonuclease G thus provides a conserved suicide strategy for prevention of paternal mtDNA transmission.

Nuclease-mediated paternal mtDNA degradation also takes place in other organisms: in *Oryzias latipes*, the elimination of the paternal mtDNA from the egg cytoplasm is achieved through stepwise degradation of paternal mtDNA during spermatogenesis and concludes after fertilization, but before destruction of mitochondrial structure (*89*). In isogamous *Physarum polycephalum*, two kinds of nucleases, Mn^{2+}-dependent and Ca^{2+}-dependent nucleases, have been identified as the candidates for selective digestion of mtDNA in zygotes, although these nucleases have not been identified molecularly (*90-92*). A Ca^{2+}-dependent nuclease activity has been detected specifically in mating type + gametes of *Chlamydomonas reinhardtii*, which selectively degrades DNA in chloroplasts (cpDNA) (*93*). In plants, such as *Arabidopsis thaliana*, a pollen-specific Mg2+ dependent exonuclease is responsible for paternal mtDNA degradation (*94*). Thus, the nuclease mechanism is a prevailing strategy utilized to degrade mtDNA in prevention of paternal mtDNA transmission.

1.8 Why does strict maternal mitochondrial inheritance occur?

1.8.1 The adaptive advantage theory

The core evolutionary theory is the adaptive advantage. The maternal inheritance mode of mitochondria is almost 100% conserved in animal kingdom, suggesting the strong adaptive advantage and predicting a disadvantageous outcome may result from failed paternal mitochondria elimination. The canonical hypothesis is that during fertilization millions of sperm compete to be the one that fertilizes the oocyte and during this process sperm generate and consume a greatly increased level of ATP and thus produce an increased level of reactive oxygen species (ROS) as the by-products, which cause damage to mtDNA. In combination with nearly absence of DNA repair mechanisms in mitochondria, sperm mtDNA mutates at a faster

rate than nuclear DNA (*32, 33, 95*). A patient with myopathy has been reported as a consequence of failed complete removal of paternal mitochondria. Etiologically, this patient inherits paternal mitochondria harboring a 2-bp mtDNA deletion in the *ND2* gene, which encodes a subunit of the enzyme complex I of the mitochondrial respiratory chain. The mtDNA harboring this mutation are found in 90% of the muscle tissue of the patient in a mosaic manner (*96*). Using *C. elegans* as the genetic model to interrogate the consequence of failed paternal mitochondrial elimination, we observed increased embryonic lethality and reduced cell division rate in cross progenies where paternal mitochondria elimination are delayed (*14*). However, the increased embryonic lethality phenotype is quite mild.

An alternative hypothesis for maternal mitochondrial inheritance is that it is an incidental by-product of DNA abandonment, a process that lowers the metabolic cost to repair organelle DNA (*97*). In unicellular eukaryotes, such as the isogamous yeast, meiosis and sexual reproduction occurs when vegetative cells are deprived of nitrogen. However, yeast is not an ideal model to explain the significance of PME, since mitochondria is not an essential organelle in yeast; which can grow anaerobically by relying on glycolysis. The first generation of zygotes from the mating is heteroplasmic with mtDNAs from both parents in yeast. During the ensuing cell divisions, all progeny in the zygote become largely or completely homoplasmic of mtDNA from either parent, which is not correlated with mating type (*98*). This phenomenon is better explained by the DNA abandonment theory, where most of the mtDNAs is degraded in the zygote with only a few left that can repopulate (*97*). Since nitrogen deprivation leads to increased oxidative stress and mutations in mtDNA, this DNA abandonment strategy in yeast allows the highest quality to cost ratio by minimizing the number of mtDNAs that need to be repaired. Thus, the benefit behind this hypothesis is to save costs on repairing potentially damaged mtDNA that is highly susceptible to damage from oxidative stress during fertilization.

1.8.2 The risk of heteroplasmy incompatibility

There may be some evidence that argues against the adaptive advantage of PME. It was reported that when a *Mus musculus* strain was mated with a *Mus spretus* strain, the paternal mitochondrial mtDNA can persisted for several generations of successive backcrossing (*99*). Another parallel evidence is that mitochondria exist beyond the third embryonic cell division when bovine species are intercrossed, suggesting that paternal mitochondria from a different species are not eliminated efficiently (*100*). Moreover, when extracted liver mitochondria are microinjected into pronucleus-stage embryos, the alien mtDNA still remains in developed embryos (*101*). These interspecies experiments and microinjection experiments suggest that the markers of paternal mitochondria facilitating discrimination from maternal mitochondria are only present in a certain context or recognized within the same species. Interestingly, mating between two wild-type *C. elegans* strains, the Bristol strain (N2) and the Hawaii strain, does not seem to delay paternal mitochondria elimination, but will cause an increased embryonic lethality phenotype, which is perhaps due to mitochondrial pool incompatibility when paternal mitochondria elimination is delayed (*14*). A recent study reports unexpected paternal mitochondrial transmission in hybrids from mating between different *Caenorhabditis briggsae* variants, where progeny from the some of the mating experiments contain paternal mitochondrial DNA. This finding likely suggests that the PME mechanism may have been compromised in some of *C. briggsae* variants (*102*). There are observations suggesting that homoplasmy of mtDNA is preferred in individuals. For example, it has been reported that the artificial heteroplasmic-state of two different wild-type mtDNAs in mice results in reduced activity, low metabolic rate, and impaired cognition compared to their homoplasmic counterparts (*103*). Thus, failure in elimination of paternal mitochondria eventually leads to mitochondrial heteroplasmy, which may potentially cause incompatibility risk.

1.9 PME is ensured with the double-latch combination.

Diverse mechanisms have been proposed to promote PME. Given the importance of PME to animal development, it appears that multiple mechanisms have been implemented to make sure that PME occurs properly. In *C. elegans*, the external allophagy pathway and the internal endonuclease G suicide pathway cooperate to ensure no transmission of paternal mitochondria or mtDNA to the next generation (*14, 34-37*). In *Drosophila*, the degradation of mtDNA mediated by the endonuclease G takes place during spermatogenesis before fertilization, whereas the allophagy pathway after fertilization guarantees complete destruction of the mitochondria structure (*45, 47*). In addition, there is a separate pathway as the backup strategy to remove paternal mtDNA when the endonuclease G pathway is defected in *Drosophila* (*45*). During spermatid individualization, actin-containing structures called investment cones move along the axoneme and sweep extraneous cytoplasm into a waste bag (*45, 104*). In EndoG mutants, the remaining mtDNA nucleoids are accumulated in the waste bag by the investment cones and eliminated from mature sperm (*45*). Thus, it is a common phenomenon under a wide variety of circumstances, and multiple different strategies act as redundancies to make sure that PME occurs. These redundancies along with their conservation in the animal kingdom lend credence to the enormous importance of maternal inheritance and PME.

Chapter 2

Endonuclease G mediates mtDNA degradation in PME.

Mitochondria are inherited maternally in most animals, but the mechanisms by which paternal mitochondria are selectively removed in embryos are poorly understood. Using electron tomography analyses, we monitor the fate of paternal mitochondria in *C. elegans* embryos and find that paternal mitochondria rapidly lose their inner membrane integrity following fertilization and become empty ghosts by the 2-4 cell embryonic stage. Using a candidate-based RNAi screen, we identify CPS-6, a mitochondrial endonuclease G, as a resident mitochondrial factor critical for paternal mitochondrial elimination (PME). Localization of CPS-6 in paternal mitochondria is required for its role in PME and CPS-6 acts in parallel to the maternal autophagy and proteasome pathways to promote PME. Immunoelectron microscopy analysis demonstrates relocation of CPS-6 from the intermembrane space of paternal mitochondria to the matrix following fertilization, leading to degradation of mitochondrial DNA (mtDNA). Loss of *cps-6* delays breakdown of mitochondrial inner membrane structures, autophagosome enclosure of paternal mitochondria, and destruction of paternal mitochondria. Moreover, delayed removal of paternal mitochondria in *C. elegans* embryos results in prolonged cell divisions and increased embryonic lethality, demonstrating that PME is important for healthy embryonic development and may provide an evolutionary advantage. Thus, CPS-6 functions as a paternal mitochondrial suicide factor during early animal development, in addition to its established role as an apoptotic nuclease that fragments chromosomes.

2.1 Background of maternal inheritance of mitochondria.

Mitochondria play critical roles in many cellular processes, including cellular respiration, apoptosis, and stress responses (*105, 106*). They are unique membrane-enclosed organelles

that possess their own genome (mtDNA), which encodes multiple components of the oxidative phosphorylation (OXPHOS) protein complexes, ribosomal RNAs, and tRNAs (*107*). mtDNA coordinates with the nuclear genome to maintain proper functions, activities and structures of mitochondria and cells (*106, 107*), including production of adenosine triphosphate (ATP), the major energy source for the cell. Mutations in mtDNA can lead to compromised mitochondria and numerous human diseases, including Leigh Syndrome, mitochondrial encephalomyopathy, lactic acidosis, stroke-like episodes, Kearns-Sayre Syndrome, and Leber hereditary optic neuropathy (*107, 108*).

Interestingly, mitochondria are inherited maternally in most eukaryotes (*109-111*). The mechanisms and reasons for this uniparental inheritance of mitochondria are poorly understood. Several models have been proposed to account for selective elimination of paternal mitochondria, including denied entry of sperm mitochondria into the oocyte, dilution or selective destruction of paternal mitochondria in the dividing embryo, and restricted localization of paternal mitochondria to a specific region of the fertilized egg (*109, 112-114*). Recently, several studies report that the autophagy-lysosomal pathway in *C. elegans* embryos is actively involved in eliminating paternal mitochondria, providing direct evidence for the model of selective degradation of paternal mitochondria (*36, 115, 116*). However, how paternal mitochondria, but not maternal mitochondria, are specifically recognized and degraded by the autophagy machinery in embryos is unknown. It is also unclear whether the autophagy process is sufficient to mediate PME and whether additional mechanisms, derived either paternally or maternally, are required to facilitate this process. Finally, the physiological significance of PME to animal development and organismal fitness remains to be determined.

Using high-resolution electron tomography (ET) analyses, we follow the fate of paternal mitochondria before and after fertilization and discover that paternal mitochondria undergo rapid internal breakdown and self-destruction upon entry into the oocyte. A candidate-approach RNAi

screen targeting 217 *C. elegans* nuclear-encoded mitochondrial proteins identifies CPS-6, a mitochondrial endonuclease, as a paternal factor critical for PME. Following fertilization, CPS-6 relocates from the intermembrane space of paternal mitochondria to the matrix to destroy mtDNA. Inactivation of CPS-6 delays internal breakdown, autophagosome enclosure, and degradation of paternal mitochondria. Moreover, CPS-6 acts in paternal mitochondria and in parallel to the maternal autophagy and proteasome pathways to promote PME. Our study thus uncovers a series of important cellular events that coordinate both self-destruction and maternal degradation of paternal mitochondria. Finally, we show that delayed removal of paternal mitochondria adversely affects cell division and embryo development, providing support to the theory that PME is important for organismal fitness.

2.2 Experimental Results

2.2.1 Electron tomography analysis of the PME process

To understand how sperm mitochondria are selectively recognized and removed in embryos, we examined paternal mitochondria in spermatozoa and embryos by electron microscopy and tomography (Fig. 2.1). The EM examination is done in collaboration with Dr. Byung-Ho Kang's group, who were in the University of Florida during our cooperation. I have prepared almost 100% of the samples that are sent to Florida for EM analysis. Mitochondria in wild-type spermatozoa are spherical and located around the nucleus (Fig. 2.1A), with an average diameter of 464 nm (SD: 68 nm). Paternal mitochondria in wild-type zygotes are readily distinguished from maternal mitochondria because the latter are tubular and thinner, with an average width of 238 nm (SD: 57 nm) (Fig. 2.1B). In spermatozoa, mitochondria have smooth cristae uniformly distributed in the matrix (Fig. 2.1C). By contrast, paternal mitochondria in wild-type zygotes have dark aggregates (agg) that form at multiple sites in the matrix (Fig. 2.1D). Since every paternal mitochondrion in the one-cell stage embryos has aggregates of different

sizes (Fig. 2.1G), this finding suggests that the aggregates form soon after fertilization. Based on their internal morphology, paternal mitochondria with small aggregates and without nearby autophagosome membranes are named “small agg PM” (Fig. 2.1D), those with larger aggregates and associated with autophagosome membranes are named “large agg PM” (Fig. 2.1E), and those with few cristae and enclosed in an autophagosome are named “ghost PM” (Fig. 2.1F). Many small agg PM in 1-cell stage embryos appear to arise independently of the autophagy machinery (Fig. 2.1, D and G). Partial enclosure (large agg PM) or complete enclosure (ghost PM) of paternal mitochondria by autophagosomes is also observed in 1-cell embryos, but mostly seen in 2- or 4-cell stage embryos (Fig. 2.1, E to G).

In large agg PM, cristae are rapidly cleared from the central region as the aggregates enlarge in the matrix (Fig. 2.1E) and this process occurs before autophagosomes quarantine paternal mitochondria into their lumen. Once enclosed by autophagosomes, paternal mitochondria lose matrix contents except for residual aggregates, but their outer membrane does not rupture until most of the cristae have been dissolved (Fig. 2.1F). These results suggest that paternal mitochondria in fertilized oocytes are destroyed by two means, firstly, by self-initiated internal breakdown prior to the autophagosome assembly, and secondly, by the autophagy machinery that eventually degrades the mitochondria.

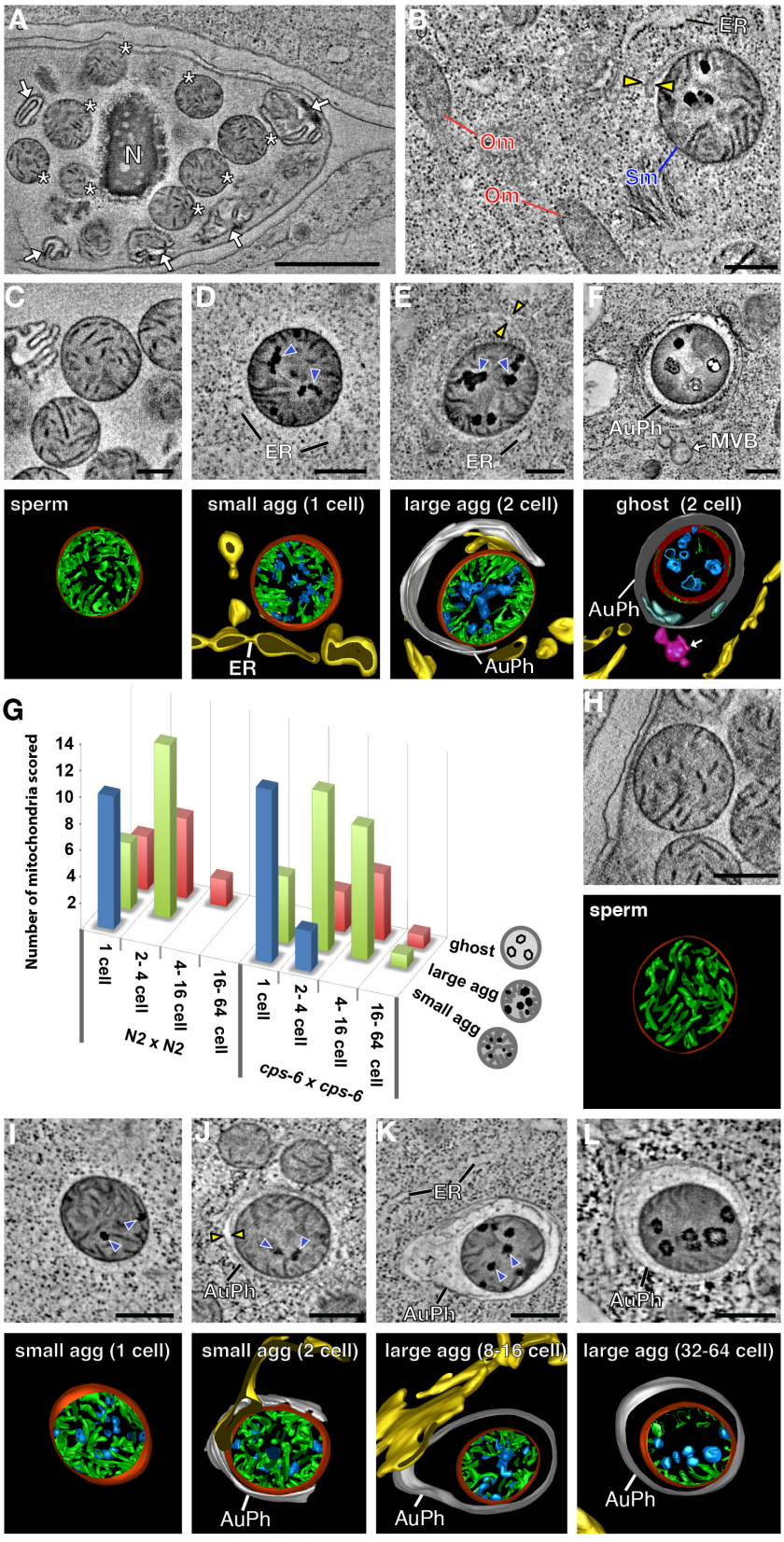
A
N
B
ER
Om
Sm
Om
C
D
ER
E
ER
F
AuPh
MVB
sperm
small agg (1 cell)
ER
large agg (2 cell)
AuPh
ghost (2 cell)
AuPh
G
Number of mitochondria scored
14
12
10
8
6
4
2
1 cell
2-4 cell
4-16 cell
16-64 cell
N2 x N2
1 cell
2-4 cell
4-16 cell
16-64 cell
cps-6 x cps-6
ghost
large agg
small agg
H
sperm
I
J
AuPh
K
ER
AuPh
L
AuPh
small agg (1 cell)
small agg (2 cell)
AuPh
large agg (8-16 cell)
AuPh
large agg (32-64 cell)
AuPh

Fig. 2. 1. Loss of *cps-6* delays internal breakdown of paternal mitochondria following fertilization. (**A**) An electron tomographic slice image of a wild-type spermatozoon showing the nucleus (N), mitochondria (asterisks), and membranous organelles (arrows). (**B**) An electron tomographic slice image of a sperm mitochondrion (Sm) in a wild-type zygote. Arrowheads denote limiting double membrane of an autophagosome being assembled around the sperm mitochondrion. Oocyte Mitochondria from the oocyte (Om) and endoplasmic reticulum (ER) are easily recognized in the image. (**C** to **F**) Images of electron tomographic slices and corresponding 3D models of a mitochondrion in a wild-type spermatozoon prior to fertilization (C) and a sperm mitochondrion in a 1- or 2-cell stage wild-type embryo after fertilization (D to F). 3D models of autophagosomes (AuPh) and ER (yellow) are also shown in the model panels. Mitochondrial membranes, cristae, and aggregates in the matrix are colored in red, green, and blue, respectively. By morphological criteria, paternal mitochondria in embryos are classified into three types: mitochondria with “small agg” (small aggregates scattered in the matrix), “large agg” (larger aggregates in the central matrix to which cristae have retracted), and “ghost” (empty mitochondria with few cristae). **(G)** A histogram illustrating the numbers of different classes of paternal mitochondria in different stages of cross-fertilized embryos from mating of wild-type (N2) males and hermaphrodites (n=45) or from mating of *cps-6(tm3222)* males and hermaphrodites (n=56). (**H** to **I**) Images of electron tomographic slices and corresponding 3D models of a mitochondrion in a *cps-6(tm3222)* spermatozoon prior to fertilization (H) and a sperm mitochondrion in a 1-cell stage (I), 2-cell stage (J), 8-16-cell stage (K), or 32-64-cell stage (L) *cps-6(tm3222)* embryo. Dark aggregates in the matrix and the autophagosome membrane are indicated with blue and yellow arrowheads (B to E, and I to K), respectively, on the tomographic slice images. Scale bar in A: 1 μm. Scale bars in B to F, and H to L: 300 nm. (I contribute Figure 1, in collaboration with Dr. Byung-ho).

2.2.2 CPS-6 is a mitochondrial factor important for PME.

The finding that paternal mitochondria self-initiate inner membrane breakdown upon entry into the oocyte suggests that intrinsic mitochondrial factors may be involved in this process. We thus performed a candidate RNAi screen against 217 nuclear genes in the *C. elegans* genome predicted to encode mitochondrial proteins (Table 2.1 in appendix and Materials and methods). Dr. Qinghua Zhou and Dr. Haimin Li designed and dominate the RNAi screening experiment, and I assisted them to do part of the screening. To assist the RNAi screen, we employed a sensitive polymerase chain reaction (PCR)-based method to track the fate of paternal mitochondria and their mtDNA using a 3 kb deletion allele (*uaDf5*) in mtDNA (Fig. 2.2A) (*36, 117*). When *C. elegans* males heteroplasmic for *uaDf5* mtDNA (*uaDf5/+*) were mated with wild-type (N2) hermaphrodites and their cross progeny were examined by PCR

analysis, *uaDf5* could be detected in one-cell stage embryos but not in stage 4 (L4) cross-fertilized larvae (right panel, Fig. 2.2A) (*36*), suggesting that paternal mitochondria are eliminated during embryonic development. By contrast, when wild-type N2 males were mated with *uaDf5/+* hermaphrodites, *uaDf5* was present in cross-progeny throughout embryonic and larval development (Fig. 2.2A) (*36*), confirming that mitochondria are maternally inherited in *C. elegans* and that the phenomenon of PME is conserved (*36, 109, 115, 116, 118, 119*).

In this screen, we looked for genes whose knockdown by RNAi delayed the removal of paternal *uaDf5* mtDNA. RNAi of the *cps-6* gene, which encodes a homolog of human mitochondrial endonuclease G (*120, 121*), resulted in persistence of paternal *uaDf5* mtDNA until the late stages of embryogenesis (Fig. 2.2B), a finding that was not observed in embryos treated with RNAi against other candidate genes (Fig. 2.2B and Materials and methods). To confirm the role of *cps-6* in elimination of paternal mtDNA during embryo development, we examined if a 336 bp deletion *(tm3222)* in *cps-6* that removes the catalytic site of CPS-6 has the same effect as *cps-6(RNAi)* (*122*). *cps-6(tm3222); uaDf5/+* males were mated with *cps-6(tm3222)* hermaphrodites and single cross-fertilized embryos or larvae at various developmental stages were isolated and analyzed by PCR. *uaDf5* paternal mtDNA was detected throughout embryonic development, but was absent in larvae (Fig. 2.2C). By contrast, in crosses between *uaDf5/+* males and N2 hermaphrodites, *uaDf5* paternal mtDNA was only detected in 64-cell stage or earlier fertilized eggs (Fig. 2.2D). These results indicate that *cps-6* promotes rapid removal of paternal mtDNA during the first several cell divisions of embryogenesis.

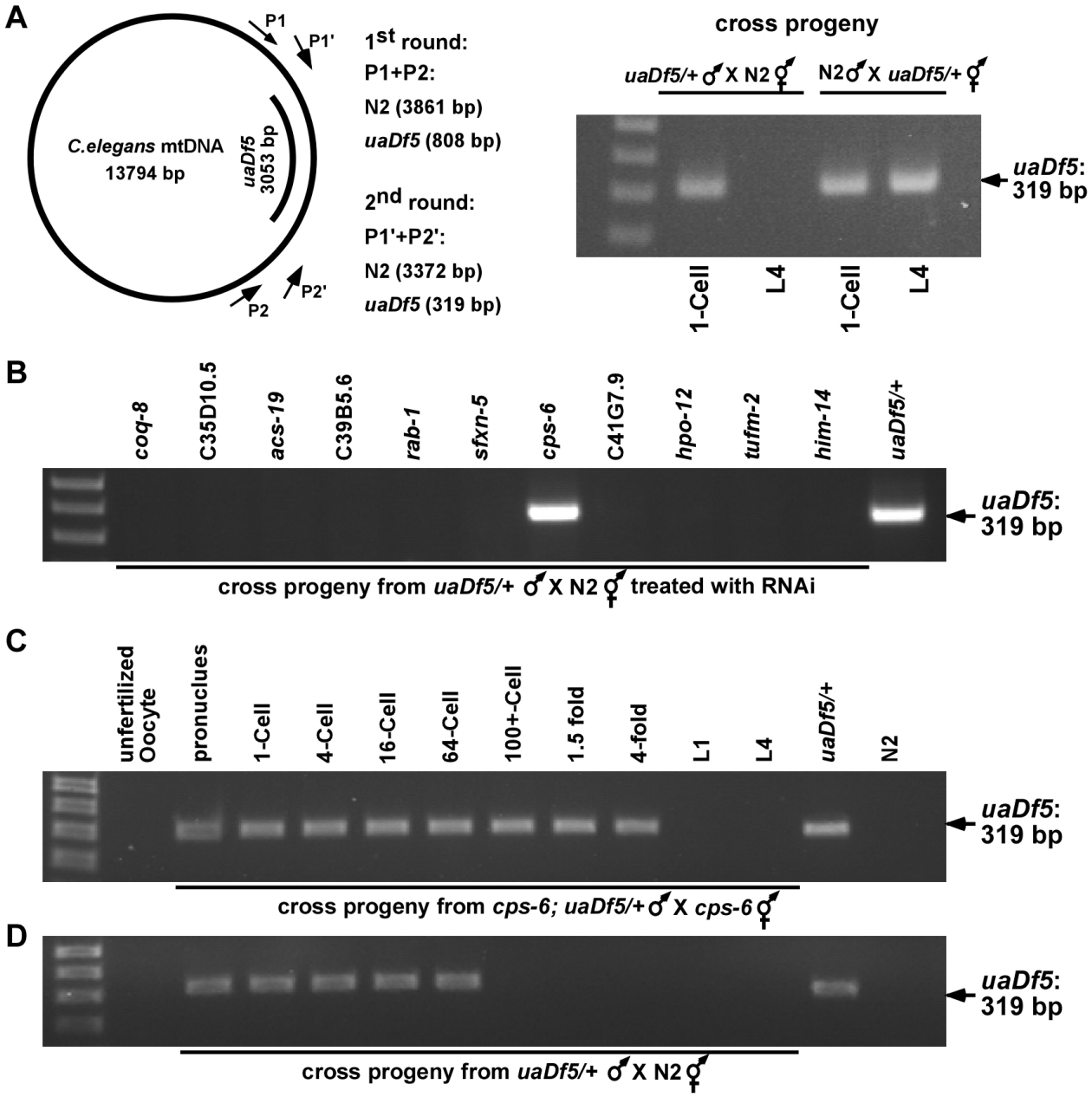

Fig. 2. 2. The CPS-6 endonuclease is a mitochondrial factor critical for paternal mtDNA elimination in *C. elegans.* (**A**) *C. elegans* mtDNA is maternally inherited. **Left panel**, a schematic diagram of *C. elegans* mtDNA, the *uaDf5* deletion, and the positions of two pairs of primers used in the nested PCR assays to detect *uaDf5*. The expected sizes of PCR products from two rounds of PCR amplification in N2 and *uaDf5/+* animals are indicated. **Right panel**, single cross-fertilized 1-cell stage embryo or L4 larva derived from mating of *smIs42; uaDf5/+* males with wild-type N2 hermaphrodites, or from mating of *smIs42* males with *uaDf5/+* hermaphrodites was analyzed by PCR for the presence of *uaDf5* mtDNA. *smIs42* is an integrated $P_{sur\text{-}5}$*sur-5::gfp* transgene that directs GFP expression in many cells (*123*) and was used to track cross progeny. MitoTracker Red (MTR) was also used to stain males before mating to facilitate isolation of the zygote. The expected PCR product from wild-type mtDNA was not detecunder the PCR conditions used. (**B**) A candidate RNAi screen identified *cps-6* as

a mitochondria-specific gene involved in paternal mtDNA elimination. A representative PCR screen is shown, in which RNAi of *cps-6* led to persistence of *uaDf5* mtDNA in 4-fold cross-fertilized embryos from mating of *smIs42; uaDf5/+* males with N2 hermaphrodites. RNAi treatment of the other nine genes predicted to encode mitochondrial proteins did not produce detectable *uaDf5*-specific product. *him-14* was used as an RNAi control to demonstrate that the bacterial feeding protocol of RNAi worked well, because an increased frequency of males were produced. See table S1 for the list of nuclear genes screened that encode mitochondrial proteins. (**C** and **D**) Inactivation of *cps-6* delays paternal mtDNA elimination. *cps-6(tm3222); smIs42; uaDf5/+* males or *smIs42; uaDf5/+* males were pre-stained with MTR before mated with *cps-6(tm3222)* or N2 hermaphrodites, respectively. Single unfertilized oocyte (MTR negative) or single cross-fertilized embryo (MTR or GFP positive) at different developmental stages was dissected from the mated hermaphrodites and analyzed by PCR to detect the presence of *uaDf5* mtDNA. The stages of the oocyte, embryo or larva (GFP positive) analyzed are: unfertilized oocyte, fertilized oocyte before the pronucleus fusion, embryo at 1-cell, 4-cell, 16-cell, 64-cell, over-100-cell, 1.5-fold, and 4-fold stage, L1 and L4 stage larva. *uaDf5/+* and N2 hermaphrodites were used as positive and negative controls, respectively.

To demonstrate that loss of paternal mtDNA corresponds to elimination of paternal mitochondria, we performed microscopic analysis of fertilized embryos to monitor the disappearance of paternal mitochondria stained by a mitochondria-specific dye, Mitotracker Red (MTR) (*36, 115, 116*). When MTR-stained N2 males were mated with unstained N2 hermaphrodites, cross-fertilized embryos examined soon after fertilization showed that paternal mitochondria vanished by the 64-cell stage (Fig. 2.3, A to F), suggesting that PME occurs in concert with the removal of paternal mtDNA (Fig. 2.2D). Conversely, when MTR-stained *cps-6(tm3222)* males were mated with *cps-6(tm3222)* hermaphrodites, MTR-stained paternal mitochondria could still be detected in embryos at around the 550-cell stage (Fig. 2.3, H to N). Therefore, CPS-6 promotes rapid clearance of both paternal mitochondria and their mtDNA in fertilized oocytes.

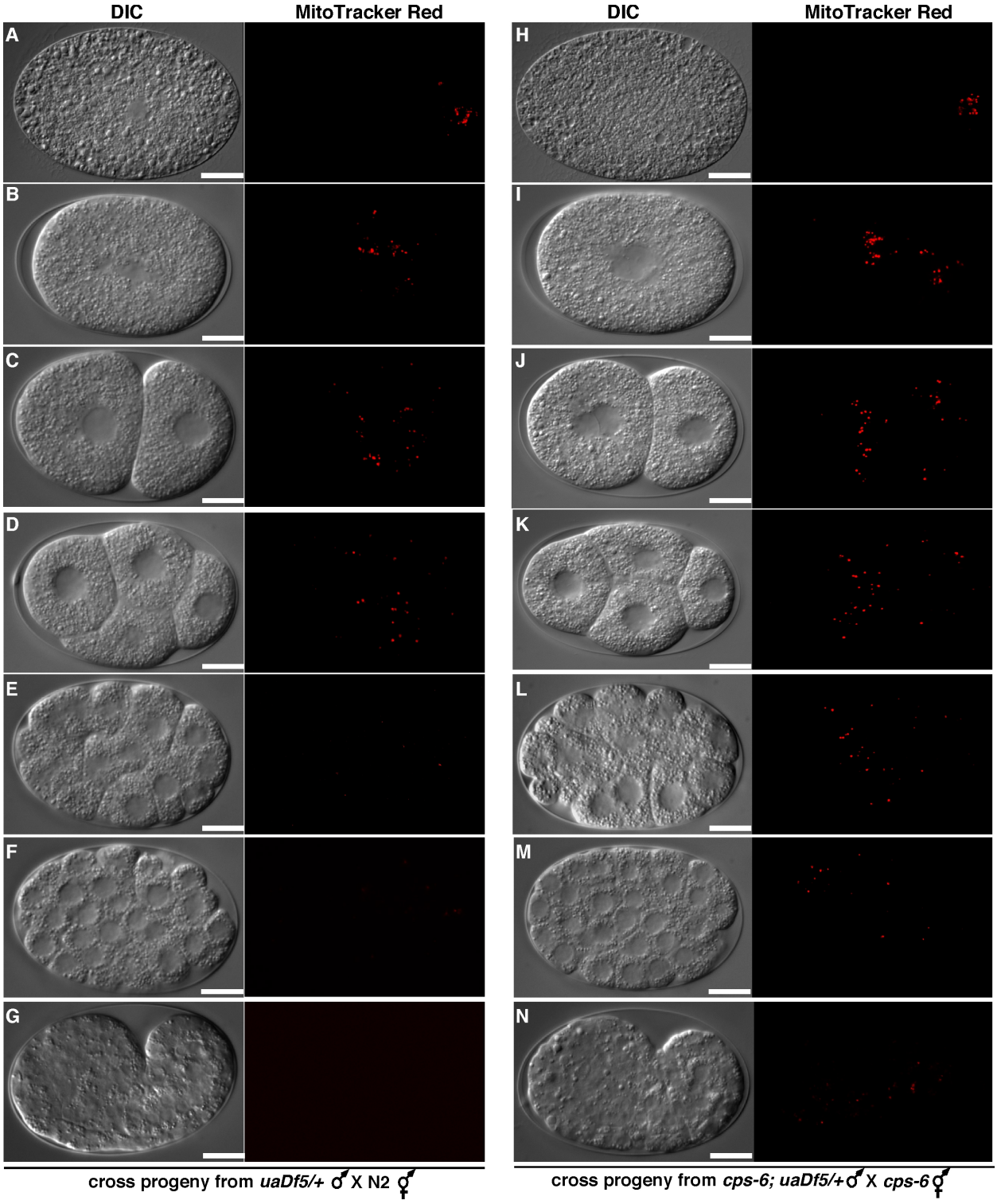

Fig. 2. 3. Inactivation of *cps-6* delays PME in *C. elegans.* (**A** to **N**) MTR-stained *uaDf5/+* males (A to G) or *cps-6(tm3222); uaDf5/+* males (H to N) were mated with unstained N2 hermaphrodites or *cps-6(tm3222)* hermaphrodites, respectively. Cross-fertilized embryos were dissected from mated hermaphrodites. Differential interference contrast (DIC) and MTR images of the embryos are shown. The red dots are paternal mitochondria clusters stained by MTR. The

stages of the embryos examined are: A zygote right after sperm entry (A and H), 1-cell stage (B and I), 2-cell stage (C and J), 4-cell stage (D and K), 32-cell stage (E and L), 64-cell stage (F and M), and comma stage embryos (G and N). Scale bars represent 10 μm.

2.2.3 CPS-6 is paternally required to promote PME.

cps-6 was first identified as a nuclease-encoding gene that acts downstream of the CED-3 caspase to mediate chromosome fragmentation during apoptosis (*120*). Inactivation of *cps-6* causes a delay in embryonic cell death and accumulation of 3′ hydroxyl DNA breaks that can be labeled by TUNEL (terminal deoxynucleotidyl transferase (TdT)–mediated dUTP nick end labeling) (*120*). CPS-6 resides in mitochondria in normal cells, but is released from mitochondria during apoptosis and translocates to the nucleus to promote chromosome fragmentation (*120, 121*). A non-apoptotic role of CPS-6 in *C. elegans* has not been reported. We first examined if the activity of CPS-6 is required paternally, maternally, or both to promote PME. *uaDf5/+* males or *cps-6(tm3222); uaDf5/+* males stained by MTR were mated with either N2 hermaphrodites or *cps-6(tm3222)* hermaphrodites. 64-cell stage cross-fertilized embryos were scored for the number of MTR-stained mitochondrial clusters by microscopic analysis (Fig. 2.4A). In parallel, we examined the presence of *uaDf5* paternal mtDNA by PCR analysis of cross-fertilized embryos at approximately 100-cell stage (Fig. 2.4B). We found that a significant portion of paternal mitochondria and mtDNA persisted past the 64-cell embryonic stage when *cps-6* was eliminated from the paternal lineage (Fig. 2.4, A and B, mating 3, 4). On the other hand, absence of maternal *cps-6* in the oocyte still resulted in rapid and close to complete PME by the 64-cell stage as in N2 fertilized oocytes (Fig. 2.4, A and B, mating 2). These results indicate that paternal CPS-6, but not maternal CPS-6, is specifically required to promote PME.

2.2.4 Nucleases activity of CPS-6 is crucial for PME.

We next examined if CPS-6 is required within paternal mitochondria to mediate PME. CPS-6 contains a mitochondrial targeting sequence (amino acids 1-21) that is critical for its mitochondrial localization (*120*). A CPS-6 mutant protein without this targeting sequence, CPS-6**Δ**N, localizes instead to the nucleus (*120*). We generated *cps-6(tm3222); uaDf5/+* transgenic animals expressing wild-type CPS-6 or CPS-6**Δ**N under the control of the promoter of the *dpy-30* gene ($P_{dpy\text{-}30}$CPS-6 and $P_{dpy\text{-}30}$CPS-6**Δ**N), which is ubiquitously expressed in *C. elegans* (*124*). Transgenic *cps-6(tm3222); uaDf5/+* males were mated with N2 hermaphrodites and cross-fertilized transgenic embryos at approximately the 100-cell stage were analyzed by PCR for the presence of *uaDf5* paternal mtDNA. Expression of wild-type CPS-6 in *cps-6(tm3222)* males rescued the defect in paternal mtDNA elimination (Fig. 2.4C, mating 1, 2, 7), whereas expression of CPS-6**Δ**N failed to do so (Fig. 2.4C, mating 5, 6). This result indicates that localization of CPS-6 in paternal mitochondria is required for CPS-6 to mediate PME. On the other hand, expression of either CPS-6 or CPS-6**Δ**N was sufficient to rescue the delay-of-cell-death defect in the *cps-6(tm3222)* mutant, in which some of the early embryonic cell deaths were delayed until the mid- or late embryonic stages (2-fold, 2.5-fold and 3-fold stages), resulting in the peak of embryonic cell deaths at the 2-fold embryonic stage (*120*). This result indicates that the pro-apoptotic function of CPS-6 is distinct from its non-apoptotic function in PME. However, the nuclease activity of CPS-6 is required for both functions, as expression of CPS-6(H148A), which has no nuclease activity due to the replacement of the catalytic residue His148 by Ala (*122*), failed to rescue the defects in both cell death and PME (Fig. 2.4C, mating 3, 4). Therefore, both the nuclease activity and mitochondrial localization are required for CPS-6 to mediate PME.

The paternal dependency experiment and the rescue experiment are 100% done by Dr. Qinghua Zhou, who used to be a graduate student in the lab.

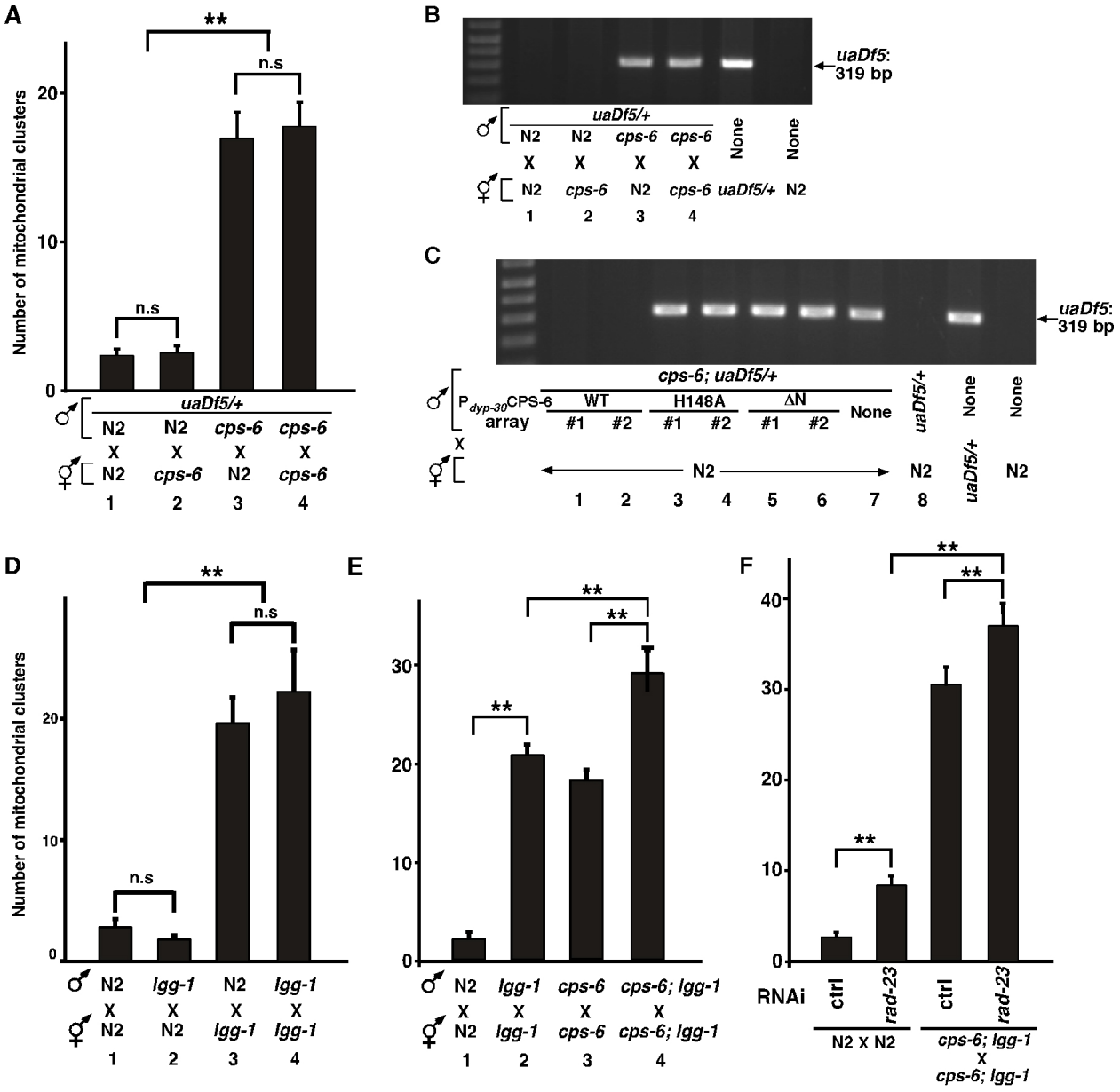

Fig. 2. 4. **CPS-6 acts paternally in mitochondria and in parallel to the maternal autophagy and proteasome pathways to promote PME.** (**A,** and **D** to **F)** Quantification of MTR-stained paternal mitochondrial clusters in 64-cell stage cross-fertilized embryos from mating of MTR-stained males and unstained hermaphrodites with the indicated genotypes. The number of MTR-positive mitochondrial clusters was counted from the deconvolved image of the cross-fertilized embryo. 20 embryos were scored for each experiment. Error bars represent SEM. The significance of differences between results from different mating experiments was determined by unpaired Student's *t*-test. ** $P < 0.0001$. "n.s." indicates no significant difference. (**B**) Loss of paternal *cps-6* delays elimination of paternal mtDNA. Five cross-fertilized embryos at approximately 100-cell stage from the indicated crosses were analyzed by PCR to detect the presence of *uaDf5* mtDNA. (**C**) The endonuclease activity and localization to paternal mitochondria are required for CPS-6 to mediate elimination of paternal mtDNA. *cps-6(tm3222); uaDf5/+* males carrying the indicated P_{dpy-30}CPS-6 transgenes were mated with N2

hermaphrodites. Five cross-fertilized transgenic embryos at approximately 100-cell stage were analyzed by PCR to detect the presence of *uaDf5* mtDNA. *lgg-1(bp500)* and *cps-6(tm3222)* alleles were used where indicated. In F, males and hermaphrodites were treated with control RNAi (Ctrl) or *rad-23* RNAi during mating, as the *cps-6(tm3222); lgg-1(bp500) rad-23(tm2595)* mutant is sick. (this figure is 100% contributed by Dr. Qinghua Zhou, and it is included in my dissertation because of the logic coherence).

2.2.5 Loss of CPS-6 delays internal breakdown of paternal mitochondria.

We examined how loss of *cps-6* affects PME structurally by electron tomography. In 1-cell stage cross-fertilized *cps-6(tm3222)* embryos, dark aggregates were still visible in paternal mitochondria, but less severe than wild-type 1-cell stage embryos, and in particular, no ghost paternal mitochondria were detected (Fig. 2.1, G to I). These findings suggest that CPS-6 is involved in, but not solely responsible for, causing internal damages to paternal mitochondria following fertilization. The double-limiting membranes of autophagosomes started to assemble around paternal mitochondria in 2- or 4-cell stage embryos and completely enclosed them by 8- or 16-cell stage embryos (Fig. 2.1, J and K), showing a significant delay in autophagosome formation on paternal mitochondria, compared with those observed in wild-type embryos where autophagosome assembly started at the 1-cell stage and completed the enclosure by 2- or 4-cell stage embryos (Fig. 2.1, E to G). Despite the assembly of autophagosomes, internal breakdown of paternal mitochondria was clearly delayed in cross-fertilized *cps-6(tm3222)* embryos (Fig. 2.1, J and K), as a significant portion of matrix and cristae in paternal mitochondria remained superficially intact and less than 40% of paternal mitochondria transited into ghost PM, even in 16-cell stage embryos (Fig. 2.1G). Some large agg PM even lingered on in 64-cell stage embryos (Fig. 2.1L). In comparison, 100% of paternal mitochondria in wild-type embryos either had become ghost PM or had already been eliminated by 4-cell stage embryos and no paternal mitochondrion was observed by EM after 16-cell stage. These results suggest that CPS-6 plays an important role in mediating internal breakdown of paternal mitochondria.

2.2.6 Paternal mitochondria are depolarized upon entry into the oocyte.

Compromised mitochondria are often accompanied by loss of mitochondrial membrane potential, which can be detected by potential-sensitive mitochondrial dyes, such as tetramethylrhodamine ethyl ester (TMRE) (*125*). When TMRE-stained *uaDf5/+* males were mated with unstained N2 hermaphrodites, TMRE staining of sperm mitochondria was completely lost upon their entry into the oocyte (Fig. 2.5A, left panel). In comparison, staining of sperm mitochondria by potential-insensitive dye MTR persisted in fertilized oocytes (Fig. 2.5A, right panel). To confirm the presence of paternal mitochondria in zygotes, males were stained with both the nucleic acid dye SYTO11 and MTR or TMRE and mated with unstained N2 hermaphrodites. SYTO11 stayed visible in paternal mitochondria after fertilization and co-localized with MTR (Fig. 2.5B). Conversely, when N2 males stained with both TMRE and SYTO11 were mated with unstained N2 hermaphrodites, SYTO11 was visible in zygotes, but TMRE staining was lost (Fig. 2.5C). Importantly, when we mated SYTO11-stained N2 males with N2 hermaphrodites in the presence of TMRE, which would stain both paternal and maternal mitochondria in zygotes, only maternal mitochondria were stained by TMRE and the SYTO11-positive paternal mitochondria were completely TMRE-negative (Fig. 2.5D). This result confirms the selective loss of membrane potential in paternal mitochondria in zygotes, which precedes mtDNA degradation. These findings indicate that paternal mitochondria are depolarized and damaged upon entry into the oocyte and that this is an early signature event preceding degradation of their mtDNA and PME.

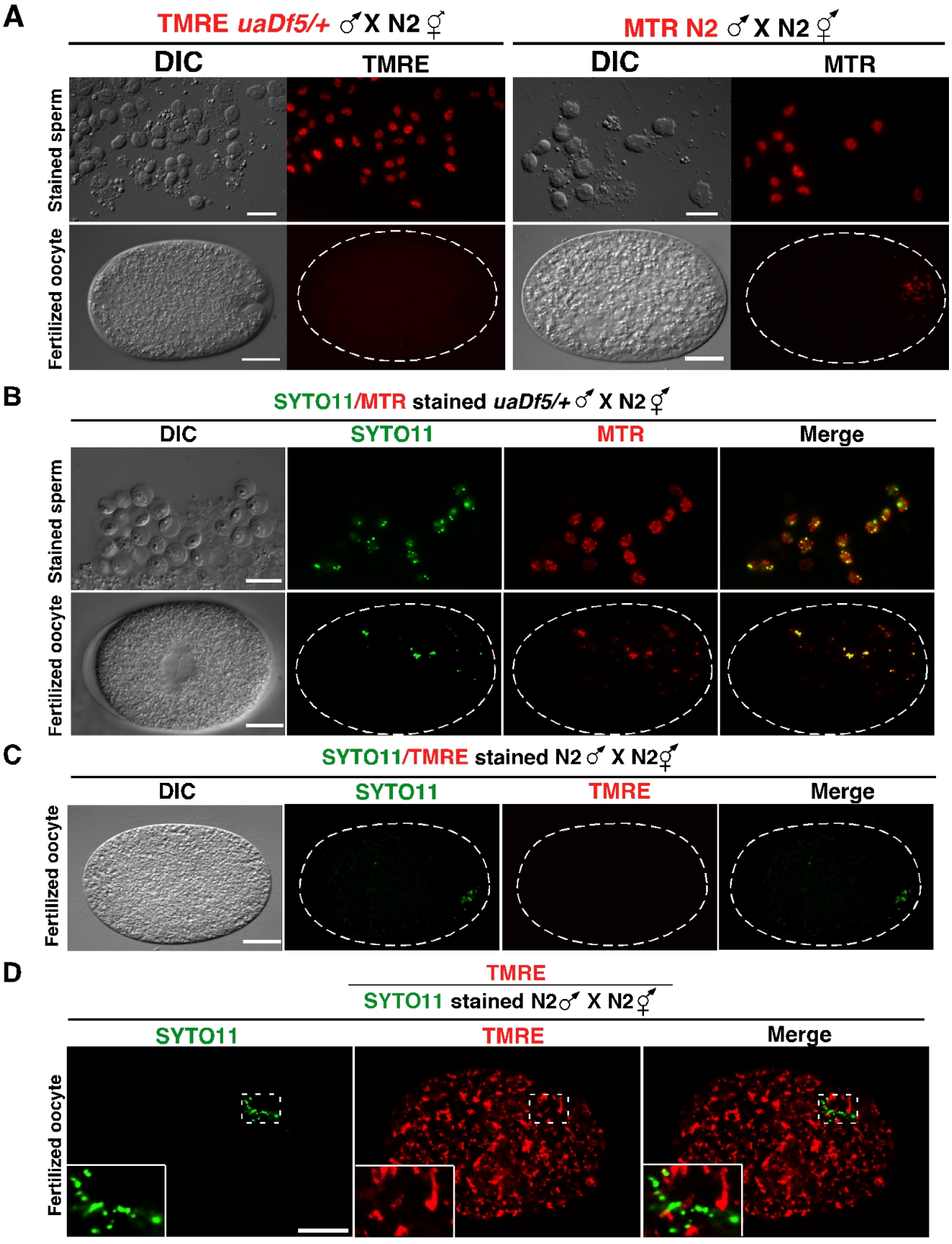
A
TMRE uaDf5/+ ♂ X N2 ♀
MTR N2 ♂ X N2 ♀
DIC
TMRE
DIC
MTR
Stained sperm
Fertilized oocyte
B
SYTO11/MTR stained uaDf5/+ ♂ X N2 ♀
DIC
SYTO11
MTR
Merge
Stained sperm
Fertilized oocyte
C
SYTO11/TMRE stained N2 ♂ X N2 ♀
DIC
SYTO11
TMRE
Merge
Fertilized oocyte
D
TMRE
SYTO11 stained N2 ♂ X N2 ♀
SYTO11
TMRE
Merge
Fertilized oocyte

Fig. 2. 5. Paternal but not maternal mitochondria are depolarized following fertilization. (**A** to **C**) DIC and fluorescence images of spermatozoa pre-stained with the indicated dyes (A and B) and corresponding images of cross-fertilized embryos from the indicated crosses with unstained N2 hermaphrodites are shown. The presence of *uaDf5* paternal mitochondria in the oocyte right after fertilization by the TMRE-stained spermatozoon (left panel, A) was confirmed by PCR analysis after recovery of the imaged zygote. (**D**) SYTO11, TMRE, and TMRE/SYTO11 merged images of a fertilized embryo right after sperm entry from mating of SYTO11-prestained N2 males with N2 hermaphrodites in the presence of TMRE. In this experiment, TMRE had equal access to both maternal and paternal mitochondria in the zygote. Scale bars represent 10 μm in all panels. (I contributed to the figure 2.5.C and repeated the rest of the figures by myself)

2.2.7 CPS-6 relocates from the intermembrane space of paternal mitochondria to the matrix.

Because CPS-6 acts in paternal mitochondria to mediate PME, we examined if loss of the inner membrane integrity in paternal mitochondria results in entry of CPS-6 from the intermembrane space into the mitochondrial matrix. We performed 40 mmune-electron microscopy analysis using an anti-CPS-6 antibody (*122*). In N2 spermatozoa, CPS-6-specific immunogold particles were predominantly associated with the mitochondrial membrane (arrowheads in Fig. 2.6A and Fig. 2.6E), in agreement with CPS-6's localization in the mitochondrial intermembrane space. By contrast, no CPS-6-specific immunogold particles were seen in *cps-6(tm3222)* spermatozoa, indicating that the antibody recognizes specifically the CPS-6 protein. In 1-cell stage embryos derived from mating of N2 males with *cps-6(tm3222)* hermaphrodites, CPS-6-specific immunogold particles were often located inside paternal mitochondria, away from the mitochondrial membrane (arrowheads in Fig. 2.6B and Fig. 2.6E). Since some of the paternal mitochondria had not been associated with autophagosomes (Fig. 2.6B), this indicates that CPS-6 enters the matrix prior to the initiation of autophagosome formation. When the localization patterns of CPS-6 before and after fertilization are compared with those of a genuine mitochondrial matrix protein, the E2 subunit of pyruvate dehydrogenase (Fig. 2.6, C to E), relocation of CPS-6 into the matrix after fertilization is clearly discerned.

Collectively, these fluorescence microscopy, electron tomography, and 41mmune-EM analyses provide strong evidence that paternal mitochondria are depolarized and damaged upon entry into the oocytes, leading to the entry of CPS-6 into the mitochondrial matrix to catalyze the degradation of mtDNA and internal breakdown of paternal mitochondria.

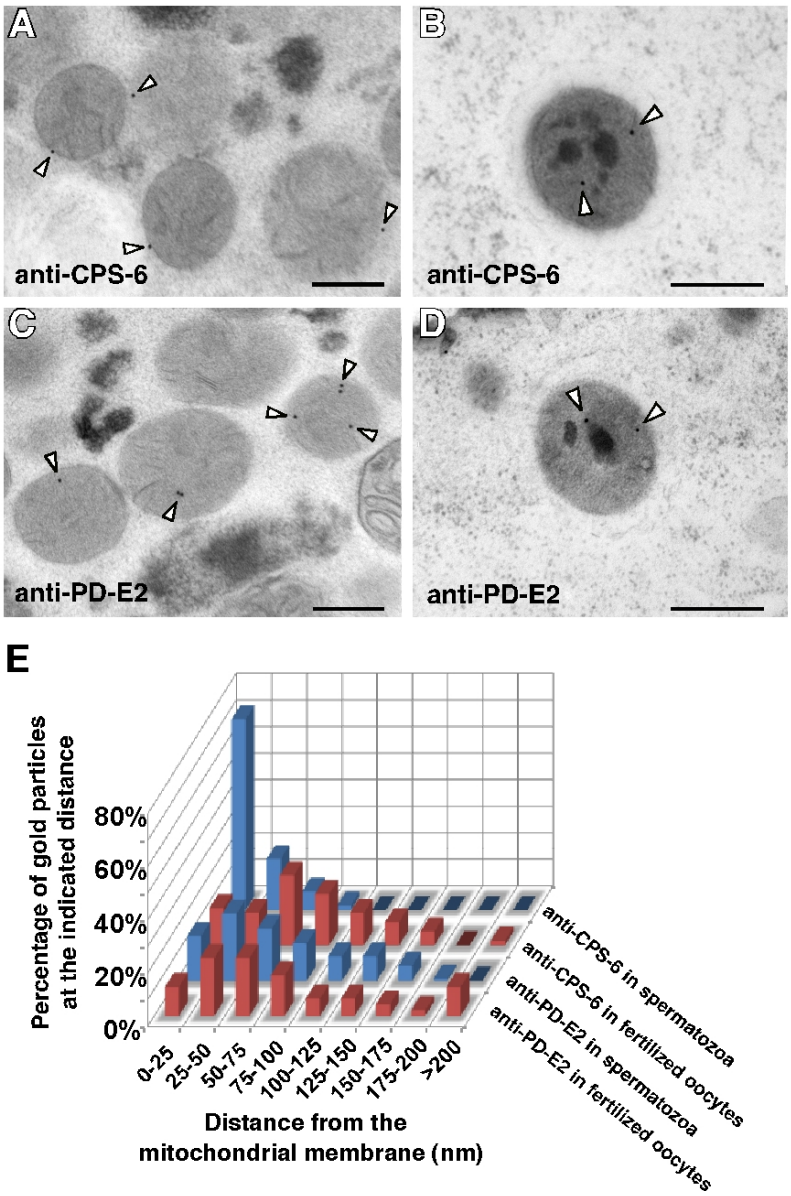

Fig. 2. 6. Immuno-electron microscopy localization of CPS-6 in paternal mitochondria before and after fertilization. (**A** to **D**) Representative 41mmune-EM images observed in mitochondria of N2 spermatozoa (A and C) and in a paternal mitochondrion in a zygote from mating of N2 males with *cps-6(tm3222)* hermaphrodites (B and D). CPS-6-specific (A and B**)** and PD-E2-specific (C and D) immunogold particles are marked with arrowheads. Dark

aggregates are seen in the matrix of paternal mitochondria in zygotes (B and D), but are absent in sperm mitochondria (A and C). Scale bars indicate 300 nm**.** (E) Histogram of the distances of 15 nm immunogold particles from the mitochondrial membrane. The histogram is based on measurements of 57 (anti-CPS-6 in spermatozoa), 57 (anti-CPS-6 in zygotes), 143 (anti-PD-E2 in spermatozoa), and 46 (anti-PD-E2 in zygotes) immunogold particles from 82 and 74 paternal mitochondria for each antibody, respectively.

2.2.8 CPS-6 acts in parallel to the maternal autophagy and proteasome pathways.

The autophagy process and the proteasome pathway have been shown to promote PME in *C. elegans* (*36, 115, 116*). We examined if LGG-1, the *C. elegans* LC3/Atg8 homolog necessary for autophagosome formation (*126, 127*), and RAD-23, one of the ubiquitin receptors that target ubiquitylated substrates for proteasomal degradation (*128*), act paternally or maternally to promote PME *(13)*, using a loss-of-function *lgg-1(bp500)* mutation and a loss-of-function *rad-23(tm2595)* deletion mutation. We quantified the number of paternal mitochondrial clusters in 64-cell stage cross-fertilized embryos derived from MTR-stained N2 or mutant males mated with unstained N2 or the corresponding mutant hermaphrodites. In both cases, when maternal *lgg-1* or *rad-23* was deficient, significantly more MTR-stained paternal mitochondria persisted regardless of the male genotype (Fig. 2.4D), with *rad-23(tm2595)* showing a weaker effect. These results indicate that unlike CPS-6 both LGG-1 and RAD-23 act maternally to promote PME.

We examined the relationship between *cps-6* and the two maternal degradation pathways. N2, *cps-6(tm3222), lgg-1(bp500),* and *cps-6(tm3222); lgg-1(bp500)* males stained by MTR were mated with respective unstained hermaphrodites. The resulting 64-cell stage cross-fertilized embryos were scored for the number of MTR-stained mitochondrial clusters (Fig. 2.4E). Cross-fertilized *cps-6(tm3222)* embryos and *lgg-1(bp500)* embryos had comparable numbers of MTR-stained paternal mitochondria, which were significantly higher than that from cross-fertilized N2 embryos (Fig. 2.4E, mating 1-3). Importantly, loss of both *cps-6* and *lgg-1*

resulted in a greater increase in MTR-stained paternal mitochondria compared to either mutant alone (Fig. 2.4E, mating 4), indicating that *cps-6* and *lgg-1* act in different pathways to promote PME. This was confirmed by time-lapse microscopic analysis of cross-fertilized embryos at multiple stages of embryo development (Fig. 2.7B). Similarly, loss of both *cps-6* and *rad-23* resulted in a significantly higher number of persistent paternal mitochondria than in either single mutant alone (Fig. 2.7C), indicating that *cps-6* and *rad-23* also act in different pathways to promote PME. Finally, an even higher number of persistent paternal mitochondria was observed in *cps-6(tm3222); lgg-1(bp500)* cross-fertilized embryos treated with *rad-23(RNAi),* which is as efficient as *rad-23(tm2595)* in delaying PME (Fig. 2.4F, Fig. 2.7A), than in *cps-6(tm3222); lgg-1(bp500)* cross-fertilized embryos treated with control RNAi (Fig. 2.4F). These results indicate that *cps-6, lgg-1,* and *rad-23* function in three independent pathways and utilize distinct mechanisms (mitochondrial self-destruction, autophagy, and proteasomal degradation, respectively) to coordinate swift removal of paternal mitochondria.

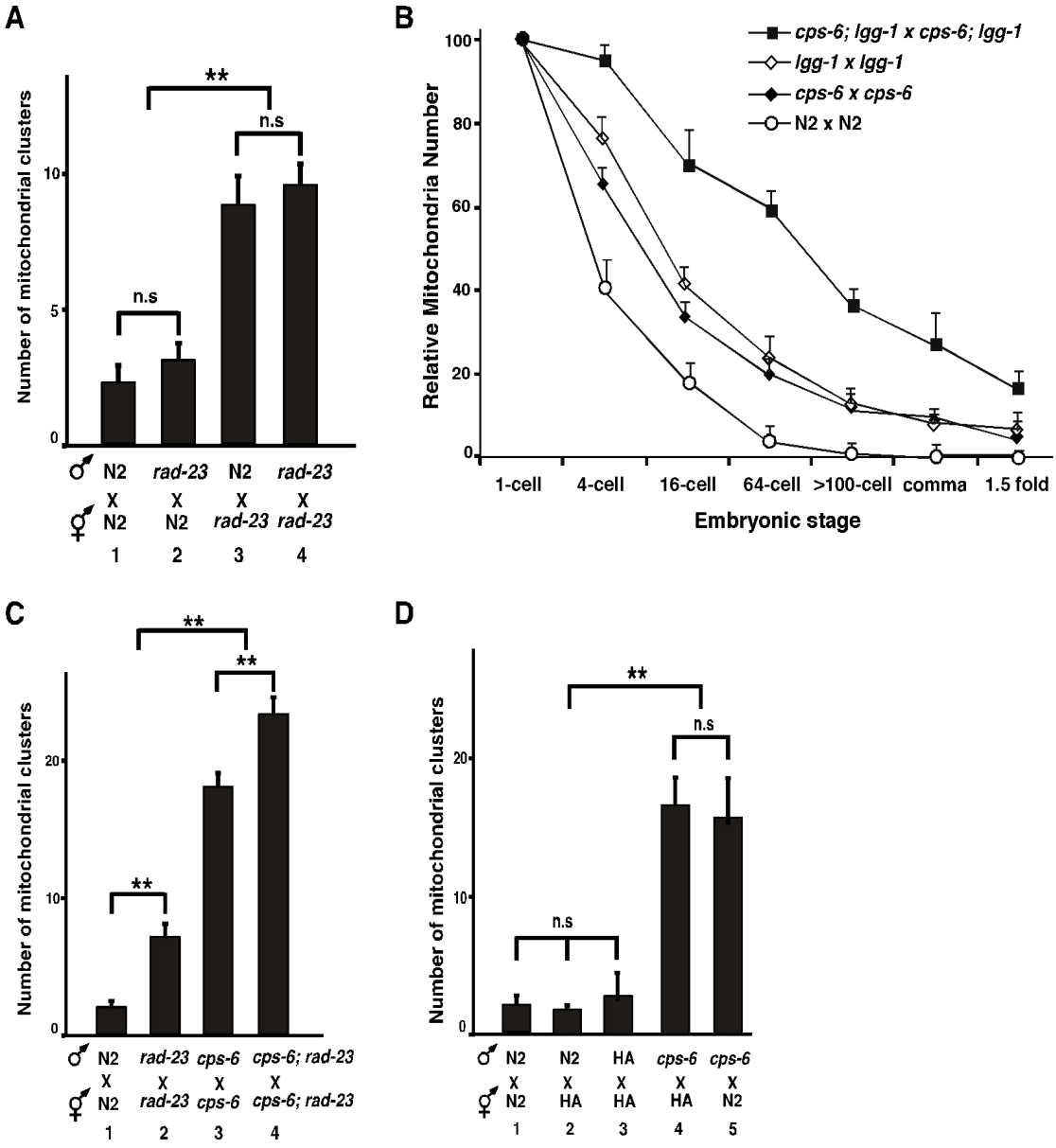

Fig. 2. 7. Paternal CPS-6 acts in parallel to the maternal autophagy and proteasome pathways to promote PME. (**A**, **C and D**) Quantification of MTR-stained paternal mitochondrial clusters in 64-cell stage embryos derived from mating of males and hermaphrodites with the indicated genotypes. *rad-23(tm2595)* and *cps-6(tm3222)* alleles were used in these experiments. HA: wild-type *C. elegans* Hawaii strain. MTR staining of males, mating with unstained hermaphrodites, and quantification of MTR-stained mitochondrial clusters were performed as described in Fig. 4A. n=20 for each experiment. The significance of differences between results from different experiments was determined by unpaired *t*-test, ** $P <$ 0.005, "n.s." indicates no significant difference. (**B**) Quantification of relative paternal mitochondrial numbers in cross-fertilized embryos from the indicated mating. The numbers of MTR-stained paternal mitochondrial clusters were scored from deconvolved images of the dividing embryo at different embryonic stages. The relative paternal mitochondrial number in each zygote right after fertilizationwas set artificially at 100. Relative paternal mitochondrial

numbers in other embryonic stages of the same embryo were normalized with the number of the zygote. Three embryos were scored for each mating experiment. *cps-6(tm3222)* and *lgg-1(bp500)* alleles were used. Error bars indicate SEM.

2.2.9 Loss of CPS-6 compromises autophagosome formation on paternal mitochondria.

Although loss of CPS-6 did not prevent the formation of autophagosomes on paternal mitochondria (Fig. 2.1, G to L), autophagosomes appear to take a longer time to encapsulate and degrade paternal mitochondria in cross-fertilized *cps-6(tm3222)* embryos, suggesting that loss of CPS-6 affects the autophagy process. We examined the formation of LGG-1 autophagosomes on paternal mitochondria by immunostaining, using a monoclonal antibody to LGG-1. In zygotes derived from mating of MTR-stained N2 males and unstained N2 hermaphrodites, bright LGG-1 staining was seen clustering around MTR-stained paternal mitochondria near the site of sperm entry (Fig. 2.8A) and approximately 81% of MTR-stained paternal mitochondrial clusters showed co-localization with LGG-1 autophagosomes (Fig. 2.8C). By contrast, in zygotes derived from mating of *cps-6(tm3222)* hermaphrodites and MTR-stained *cps-6(tm3222)* males, co-localization of paternal mitochondrial clusters with LGG-1 autophagosomes dropped to 43% (Fig. 2.8, B and C), indicating that loss of *cps-6* compromises autophagosome formation on paternal mitochondria. We then examined more closely the enclosure of MTR-stained paternal mitochondria by autophagosomes using the superresolution Structured Illumination Microscopy (SIM) and obtained similar results. In zygotes between MTR-stained N2 males and unstained N2 hermaphrodites, the majority (77%) of paternal mitochondria were fully encapsulated (enclosed) by LGG-1 autophagosomes, some (12%) were partially encapsulated (partially enclosed), and only 11% of paternal mitochondria did not associate with (isolated) with autophagosomes (Fig. 2.8, D, E and H). By contrast, in zygotes between *cps-6(tm3222)* hermaphrodites and MTR-stained *cps-6(tm3222)* males, more than one half (51%) of paternal mitochondria did not associate with autophagosomes and only 29% and

20% of paternal mitochondria were fully and partially enclosed by autophagosomes, respectively (Fig. 2.8, F to H). These findings, together with the EM observations, indicate that the CPS-6-mediated mitochondrial self-destruction process, albeit ocurring independently of the autophagy process, is important for efficient recruitment of autophagosomes to paternal mitochondria and rapid degradation of paternal mitochondria once they are encapsulated by autophagosomes.

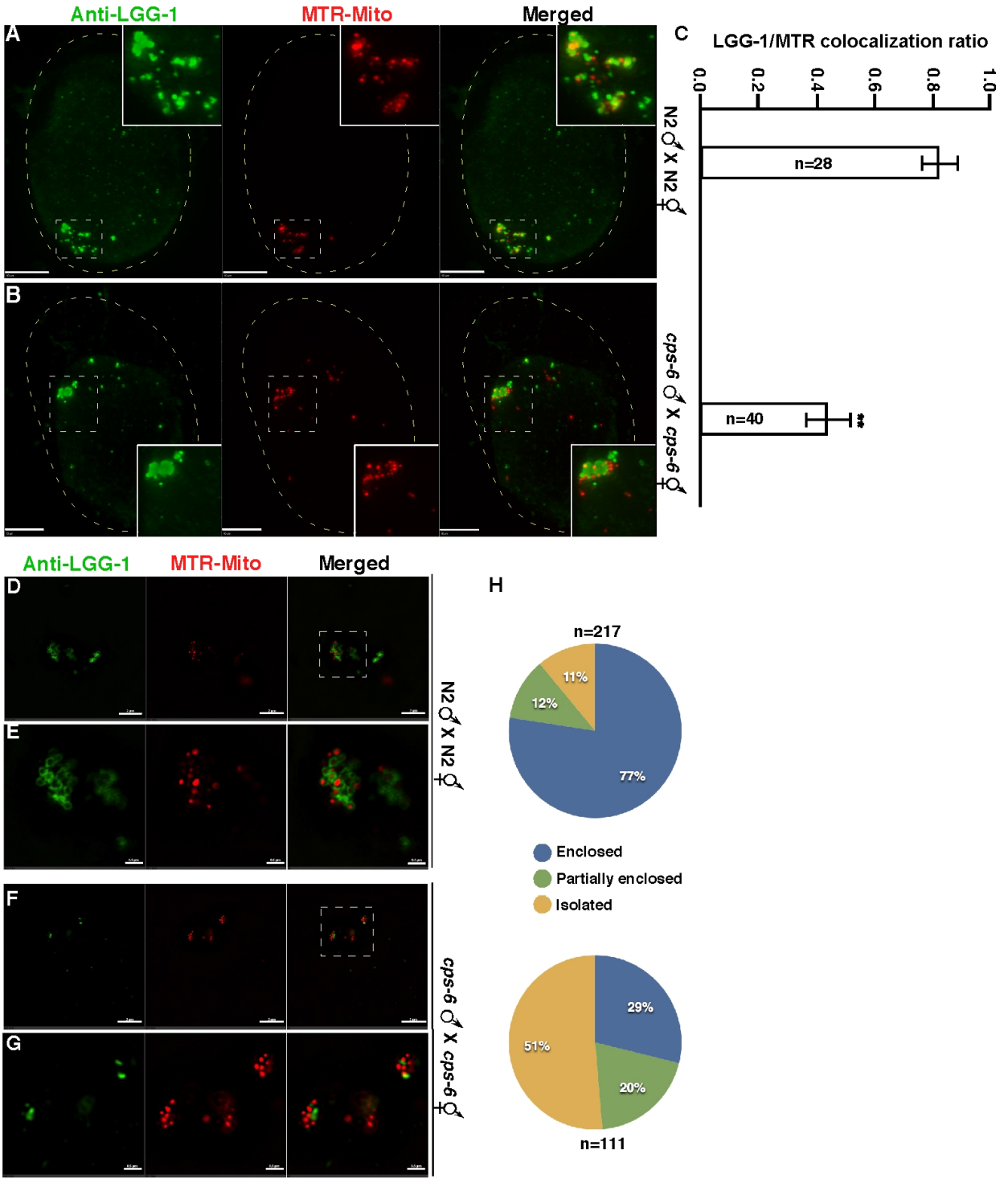

Fig. 2. 8. Loss of CPS-6 compromises autophagosome formation on paternal mitochondria. (**A, B** and **D** to **G**) Zygotes from mating of MTR-stained males with unstained hermaphrodites of the indicated genotypes were labeled with a monoclonal antibody to LGG-1. Images shown are anti-LGG-1 staining (Green), MTR-stained paternal mitochondria (Red), and anti-LGG-1/MTR merged images. Images were acquired using a Zeiss Axioplan 2 microscope (A and B) and a Nikon Structured Illumination Microscope (SIM, D to G). The *cps-6(tm3222)*

allele was used. Dash rectangles highlight the areas enlarged and shown in insets (A and B) or in figure panels below (E and G). Scale bars represent 10 μm (A and B), 2 μm (D and F) and 0.5 μm (E and G). (**C**) Quantification of the colocalization ratio of MTR-stained paternal mitochondrial clusters with LGG-1-stained autophagosomes shown in A and B. Error bars are SEM. n indicates the number of zygotes scored. The significance of difference between results from two different mating experiments was determined by unpaired Student's *t*-test. ** $P < 0.001$. (**H**) Quantification of the percentage of MTR-stained paternal mitochondrion enclosed or partially enclosed by the LGG-1 autophagosome (D to G). Three categories are scored: MTR-stained paternal mitochondrion fully encapsulated (Enclosed), partially encapsulated (Partially enclosed), and not encapsulated (Isolated) by the LGG-1 autophagosome. n indicates the number of mitochondria scored. (This whole figure is contributed by me)

2.2.10 Delayed removal of paternal mitochondria increases embryonic lethality.

We last examined the physiological consequence of delayed removal of paternal mitochondria to the proper development of animals. It has been suggested that the high rate of oxidative phosphorylation to generate energy necessary for successful fertilization of an oocyte among millions of competing spermatozoa leads to increased oxidative damage, and thus, a higher rate of mutations in paternal mtDNA (*110, 129, 130*). Failure to remove paternal mitochondria carrying mutated mtDNA may result in incompatibility with maternal mitochondria and the nuclear genome and adversely affect the fitness of the animals (*96, 130, 131*). To test this hypothesis, we first took advantage of the *uaDf5* deletion, which removes 4 of the 12 mitochondrial respiratory chain subunits encoded by mtDNA (*117*), to determine if delayed removal of mutant paternal mitochondria affects normal embryo development. Comparison of N2 and *uaDf5*/+ embryos reveals a 23-fold increase in embryonic lethality from 0.4% to 9.4% (Fig. 2.9A, assays 1 and 3), suggesting that the heteroplasmic presence of the mutant mtDNA compromises embryonic development. When *uaDf5/+* males were mated with N2 hermaphrodites, cross-fertilized embryos displayed a lethality rate of 0.9% (Fig. 2.9A, assay 5), which is comparable to that (0.8%) seen in cross-fertilized embryos between N2 males and hermaphrodites (Fig. 2.9A, assay 4). By contrast, embryos derived from mating between *cps-6(tm3222); uaD5f/+* males and *cps-6(tm3222)* hermaphrodites experienced a lethality rate of

5.9%, an 8.4-fold increase over that (0.7%) of embryos from mating between *cps-6(tm3222)* males and *cps-6(tm3222)* hermaphrodites (Fig. 2.9A, assays 6 and 7). These results support the notion that inefficient clearance of mutant paternal mitochondria, even in a heteroplasmic mixture with healthy maternal mitochondria, can significantly compromise embryo development and organismal fitness.

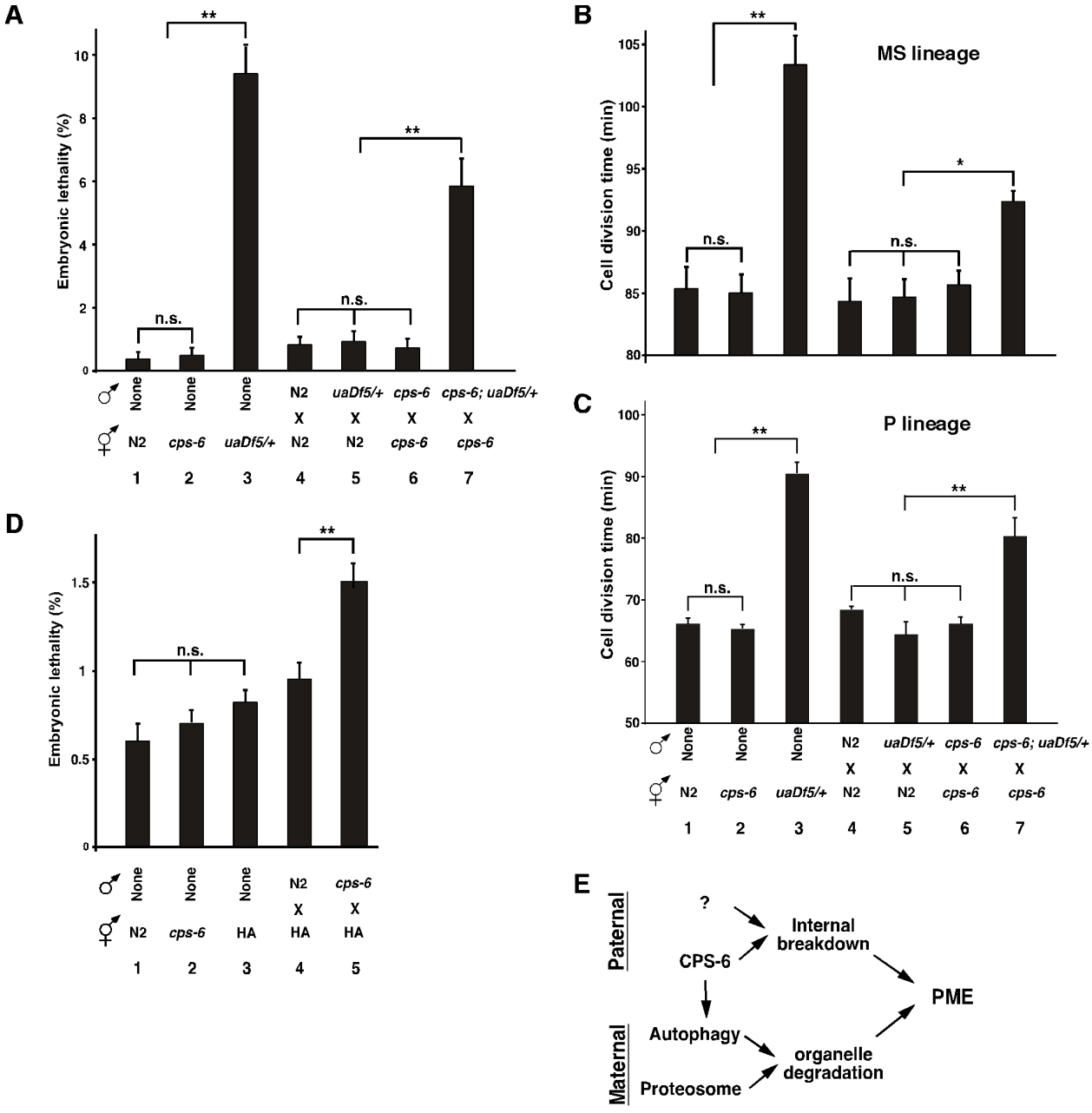

Fig. 2. 9. Delayed removal of paternal mitochondria increases embryonic lethality and prolongs cell division during embryogenesis. (**A** to **C**) The percentage of embryonic lethality (A), the duration of four cell divisions in the MS cell lineage from the MS cell to the MS.aaaa cell (B), and the duration of three cell divisions in the P cell lineage from the P1 cell to the P4 cell (C) were scored in the following embryos: self-fertilized N2, *cps-6(tm3222)*, and *uaDf5/+* embryos, respectively (**1-3**), cross-fertilized embryos from mating of *smIs42* males with N2 hermaphrodites (**4**), *smIs42; uaDf5/+* males with N2 hermaphrodites (**5**), *cps-6(tm3222); smIs42* males with *cps-6(tm3222)* hermaphrodites (**6**), and *cps-6(tm3222)*; *smIs42; uaDf5/+* males with *cps-6(tm3222)* hermaphrodites (**7**). Males were also stained with MTR to assist identification of zygotes (B and C). **(D**) The percentage of embryonic lethality was scored in the following *C. elegans* embryos: self-fertilized N2 Bristol, *cps-6(tm3222)* Bristol, and wild-type Hawaii (HA) embryos, respectively (**1-3**), cross-fertilized embryos from mating of *smIs42* Bristol males with wild-type Hawaii hermaphrodites (**4**) or *cps-6(tm3222); smIs42* Bristol males with wild-type Hawaii hermaphrodites (**5**). Over 1000 embryos from each mating experiment were scored in the embryonic lethality assays performed at 25°C (A and D). Three embryos each were followed in the cell division assays performed at 20°C (B and C). Error bars indicate SEM. The significance of differences between different experiments was determined by unpaired Student's *t*-test. ** $P < 0.001$. * $P < 0.05$. "n.s." indicates no significant difference. (**E**) Both paternal and maternal pathways contribute to PME. On the paternal side, CPS-6 and an unknown factor or mechanism promote internal breakdown of paternal mitochondria following fertilization. On the maternal side, the autophagy and proteasome pathways promote degradation and clearance of paternal mitochondria. Interestingly, loss of paternal CPS-6 impairs recruitment of autophagosomes to paternal mitochondria, indicating that paternal and maternal pathways interact and act cooperatively to promote PME. (this figure is 100% contributed by Dr. Qinghua Zhou, it is needed to be included for the purpose of coherence).

Given that mitochondria are the major energy-generating organelle and cell division is an energy-driven process, we examined if delayed removal of *uaDf5* paternal mitochondria affects the rate of cell division during embryogenesis using the invariant cell lineage in *C. elegans*. During normal embryogenesis, the MS.aaaa cell arises following 4 cell divisions of the mesodermal (MS) precursor cell and its anterior daughter cells (Fig. 2.10, A to D) (*132*). In N2 and *cps-6(tm3222)* embryos, this process occurs in about 85 minutes (Fig. 2.9B, assays 1 and 2). In *uaDf5/+* embryos, this series of cell divisions was prolonged (103 minutes; Fig. 2.9B, assay 3), indicating that the presence of mutant mitochondria interferes with proper cell division. While cross-fertilized embryos between N2 males and hermaphrodites or between *cps-6(tm3222)* males and hermaphrodites showed normal MS to MS.aaaa durations (84-86 minutes; Fig. 2.9B, assays 4 and 6), the average duration of MS to MS.aaaa (92 minutes) in cross-fertilized embryos between *cps-6(tm3222); uaDf5/+* males and *cps-6(tm3222)* hermaphrodites

was significantly longer than that in cross-fertilized embryos between *uaDf5/+* males and N2 hermaphrodites (85 minutes; Fig. 2.9B, assays 5 and 7). Similar results were obtained with another cell lineage, the P cell lineage, in the same assay (Fig. 2.9C; Fig. 2.10, A and D). Therefore, both cell division rates and viability of embryos are compromised by delayed removal of mutant paternal mitochondria. Since *uaDf5* is used to simulate accumulation of harmful mutations in mtDNA over multiple generations or a sporadic mutation that inactivates a crucial gene in mtDNA, these findings provide the proof-of-concept evidence that impaired clearance of mutated paternal mitochondria can lead to decreased fitness at the cellular and organismal levels and presents an evolutionary disadvantage.

We last examined the consequence of delayed removal of wild-type paternal mitochondria. To interrogate this issue, we mated two different wild-type *C. elegans* strains, the Bristol strain (N2) and the Hawaii strain (HA), with each other. As in cross-fertilized N2 embryos from mating of N2 males and hermaphrodites (Fig. 2.4A), the Bristol or Hawaii paternal mitochondria are rapidly cleared by the 64-cell stage in cross-fertilized Hawaii embryos from mating of N2 Bristol males with wild-type Hawaii hermaphrodites or from mating of wild-type Hawaii males and hermaphrodites (Fig. 2.7D, mating 1-3). Likewise, loss of paternal CPS-6 significantly delayed elimination of Bristol paternal mitochondria in cross-fertilized Hawaii embryos or cross-fertilized N2 Bristol embryos (Fig. 2.7D, mating 4, 5), when *cps-6(tm3222)* Bristol males were mated with wild-type Hawaii hermaphrodites or N2 Bristol hermaphrodites. Although N2 Bristol, *cps-6(tm3222)* Bristol, and wild-type Hawaii hermaphrodites showed comparable levels of embryonic lethality (Fig. 2.9D, assays 1-3), delayed removal of *cps-6(tm3222)* Bristol paternal mitochondria in wild-type Hawaii embryos derived from mating of wild-type Hawaii hermaphrodites with *cps-6(tm3222)* Bristol males resulted in a significantly higher percentage of embryonic lethality than that observed in wild-type Hawaii embryos from mating of N2 Bristol males with wild-type Hawaii hermaphrodites (Fig. 2.9D, assays 4, 5 and

Fig. 2.7D, mating 2, 4). These results indicate that delayed clearance of wild-type paternal mitochondria also compromises the development of the animals and that transmission of paternal mitochondria among different wild-type variants in the same species is evolutionarily disadvantageous.

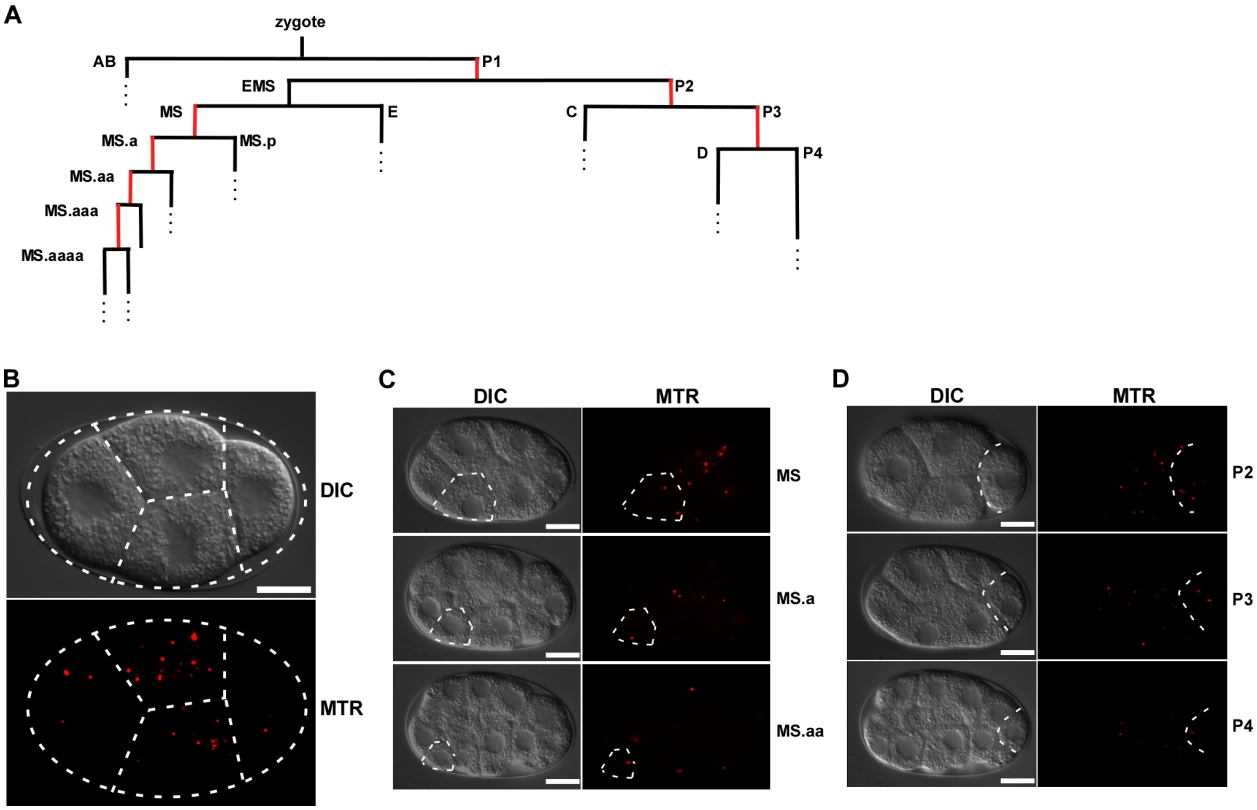

Fig. 2. 10. Persistence of *uaDf5* paternal mitochondria in the MS and the P cell lineage of embryos. (**A**) Partial lineage of *C. elegans* embryos. The horizontal axes represent the direction of cell division. The anterior daughter cell (.a) is shown at the left and the posterior daughter cell (.p) is shown at the right. The MS to MS.aaaa and the P1 to P4 cell divisions are highlighted in red. (**B**) Representative DIC and MTR images of a 4-cell stage embryo derived from mating of MTR-stained *cps-6(tm3222)*; *uaDf5/+* males with unstained *cps-6(tm3222)* hermaphrodites. MTR-stained paternal mitochondria were observed in all four blastomeres. (**C** and **D**) DIC and MTR images of a cross-fertilized embryo from mating of MTR-stained *cps-6(tm3222)*; *uaDf5/+* males with unstained *cps-6(tm3222)* hermaphrodites. MTR-stained paternal mitochondria were observed in three descendants of the MS lineage (C) and three descendants of the P lineage (D) indicated by the white dash lines. Scale bars represent 10 μm.

2.3 Discussion

One of the long-standing puzzles in developmental biology is that mitochondria are inherited maternally in most eukaryotes (*109-111*). Why and how paternal mitochondria are selectively targeted for elimination in embryos has been a major unanswered question. In this study, using high-resolution EM tomography and fluorescent microscopy, we examine the fate and ultrastructural changes of paternal mitochondria before and after fertilization. We find that upon entry into the oocyte paternal mitochondria rapidly lose their inner membrane integrity, are depolarized, and disintegrate into empty ghosts. This series of internal damages and depolarization mark paternal mitochondria specifically for autophagy degradation, as damaged and depolarized mitochondria are targeted for mitophagy (*133-135*). Using a candidate RNAi screen on nuclear genes encoding mitochondrial proteins, we identify the mitochondrial endonuclease CPS-6 as a resident paternal suicide factor that mediates self-degradation of paternal mitochondria. Our immuno-EM analysis reveals that CPS-6, normally localizing in the mitochondrial intermembrane space, abnormally moves into the mitochondrial matrix right after fertilization to degrade mtDNA, probably caused by the initial damage of mitochondria. Because *C. elegans* mtDNA encodes 12 mitochondrial proteins, two ribosomal RNAs, and 22 tRNAs, which are essential for the normal functions and maintenance of mitochondria (*136*), the degradation of mtDNA by relocalized CPS-6 is detrimental to mitochondria and accelerates rapid internal breakdown of paternal mitochondria, which in turn triggers PME by the autophagy and proteasomal machineries (Fig. 2.9E). Consistent with this model, loss of paternal *cps-6* significantly delays inner membrane breakdown of paternal mitochondria and their subsequent enclosure and degradation by the autophagy machinery. These findings also provide a simple mechanism by which paternal mitochondria are distinguished from maternal mitochondria and selectively cleared.

The CPS-6 endonuclease was first identified for its function in nuclear DNA degradation during apoptosis (*120, 121*). This study reveals a new, self-destructive role of CPS-6 in degradation of paternal mtDNA and rapid clearance of paternal mitochondria during *C. elegans* embryo development. The endonuclease activity of CPS-6 is required for both processes to degrade mitochondrial and nuclear DNA, respectively, but the two events proceed through different mechanisms. Localization of CPS-6 in paternal mitochondria is required for PME, which ensures healthy development of embryos. By contrast, CPS-6 is released from mitochondria during apoptosis and translocates to the nucleus where it promotes chromosomal DNA degradation and cellular demise (*120, 121*). These findings, in combination with the recent observations that EndoG, the CPS-6 homologue, is important for mtDNA synthesis and mitochondrial maintenance in human cardiomyocytes (*137*) and is involved in degradation of mtDNA during *Drosophila* spermatogenesis before fertilization (*138*), highlight the complex but critical roles of EndoG/CPS-6 in different cellular and developmental contexts.

PME is a developmental and reproductive process highly conserved in diverse species (*109-111, 118, 119, 139*). Why would nature select for maternal inheritance of mitochondria? It has been reported that paternal mtDNA has a higher frequency of mutations, probably due to elevated levels of oxidative phosphorylation and increased production of reactive oxygen species during the fertilization process (*110, 129, 130*). Paternal mitochondria carrying mutated mtDNA may have reduced efficiency of oxidative phosphorylation, compete with maternal mitochondria for cellular resources, lead to genetic instability, and generate incompatibility in cellular signaling between the mitochondrial and the nuclear genomes, the last of which has been documented in heteroplasmic mice carrying an admixture of two normal but different mouse mtDNAs (*131, 140, 141*). We find that delayed removal of *uaDf5* mutant paternal mitochondria caused by loss of CPS-6 significantly slows down cell divisions and increases the lethality rate in developing embryos. More importantly, delayed removal of wild-type Bristol

paternal mitochondria also significantly increases lethality in embryos of another *C. elegans* wild-type variant, the Hawaii strain. These results provide important supporting evidence that persistence of paternal mitochondria compromises embryo development and organismal fitness. This presents an evolutionary disadvantage and could provide the impetus for maternal inheritance of mitochondria.

Despite major differences between PME and apoptosis, these two critical cellular processes share interesting similarities. First, both processes proceed through a suicide mechanism. In apoptotic cells, caspases and nucleases are activated to promote self-destruction, while in paternal mitochondria the CPS-6 nuclease is relocalized after fertilization to degrade mtDNA. Second, paternal mitochondria and apoptotic cells both undergo dramatic internal ultrastructural changes and damages that distinguish them from maternal mitochondria and normal cells, respectively, and that trigger and accelerate the clearance process. Third, failure to clear paternal mitochondria or apoptotic cells compromises organismal fitness. Given the symbiotic relationship of mitochondria with the cell, apoptosis and PME, the two self-destruction processes, likely employ additional shared components and strategies.

2.4 Materials and methods

2.4.1 Identification of candidate *C. elegans* genes that encode mitochondrial proteins

To identify candidate *C. elegans* genes that encode proteins residing in mitochondria, we took advantage of the comprehensive mitochondrial compendium of 1098 genes identified from 14 mouse tissues (*142*). We blasted the *C. elegans* genome to identify orthologs of these 1098 mitochondrial proteins. Excluding those genes that are redundant or genes whose RNAi treatment results in embryonic lethality, we identified 217 candidate genes that encode mitochondrial proteins in *C. elegans* for the RNAi screen (table 2.1, Appendix).

2.4.2 RNAi screen

To identify mitochondrial proteins involved in PME, we performed RNAi screen on 217 candidate genes predicted to encode mitochondrial proteins in *C. elegans,* using a sensitive nested PCR assay to detect the presence of paternal *uaDf5* mtDNA (Fig. 2.2A). A bacterial feeding protocol of RNAi was used to treat plates containing *uaDf5/+* males and *fem-3(e1996) dpy-20(e1282)* animals, which are fertile females lacking sperm and thus cannot self-fertilize (*143*). Cross progeny at late embryonic stages or early larval stages were subject to the PCR screen to search for the presence of *uaDf5* paternal mtDNA. Each RNAi experiment was carried out in duplicate at room temperature. The RNAi experiments that produced single positive or double positive results (presence of *uaDf5* mtDNA) were retested in duplicate, and sometimes, in multiple (4 to 8) replication experiments. RNAi treatment of one gene, C41D11.8 (*cps-6*), was found to be positive in multiple retests and was analyzed further.

2.4.3 Strains

C. elegans strains were maintained at 20°C using standard methods (*144*). The alleles used for this study: LGI, *cps-6 (tm3222);* LGII, *lgg-1(bp500), rad-23(tm2595);* LGIV, *fem-*

3(e1996), *dpy-20(e1282), him-8(e1489);* mtDNA, *uaDf5* (*117*). *smIs42* is an integrated transgene generated by gamma irradiation of animals carrying an extrachromosomal array containing $P_{sur\text{-}5}$*sur-5::gfp*. It was backcrossed four times with N2 animals before being used in this study.

2.4.4 Transgenic animals

Complex transgenic arrays were generated as previously described to promote germline expression of the transgenes (*145*). Briefly, *cps-6(tm3222); uaDf5/+* worms were injected with 10 ng/µL of $P_{sur\text{-}5}$*sur-5::gfp* (injection marker), 2.5 ng/µL of $P_{dpy\text{-}30}$CPS-6 (wild-type, **Δ**N, or H148A), and 500 ng/µL Sca I-digested N2 genomic DNA.

2.4.5 MitoTracker Red (MTR), SYTO 11, and TMRE staining

1 mM MTR in dimethyl sulfoxide (DMSO) was diluted in M9 buffer (42.3 mM Na_2HPO_4, 22 mM KH_2PO_4, 8.6 mM NaCl, 18.7 mM NH4Cl) to a final concentration of 50 μM before mixing with *E. coli* OP50 to feed *C. elegans* animals. L4 larval stage males were fed with the MTR/bacteria mixture for 12 hours and then cleaned up through three rounds of "bacterial shower", in which they were transferred to a fresh plate with unstained OP50 for 15 minutes each to remove MTR from their exterior. Subsequently, MTR-stained males were mated with unstained young adult hermaphrodites for 8 hours before the mated hermaphrodites were dissected to obtain cross-fertilized MTR-stained oocytes. For SYTO11 and TMRE staining, the same protocol was used. The final concentrations of SYTO11 and TMRE used were 10 μM and 50 μM, respectively.

2.4.6 Fluorescent and time-lapse microscopy

Fluorescent and time-lapse microscopy was performed as described previously (*146*). Briefly, mated hermaphrodites as described above were dissected and embryos were released

onto an agarose pad. A coverslip was then applied on the embryos and egg salt buffer [118 mM NaCl, 48 mM KCl, 2 mM $CaCl_2$, 2 mM $MgCl_2$, and 5 mM HEPES (pH 7.5)] was pipetted into the empty space between the coverslip and the slide. The sample was sealed with a hot mixture of petrol gel and bees wax. Images were captured from the top to the bottom of the embryo using a Zeiss Axioplan 2 microscope equipped with a Cohu CCD camera and SlideBook 5 software (Intelligent Imaging Innovations, Inc.). Z-stacks were then deconvolved and projected into one plane to depict all MTR-stained mitochondria from an embryo in a single image. The duration from the MS cell to the MS.aaaa cell or from the P1 cell to the P4 cell was determined as described previously (*146*).

2.4.7 Quantification of MTR-stained paternal mitochondrial clusters in fertilized oocytes

The number of MTR fluorescent dots was scored from deconvolved images of fertilized oocytes or embryos derived from mating of MTR-stained males with unstained hermaphrodites. For each genotype, 20 cross-fertilized embryos were scored.

2.4.8 PCR analysis

Single or multiple cross-fertilized embryos or larvae at various developmental stages were dissected from mated hermaphrodites or collected from the mating plates and analyzed by PCR. The primer pairs used to detect the *uaDf5* deletion are: P1, 5' GATTAGCACAAGCTTTATTGGATGG 3' and P2, 5' AAGATCTTAACATTCCGGCTGAGGC 3'; P1', 5' TGGTATAATTGGGGCCATCCGTGC 3' and P2', 5' AGGGTCTTCTACAGTGCATTGACC 3'.

2.4.9 Electron microscopy and electron tomography

Mated *C. elegans* hermaprodites were processed by high-pressure freezing, freeze-substitution, and embedding in epoxy resin as described previously (*147*). To prepare samples

for immunogold labeling, worms were freeze-substituted in anhydrous acetone containing 0.1% UA and 0.25% glutaraldehyde and embedded in LRwhite resin. Sectioning, staining, immunogold labeling, and EM imaging were performed according to a previous protocol (*148*), with a Spirit electron microscope (FEI, Hillsboro, OR, USA). 15 nm gold particles are conjugated to a secondary antibody against rabbit immunoglobulin G. Electron tomography analysis was carried out as described previously (*149*). In brief, 250 nm thick sections were collected and the sections were coated with fiducial particles. Tilting series images from 2 orthogonal axes were collected at 15400X from $+60^{o}$ to -60^{o} with 1.5 increments using a TF20 electron microscope (FEI, Hillsboroa, OR, USA). Tomograms were calculated using the Etomo module of the IMOD software package (Boulder Laboratory of 3D Electron Microscopy of the Cell, University of Colorado at Boulder). 3D models were generated with the 3dmod program in the same package.

2.4.10 RNAi experiments

All RNAi experiments were carried out at room temperature using a bacterial feeding protocol (*145*) and RNAi bacterial clones from a *C. elegans* RNAi library (constructed by the Ahringer laboratory). For *cps-6*(RNAi) experiments, animals were treated with RNAi for two generations before their progeny were examined for defects in apoptosis and PME.

2.4.11 Embryonic lethality assays

The assays were carried out at 25°C. For self-fertilized strains, late L4 larvae were aged for 12 hours and then transferred to fresh plates to lay eggs for 6 hours before they were removed. The total number of embryos in the plates was then scored. After 24 hours, embryos that did not hatch were scored as dead embryos. Embryonic lethality rate was calculated as the number of dead embryos divided by the total number of embryos. For cross-fertilized strains,

late L4 hermaphrodites were mated with young adult *smIs42* males with the indicated genotype for 12 hours and then transferred to fresh plates to lay eggs for 6 hours before they were removed. Embryonic lethality rate was calculated similarly as the number of dead GFP-positive embryos divided by the total number of GFP-positive embryos.

2.4.12 Quantification of paternal mitochondria in dividing embryos

Quantification of paternal mitochondria in dividing embryos was conducted as described previously with minor modifications (*36*). Briefly, the numbers of MTR-stained mitochondrial clusters were scored from deconvolved images of the fertilized egg at different embryonic stages. The number of paternal mitochondrial clusters for each fertilized egg at the 1-cell stage was set artificially at 100. Relative numbers of paternal mitochondrial clusters in other embryonic stages of the same fertilized egg were normalized using the 1-cell stage number. To avoid photobleaching and to achieve maximal quantification accuracy, we followed cell divisions in the fertilized egg by DIC and acquired fluorescent images manually at specific embryonic stages.

2.4.13 Immunofluorescence imaging by widefield fluorescent microscopy and Structured Illumination Microscopy (SIM)

Immunostaining of *C. elegans* embryos was performed as described previously (*150*), using an anti-LGG-1 mouse monoclonal antibody (1:100; provided by Hong Zhang, Institute of Biophysics, Beijing, China). Secondary antibodies used are FITC-conjugated goat anti-mouse antibody (1:100; Jackson ImmunoResearch laboratories, Inc.). Stained embryos were mounted onto the slides with Vectashield Antifade Mounting Medium with DAPI. Widefield fluorescent microscopy images were captured from the top to the bottom of the embryos using a Zeiss Axioplan 2 microscope equipped with a Cohu CCD camera and a SlideBook 5 software

(Intelligent Imaging Innovations, Inc.). Z-stacks were then deconvolved and projected into one plane to depict all MTR-stained mitochondria from an embryo in a single image. SIM imaging is achieved by enlarging the Fouriet Domain of sample images about two fold with Nikon Structured Illumination Microscopy (N-SIM). Stained embryos were imaged with 488 nm and 561 nm channels (100X, oil lens).

2.4.14 Quantification of co-localization or encapsulation of paternal mitochondria by autophagosomes in fertilized oocytes

Using widefield fluorescent microscopy images, the co-localization ratio of paternal mitochondrial clusters with autophagosomes in fertilized oocytes is determined as the number of MTR-stained mitochondrial clusters that are associated with LGG-1 immunofluorescence signals divided by the total number of MTR-stained mitochondrial clusters. Using SIM images, the percentages of three classes of paternal mitochondria are determined: those fully encapsulated by autophagosomes (enclosed), those partially encapsulated by autophagosomes (partially enclosed), and those that are not associated with any autophagosome (isolated).

2.4.15 Constructs.

The *cps-6* expression constructs used in the study were made in previous studies (*120, 122*).

Chapter 3

Parkin mediates paternal mitochondrial elimination and regulates autophagy specificity

Maternal inheritance of mitochondria is conserved in most animals. In *C. elegans*, autophagy is involved in paternal mitochondrial elimination (PME) during early embryogenesis. How paternal mitochondria are selectively targeted by autophagy is poorly understood. We show that PDR-1, a worm Parkin homolog, translocates to paternal mitochondria after fertilization to mediate their specific elimination. Loss of *pdr-1* impairs selective autophagosome formation around paternal mitochondria, leading to autophagosome enclosure of other organelles, including endoplasmic reticulum and maternal mitochondria. Expression in the *pdr-1* mutant of human Parkin and PINK1, both associated with Parkinson's disease (PD), rescues the PME defect. Mutations at conserved residues of Parkin that cause PD impair translocation of PDR-1 to paternal mitochondria and its activity in PME, indicating that the function of Parkin is conserved and that *C. elegans* could be a good animal model for studying PD. Our study reveals an unknown physiological role of Parkin in PME and in determining the specificity of autophagic encapsulation. Our finding also suggests that Parkin deficiency may cause disease by blocking clearance of damaged mitochondria and by promoting indiscriminate removal of other crucial organelles, including healthy mitochondria.

3.1 Background

Parkin and PINK1 are two human genes associated with the Parkinson's disease (PD) and encode an E3 ubiquitin ligase and a mitochondrial Serine/Threonine kinase, respectively *(151-154)*. They appear to act in the same pathway to remove damaged mitochondria and to maintain a healthy mitochondrial pool *(154-157)*. In healthy mitochondria, PINK1 is constitutively imported into the mitochondrial matrix, where it is cleaved by presenilin-associated rhomboid-

like protease (PARL) and further degraded through the N-end rule pathway *(154, 158-162)*. In damaged mitochondria, reduced mitochondrial membrane potential leads to stalled import of PINK1 and its ectopic presence on the surface of mitochondria *(163-166)*. Parkin is then recruited to depolarized mitochondria and activated by PINK1 phosphorylation at its Serine 65 residue and by binding to phosphorylated ubiquitin *(163-172)*. Activated Parkin catalyzes polyubiquitination of mitochondrial substrates, which recruit the autophagy machinery to encapsulate damaged mitochondria, ushering them to lysosomes for degradation *(163, 173-176)*.

3.2 Experimental Results

3.2.1 PDR-1, the *C. elegans* homolog of Parkin, is maternally involved in PME.

C. elegans sperm mitochondria are depolarized and damaged upon entry into the oocyte and are selectively targeted by the autophagy machinery, whereas maternal mitochondria stay untouched *(177)*. Since PDR-1, the *C. elegans* Parkin homolog (Fig. 3.1, A and B), and PINK-1, a worm PINK1 homolog (Fig 3.1, C and D), participate in autophagic degradation of damaged mitochondria in *C. elegans (178)*, we examined if PDR-1 and PINK-1 affect paternal mitochondrial elimination (PME) during *C. elegans* development. Using a polymerase chain reaction (PCR) based method *(34-36)*, we tracked the fate of paternal mitochondrial genomes (mtDNA) in embryos, which is directly tied to the fate of paternal mitochondria. Males heteroplasmic for mitochondria carrying a 3 kb deletion (*uaDf5*) in their mtDNA were mated with wild-type (N2) hermaphrodites (Fig. 3.2, A and B). Single cross-fertilized embryos at different stages were isolated and analyzed by PCR. *uaDf5* paternal mtDNA was detected in embryos before the 64-cell stage, but disappeared from embryos at 64-cell or later stages (Fig. 3.2B) *(36)*. In contrast, when *pdr-1(tm598); uaDf5/+* males, carrying a 697 bp deletion that removes half of the *pdr-1* coding region (Fig. 3.1E), were mated with *pdr-1(tm598)* hermaphrodites, *uaDf5*

paternal mtDNA was detected in later stage embryos, as late as bean-stage embryos with approximately 550 cells (Fig. 3.2C). These results indicate that *pdr-1* is important for efficient removal of paternal mtDNA during embryogenesis.

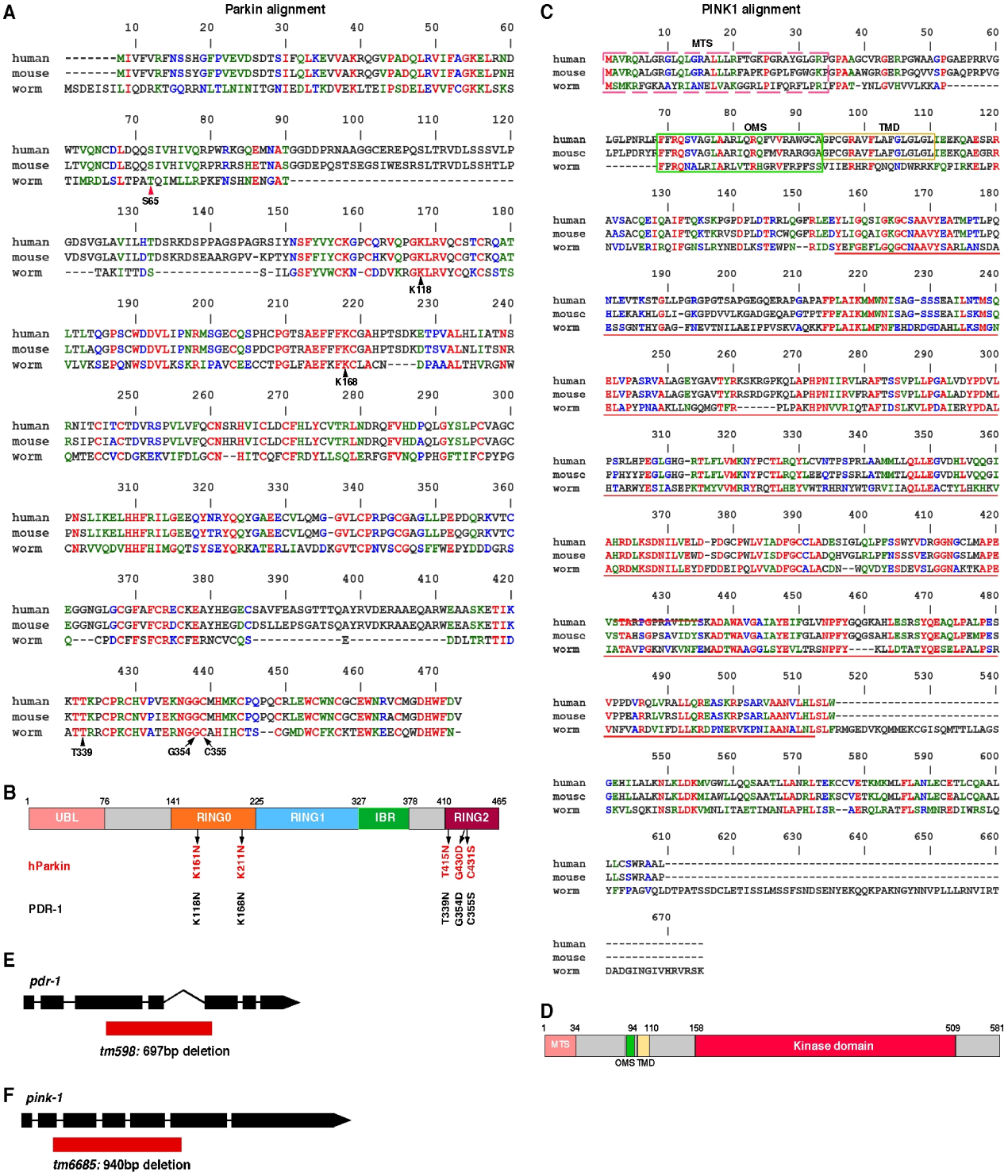

Fig. 3. 1. Comparison of *C. elegans* PDR-1 and PINK-1 proteins with human and mouse Parkin and PINK1 proteins. (**A** and **C**) Sequence alignment of Parkin and PINK1 homologs using the CLUSTALW program, respectively. Residues that are identical are highlighted in red and residues that are similar are in green. The mitochondrial targeting signals (MTS) in PINK1 proteins are indicated with a pink dash box. The putative mitochondrial outer membrane localization signals (OMS) in PINK1 proteins are indicated with a green box. The transmembrane domains (TMD) in human and mouse PINK1 are indicated with a yellow box. The kinase domains (residues 156-509) are indicated with a red line. No TMD has been identified in *C. elegans* PINK-1 using multiple programs predicting transmembrane domains. (**B**) A schematic representation of different domains found in human Parkin. Some Parkinson's disease mutations and their corresponding mutations in PDR-1 analyzed in this study are indicated below the domain structure. (**D**) A schematic representation of different domains found in human PINK1. (**E** and **F**) *C. elegans pdr-1* and *pink-1* gene structures and corresponding deletion mutations. Exons are shown as boxes and introns as lines. The filled red boxes indicate the regions of *pdr-1* and *pink-1* removed by the *tm598* and *tm6685* deletion mutations, respectively.

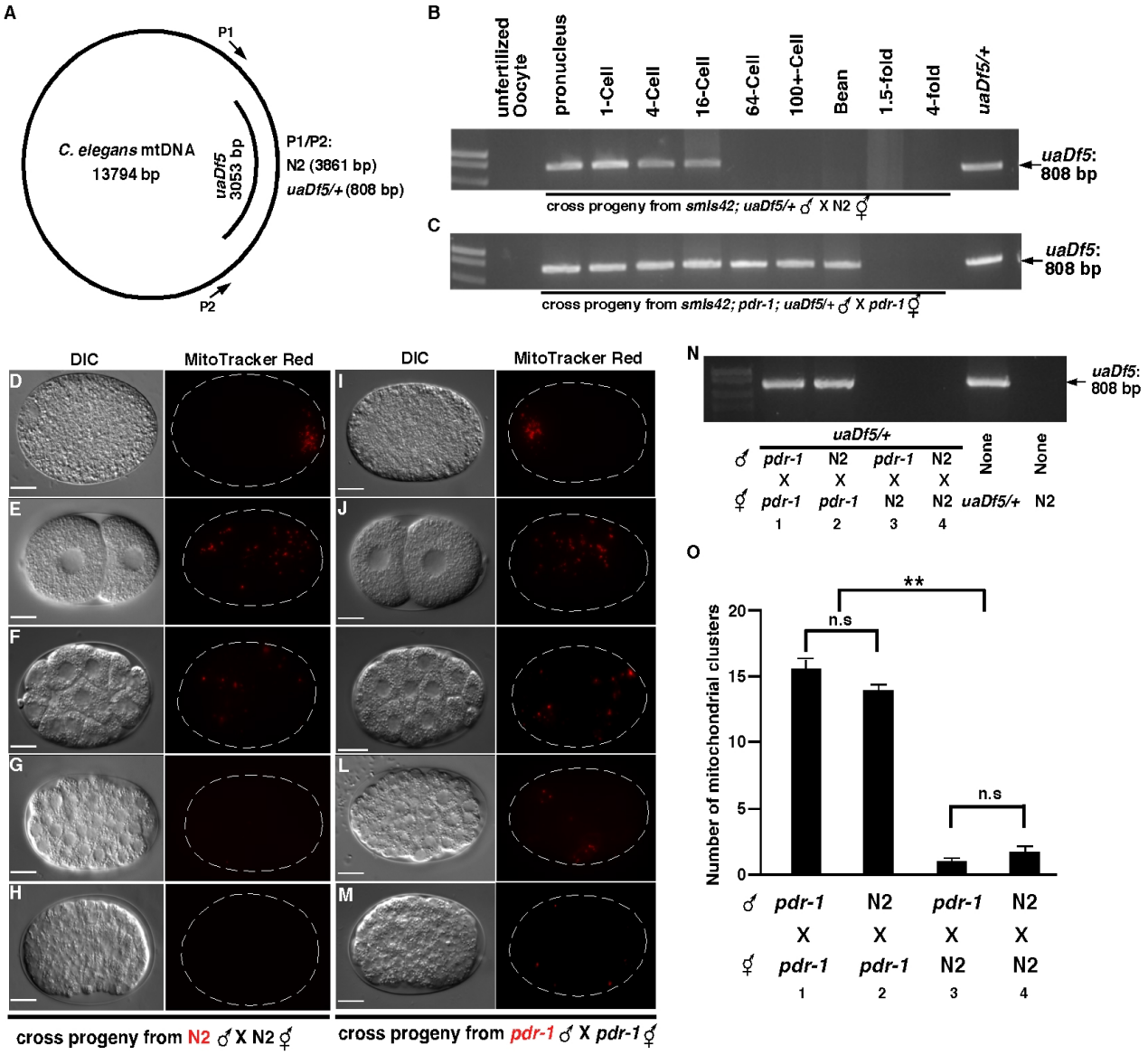

Fig. 3. 2. The *C. elegans* Parkin homolog PDR-1 acts maternally to promote PME. (**A**) A schematic diagram of *C. elegans* mtDNA, the *uaDf5* deletion, primers used in the PCR assays, and the sizes of expected PCR products. (**B** and **C**) MTR-stained males and unstained hermaphrodites of the indicated genotypes were mated. Males also carried *smIs42,* an integrated $P_{sur\text{-}5}$*sur-5::gfp* transgene used to identify cross progeny. A single unfertilized oocyte or a single cross-fertilized embryo (MTR or GFP positive) at the indicated stage was analyzed by PCR. *uaDf-5/+* hermaphrodites are positive controls. (**D** to **M**) Fluorescence microscopy tracking of paternal mitochondria. MTR-stained males and unstained hermaphrodites were mated. Cross-fertilized oocytes were dissected from mated hermaphrodites. Differential interference contrast (DIC) and MTR images of the embryos are shown. Red dots are paternal mitochondrial clusters stained by MTR. The stages of embryos examined are: the zygote (D and I), 2-cell (E and J), 16-cell (F and K), 64-cell (G and L), and comma stage (H and M). Scale bars represent 10 μm. (**N**) Single cross-fertilized embryos at approximately 100-cell stage from the indicated crosses were analyzed by PCR. (**O**) Quantification of MTR-stained paternal mitochondrial clusters in 64-cell stage embryos from the indicated crosses with MTR-stained

males. Data are means ± SEM; *n* = 30 per cross. ** *P*<0.01 (unpaired student's *t*-test). n.s, not significant. *pdr-1(tm598)* was used.

We confirmed this finding using time-lapse fluorescent microscopy, which tracks the physical presence of paternal mitochondria in embryos *(36)*. N2 males prestained by Mitotracker Red (MTR), a mitochondrion-specific dye, were mated with unstained N2 hermaphrodites and the fates of MTR-stained paternal mitochondria were monitored in developing embryos using time-lapse microscopy *(34-36)*. Consistent with the observations from the PCR assays, MTR-stained paternal mitochondria disappeared in N2 embryos at approximately the 64-cell stage (Fig. 3.2, D to H, and Fig. 3.2O, mating 4). In contrast, when MTR-stained *pdr-1(tm598)* males were mated with *pdr-1(tm598)* hermaphrodites, MTR-stained paternal mitochondria persisted significantly longer, to the bean-stage embryos (Fig. 3.2, I to M, and Fig. 3.2O, mating 1). Thus, loss of *pdr-1* causes a significant delay in PME. We similarly analyzed if *C. elegans pink-1* affects PME and found that inactivation of *pink-1* by a deletion mutation (*tm6685*) that removes the first half of the *pink-1* coding region mildly delayed PME (Fig. 3.1F and Fig. 3.3A). Since the PME defect of *pink-1* is significantly weaker than that of *pdr-1*, additional kinases or factors may cooperate with PDR-1 to remove damaged paternal mitochondria in fertilized eggs.

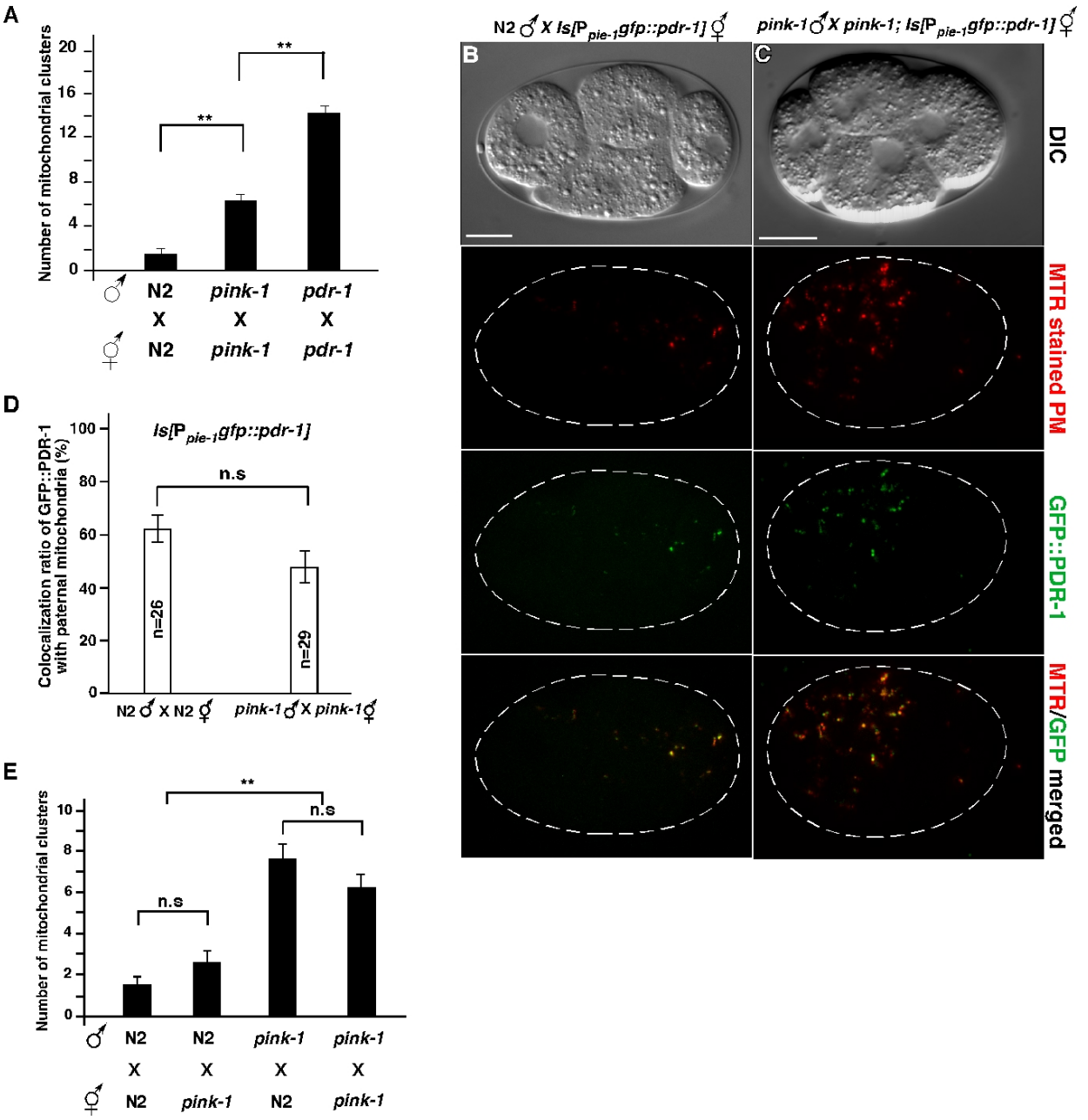

Fig. 3. 3. *C. elegans pink-1* plays a minor paternal role in mediating PME. (**A** and **E**) Quantification of MTR-stained paternal mitochondrial clusters in 64-cell stage embryos from the indicated crosses with MTR-stained males. Means ± SEM; *n*=20 per cross. ** $P < 0.01$ using unpaired Student's *t*-test. *pdr-1* and *pink-1* alleles used are *tm598* and *tm6685,* respectively. (**B** and **C**) GFP::PDR-1 translocation to paternal mitochondria in 4-cell embryos is not affected by loss of *C. elegans* PINK-1. DIC and fluorescence images of 4-cell embryos from the indicated crosses are shown. MTR-stained males were mated with hermaphrodites carrying the integrated $P_{pie\text{-}1}$*gfp::pdr-1* transgene. Scale bars represent 10 μm. (**D**) Quantification of the colocalization ratio of GFP::PDR-1 with paternal mitochondria in 1 to 4-cell stage embryos from the indicated

mating (see Materials and Methods). N2 or *pink-1(tm6685)* males were stained with MTR and mated with unstained N2 or *pink-1(tm6685)* hermaphrodites carrying the integrated P_{pie-1}*gfp::pdr-1* transgene, respectively. Data shown are Means ± SEM. "n.s", no significant difference based on unpaired student's *t*-test.

3.2.2 Translocation of maternal PDR-1 onto paternal mitochondria after fertilization

It has been shown that the normally diffuse Parkin protein translocates to damaged mitochondria in mammalian cells *(163-166)*. This translocation is likely triggered by PINK1 exposure on the surface of damaged mitochondria and leads to autophagosome formation on damaged mitochondria and their selective degradation *(163-166)*. Since paternal mitochondria are damaged after fertilization *(177)*, we examined whether *C. elegans* PDR-1 is recruited to paternal mitochondria in early embryos. To observe PDR-1 localization in *C. elegans*, we generated a low-copy integrated transgene carrying P_{pie-1} *gfp::pdr-1 (179),* which drives the expression of the GFP::PDR-1 fusion in the germline and early embryos under the control of the promoter of the *pie-1* gene *(180)*. This transgene rescues the PME defect in *pdr-1(tm598)* embryos (Fig. 3.4A, assays 1-3), suggesting that GFP::PDR-1 localizes to its functional sites. GFP::PDR-1 was not detected in unfertilized oocytes from P_{pie-1} *gfp::pdr-1* hermaphrodites (Fig. 3.4B), but became visible and was largely colocalized with MTR-stained paternal mitochondria in embryos from mating of P_{pie-1} *gfp::pdr-1* hermaphrodites with MTR-stained N2 males (Fig. 3.4C), indicating translocation and clustering of PDR-1 onto paternal mitochondria. Loss of *pink-1* did not obviously affect colocalization of GFP::PDR-1 with MTR-stained paternal mitochondria (Fig. 3.3, B to D), which is consistent with the weak PME defect of *pink-1*.

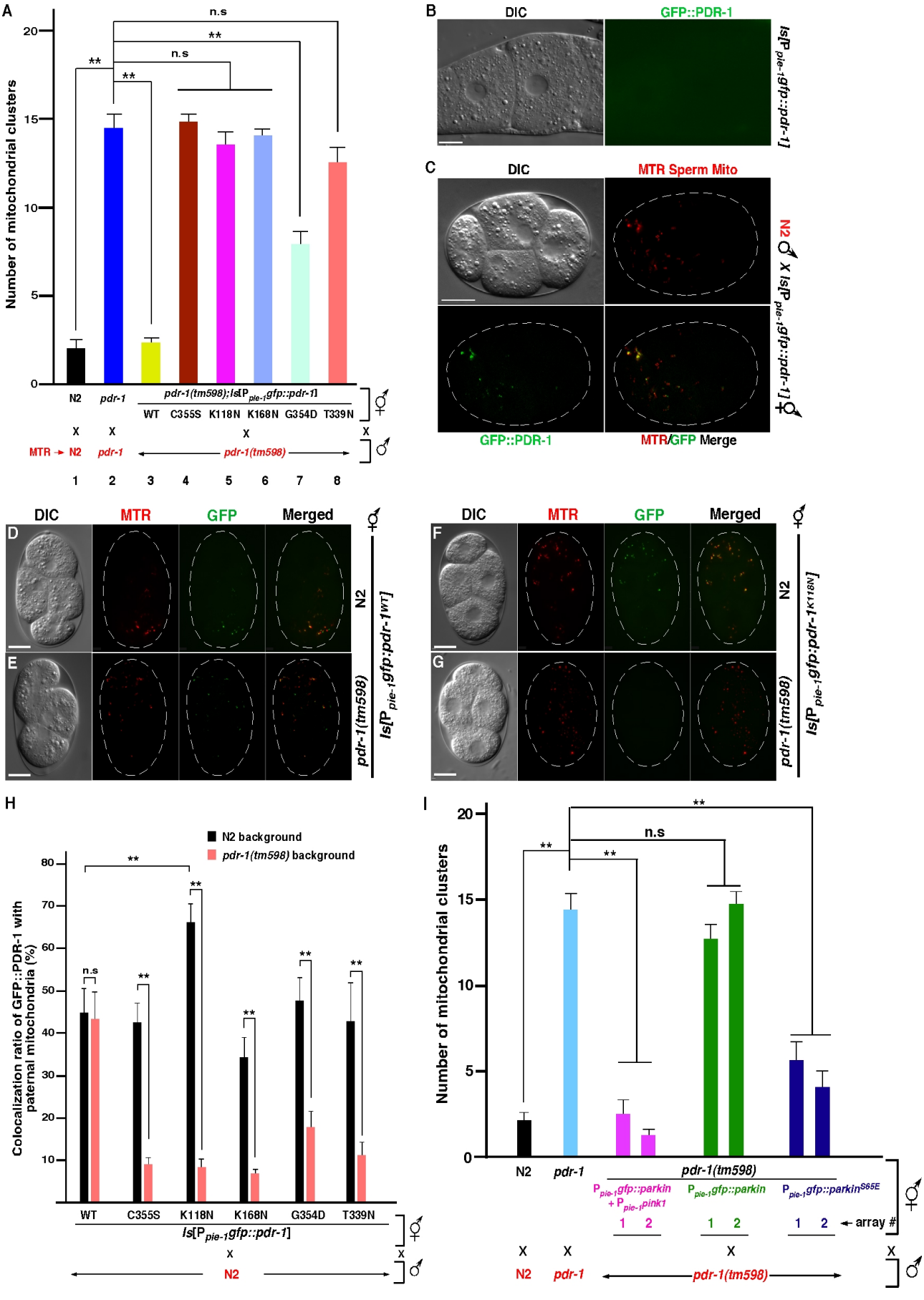
A
Number of mitochondrial clusters
n.s
**
n.s
**
**
N2
pdr-1
pdr-1(tm598);Is[Ppie-1gfp::pdr-1]
WT C355S K118N K168N G354D T339N
MTR → N2
pdr-1
pdr-1(tm598)
1 2 3 4 5 6 7 8
B
DIC
GFP::PDR-1
Is[Ppie-1gfp::pdr-1]
C
DIC
MTR Sperm Mito
N2 ♀ X Is[Ppie-1gfp::pdr-1] ♂
GFP::PDR-1
MTR/GFP Merge
D
DIC MTR GFP Merged
N2 ♀
Is[Ppie-1gfp:pdr-1WT] ♂
E
pdr-1(tm598) ♀
Is[Ppie-1gfp:pdr-1WT] ♂
F
DIC MTR GFP Merged
N2 ♀
Is[Ppie-1gfp:pdr-1K118N] ♂
G
pdr-1(tm598) ♀
Is[Ppie-1gfp:pdr-1K118N] ♂
H
N2 background
pdr-1(tm598) background
Colocalization ratio of GFP::PDR-1 with paternal mitochondria (%)
n.s
**
WT C355S K118N K168N G354D T339N
Is[Ppie-1gfp::pdr-1]
x
N2
I
Number of mitochondrial clusters
**
n.s
**
**
N2
pdr-1
pdr-1(tm598)
Ppie-1gfp::parkin + Ppie-1pink1
Ppie-1gfp::parkin
Ppie-1gfp::parkinS65E
1 2 1 2 1 2 ← array #
N2
pdr-1
pdr-1(tm598)

Fig. 3. 4. Characterization of the activity and localization of PDR-1 proteins with Parkinson's disease mutations during PME. (**A** and **I**) Quantification of MTR-stained paternal mitochondrial clusters in 64-cell transgenic embryos derived from mating of MTR-stained *pdr-1(tm598)* males with *pdr-1(tm598)* hermaphrodite carrying the integrated transgenes as indicated (A) or two independent complex transgenic arrays #1 and #2 (I). N2 and *pdr-1(tm598)* cross-fertilized embryos are positive and negative controls. Data shown are means ± SEM; n = 15 per cross. ** $P < 0.01$ (unpaired student's t-test). (**B** and **C**) GFP::PDR-1 is not visible in unfertilized oocytes (B) and translocates to and clusters on paternal mitochondria after fertilization (C). DIC and fluorescence images of an unfertilized oocyte (B) or a cross-fertilized embryo (C) derived from mating of N2 hermaphrodites carrying a low-copy integrated $P_{pie\text{-}1}$*gfp::pdr-1* transgene with MTR-stained N2 males. Scale bars represent 10 μm. (**D** to **G**) Localization patterns of GFP::PDR-1 and GFP::PDR-1^{K118N} in embryos with the indicated maternal background. MTR-stained N2 males were mated with N2 or *pdr-1(tm598)* hermaphrodites carrying the indicated transgene. Scale bars represent 10 μm. (**H**) Quantification of the colocalization ratio of GFP::PDR-1 (wild-type and mutant) with MTR-stained paternal mitochondria in embryos with an N2 (black bar) or *pdr-1(tm598)* (red bar) maternal background. N2 males were stained with MTR. Data shown are means ± SEM; n = 15 per cross (except n = 13 for T339N black bar). ** $P < 0.01$ (unpaired student's t-test). n.s, not significant.

Because maternally expressed PDR-1 is recruited to paternal mitochondria after fertilization, we examined if maternal *pdr-1* is sufficient to mediate PME and found that loss of only maternal *pdr-1* recapitulated the PME defect observed in cross progenies from mating of *pdr-1(tm598)* males and hermaphrodites (Fig. 3.2, N and O, matings 1 and 2). Loss of paternal *pdr-1* alone did not affect PME (Fig 3.2, N and O, mating 3), confirming that *pdr-1* is required maternally to promote PME. In contrast, *pink-1* is required paternally to mediate PME (Fig. 3.3E), suggesting that PINK-1 either acts in paternal mitochondria or is contributed paternally to promote PME.

3.2.3 Loss of PDR-1 impairs the selectivity and closure of autophagosome.

We next examined how PDR-1 recruits autophagosomes to paternal mitochondria. Shortly after their entry into the oocyte, paternal mitochondria were surrounded by autophagosomes associated with LGG-1 (Fig. 3.5A) *(34, 35, 177)*, the *C. elegans* homolog of GABARAP or Atg8 *(126)*. In zygotes derived from mating of MTR-stained N2 males with unstained N2 hermaphrodites, 81% of MTR-stained paternal mitochondrial clusters were

colocalized with LGG-1 autophagosomes (Fig. 3.5, A and C). In comparison, in zygotes derived from mating of MTR-stained *pdr-1(tm598)* males with *pdr-1(tm598)* hermaphrodites, colocalization of MTR-stained paternal mitochondria with LGG-1 autophagosomes decreased significantly to 56% (Fig. 3.5, B and C), indicating that loss of *pdr-1* impairs recruitment of autophagosomes to paternal mitochondria. We analyzed this issue further using superresolution structured illumination microscopy (SIM). In zygotes between MTR-stained N2 males and N2 hermaphrodites, the majority (72%) of MTR-stained paternal mitochondria were fully enclosed by LGG-1 autophagosomes (Fig. 3.5, D, E, and H). A low percentage (7% each) of paternal mitochondria either were partially enclosed or had nearby isolation membrane (phagophore) that might initiate extension around paternal mitochondria (initiating phagophore). Only 14% of paternal mitochondria did not associate with phagophores or autophagosomes (isolated). In contrast, in zygotes derived from mating of *pdr-1(tm598)* hermaphrodites with MTR-stained *pdr-1(tm598)* males, the number of paternal mitochondria fully enclosed by autophagosomes declined substantially from 72% to 30% (Fig. 3.5, F to H). Instead, the percentage of paternal mitochondria partially enclosed (25%) or with initiating phagophores (28%) more than tripled (Fig. 3.5, F to H). These results suggest that the phagophores have trouble to extend efficiently around a paternal mitochondrion and to fully enclose it, leading to an increased number of phagophores that fail to close and that end up accommodating other cargos and become less selective.

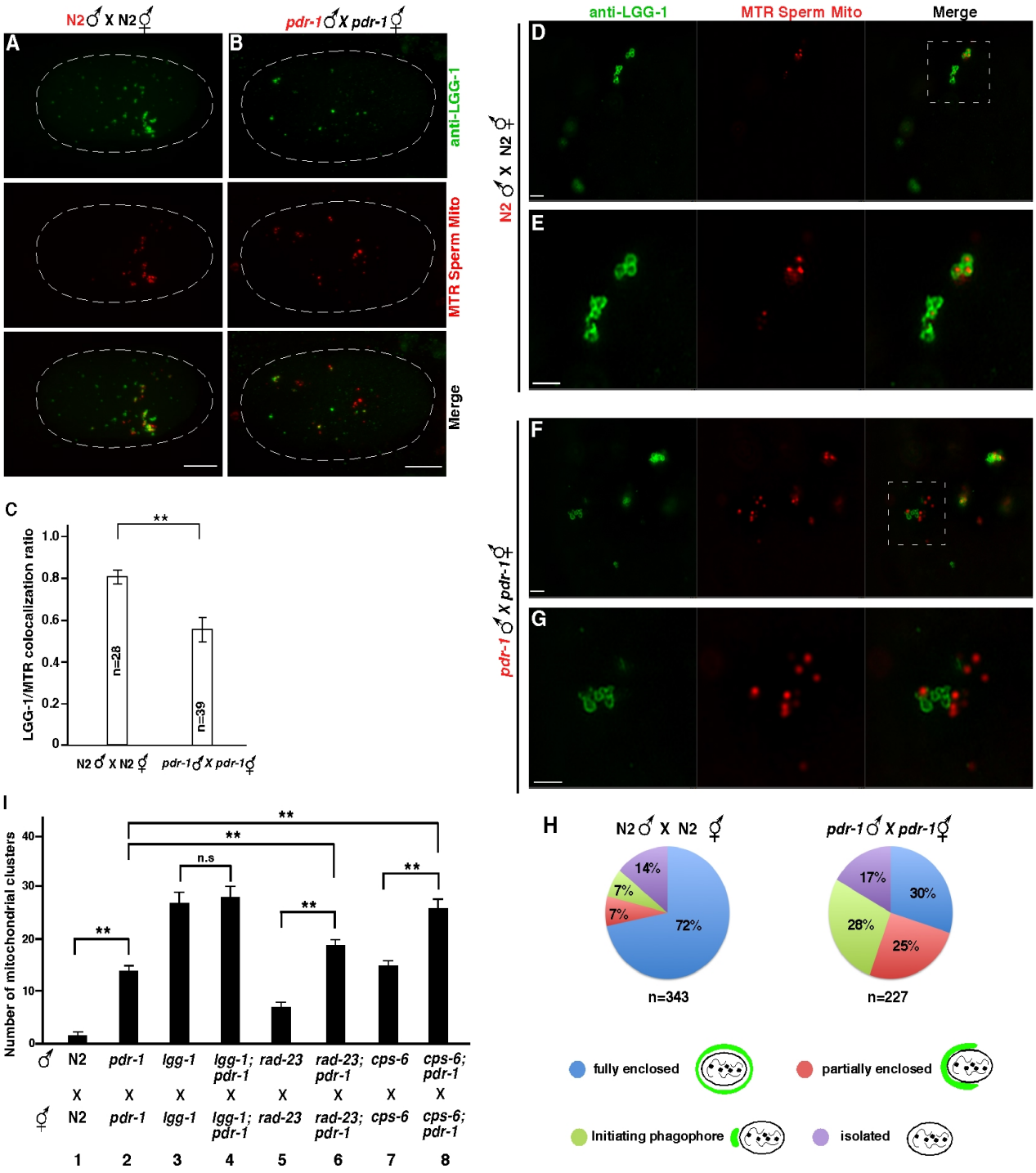

Fig. 3. 5. PDR-1 is important for phagophore extension and encapsulation of paternal mitochondrion and autophagy specificity. (**A** and **B**) Zygotes from the indicated crosses with MTR-stained males were stained with a monoclonal antibody to LGG-1. Images were acquired using a Zeiss Axioplan 2 microscope. Scale bars represent 10 μm. (**C**) Quantification of the colocalization ratio of MTR-stained paternal mitochondrial clusters with LGG-1-stained autophagosomes shown in A and B. error bars are SEM. ** $P < 0.01$ (unpaired Student's *t*-test). (**D** to **G**) Zygotes from the same immunostaining experiments (A and B) were imaged with a

Nikon SIM microscope. Dash rectangles highlight the areas enlarged and shown below (E and G). Scale bars represent 2 μm. (**H**) Quantification of four types of paternal mitochondria, those fully enclosed, partially enclosed, and not enclosed (Isolated) by the LGG-1 autophagosomes and those with a nearby initiating phagophore. (**I**) Genetic analysis of the relationships among *pdr-1*, *lgg-1, rad-23* and *cps-6* in PME. Quantification of MTR-stained paternal mitochondrial clusters in 64-cell embryos derived from the indicated crosses was performed as in Fig. 3.2O. Data are means ± SEM; n = 20 per cross, ** $P < 0.01$ (unpaired student's t-test). *pdr-1*, *lgg-1, rad-23* and *cps-6* alleles used are *tm598, bp500, tm2595,* and *tm3222,* respectively.

3.2.4 PDR-1 act in the autophagy pathway.

Given the role of PDR-1 in recruiting autophagosomes to damaged paternal mitochondria, we examined whether *pdr-1* and *lgg-1* act in the same pathway and found that loss of *pdr-1* did not enhance the PME defect of the *lgg-1* mutant (Fig. 3.5I, matings 1-4). This result suggests that *pdr-1* and *lgg-1* act in the same pathway to promote PME. On the other hand, loss of *pdr-1* resulted in a more severe PME defect when combined with a loss-of-function mutation in *rad-23,* which encodes a ubiquitin receptor in the proteasomal pathway and acts in parallel to the autophagy pathway to promote PME (Fig. 3.5I, matings 2, 5, 6) *(36, 177)*. Inactivation of *pdr-1* also enhanced the PME defect in animals deficient in *cps-6*, which encodes a mitochondrial endonuclease G that mediates paternal mitochondrial self-destruction and acts in parallel to the autophagy pathway *(177)*. Therefore, *pdr-1* appears to act in the autophagy pathway and in parallel to both the proteasomal degradation pathway and the CPS-6 self-destruction pathway to promote PME.

3.2.5 The E3 ubiquitination ligase activity is critical for PDR-1's role in PME.

We tested whether the E3 ubiquitin ligase activity of PDR-1 is important for PME by performing the rescue experiment in *pdr-1(tm598)* animals using the $P_{pie\text{-}1}$ *gfp::pdr-1* transgenes that express PDR-1 or a PDR-1 mutant with a catalytic site mutation, C355S (Fig. 3.1, A and B) *(181)*. Expression of PDR-1 using complex transgenic arrays, which allow gene expression in

early embryos *(180)*, fully rescued the PME defect in the *pdr-1(tm598)* mutant, whereas expression of PDR-1^{C355S} failed to rescue (Fig. 3.6). We also generated a low-copy transgene carrying P_{pie-1} *gfp::pdr-1*^{C355S} inserted at the same chromosomal locus as the wild-type P_{pie-1} *gfp::pdr-1* transgene *(179)* and confirmed that PDR-1^{C355S} failed to rescue the PME defect (Fig. 3.4A, assay 4). These results indicate that the E3 ubiquitin ligase activity of PDR-1 is required for its function in PME.

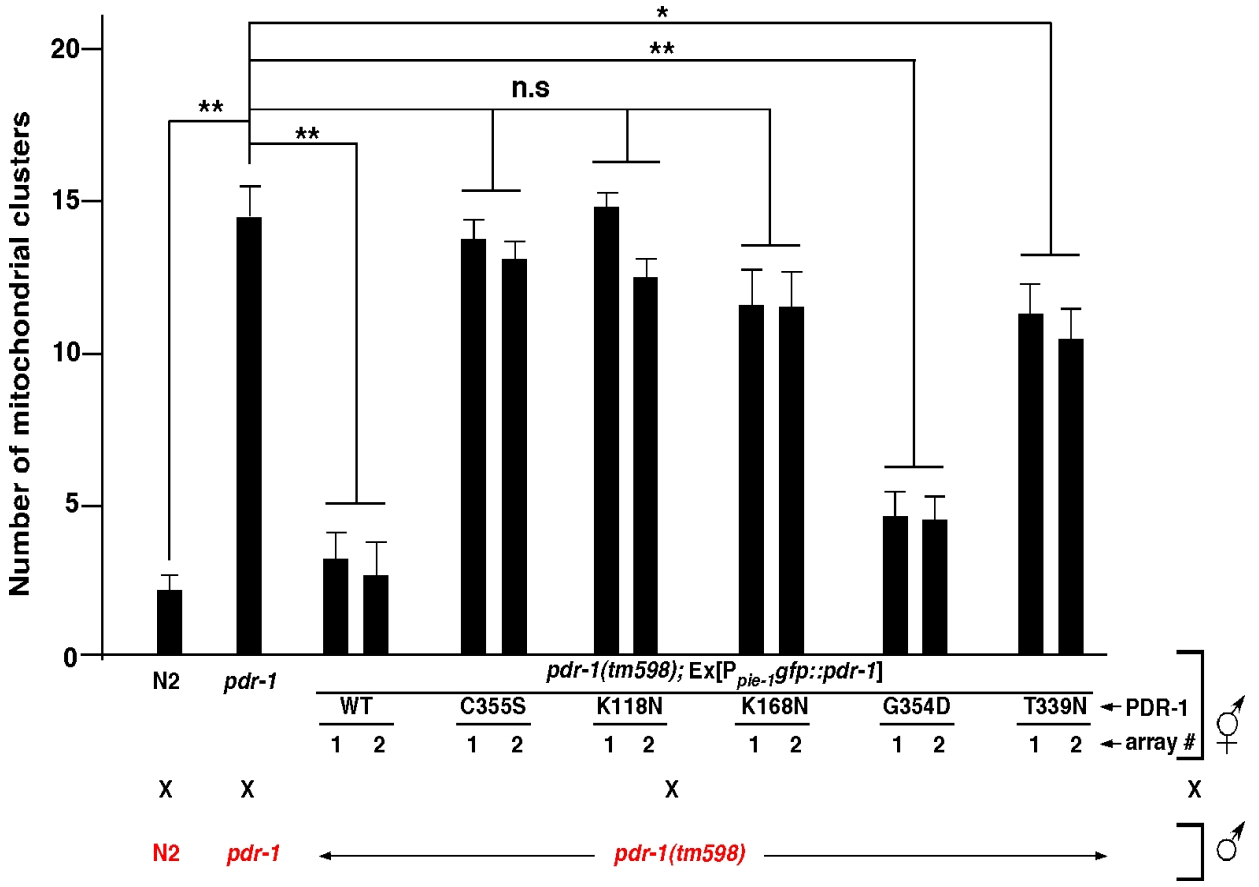

Fig. 3. 6. The ability of different GFP::PDR-1 proteins in rescuing the PME defect of *pdr-1(tm598)* embryos. Quantification of MTR-stained paternal mitochondrial clusters in 64-cell stage embryos from the indicated mating. MTR-stained males of the indicated genotypes were mated with N2 hermaphrodites, *pdr-1(tm598)* hermaphrodites, or *pdr-1(tm598)* hermaphrodite carrying two independent complex transgenic arrays, array #1 and #2, through which the GFP::PDR-1 fusion (wild-type or mutant) is expressed under the control of the *pie-1* promoter in early embryos. Data shown are Means ± SEM; *n*= 15 per cross. ** P<0.01, * P < 0.05, using unpaired student's *t*-test. "n.s", no significant difference.

3.2.6 Conservation of disease related mutations in Parkin

In patients with familial Parkinson's disease, multiple point mutations were identified that impair or compromise the activity of human Parkin *(163, 164, 182)*. We selected four human mutations, K161N, K211N, T415N, and G430D, which alter residues conserved between human Parkin and *C. elegans* PDR-1 (Fig. 3.1, A and B) and were shown to impair recruitment of Parkin to depolarized mitochondria in mammalian cells *(163, 164)*. We similarly generated low-copy P_{pie-1} *gfp::pdr-1* transgenes with four corresponding *C. elegans* mutations (Fig. 3.1B), which are inserted at the same chromosomal locus as the wild-type P_{pie-1} *gfp::pdr-1* transgene *(179)*, and tested their activities in rescuing the PME defect of *pdr-1(tm598)* embryos. PDR-1^{G354D} showed partial rescue of the PME defect, whereas PDR-1^{K118N}, PDR-1^{K168N}, and PDR-1^{T339N} failed to rescue (Fig. 3.4A, assays 5-8). We obtained similar results when expressing these PDR-1 mutants from complex transgenic arrays (Fig. 3.6). These results indicate that conserved residues critical for the activity of human Parkin are also important for the function of *C. elegans* PDR-1 in PME.

We then analyzed if these PD mutations affect recruitment of *C. elegans* PDR-1 to paternal mitochondria using the same low-copy P_{pie-1} *gfp::pdr-1* integrated transgenes. In cross-fertilized embryos derived from mating of MTR-stained N2 males with N2 hermaphrodites carrying these P_{pie-1} *gfp::pdr-1* transgenes, four mutant GFP::PDR-1 fusions (C355S, K168N, G354D, and T339N) translocated to paternal mitochondria like wild-type GFP::PDR-1 (Fig. 3.4, D and H, and Fig. 3.7, A, C, E, and G), with one mutant, GFP::PDR-1^{K118N}, showing increased translocation (Fig. 3.4, F and H). These results indicate that these mutations do not affect PDR-1 stability or association with paternal mitochondria despite inactivating the activity of PDR-1 in PME. On the other hand, in embryos derived from mating of MTR-stained N2 males with *pdr-1(tm598)* hermaphrodites carrying these P_{pie-1} *gfp::pdr-1* transgenes, all five mutant GFP::PDR-1 fusions showed greatly reduced colocalization with paternal mitochondria (Fig. 3.4, G and H,

and Fig. 3.7, B, D, F, and H), whereas wild-type GFP::PDR-1 translocated to paternal mitochondria normally (Fig. 3.4, E and H). These findings together indicate that these five PDR-1 mutants are capable of translocating to paternal mitochondria, but need wild-type PDR-1 to help or prime them for such movement, probably by catalyzing ubiquitination of substrates on paternal mitochondria that recruit PDR-1.

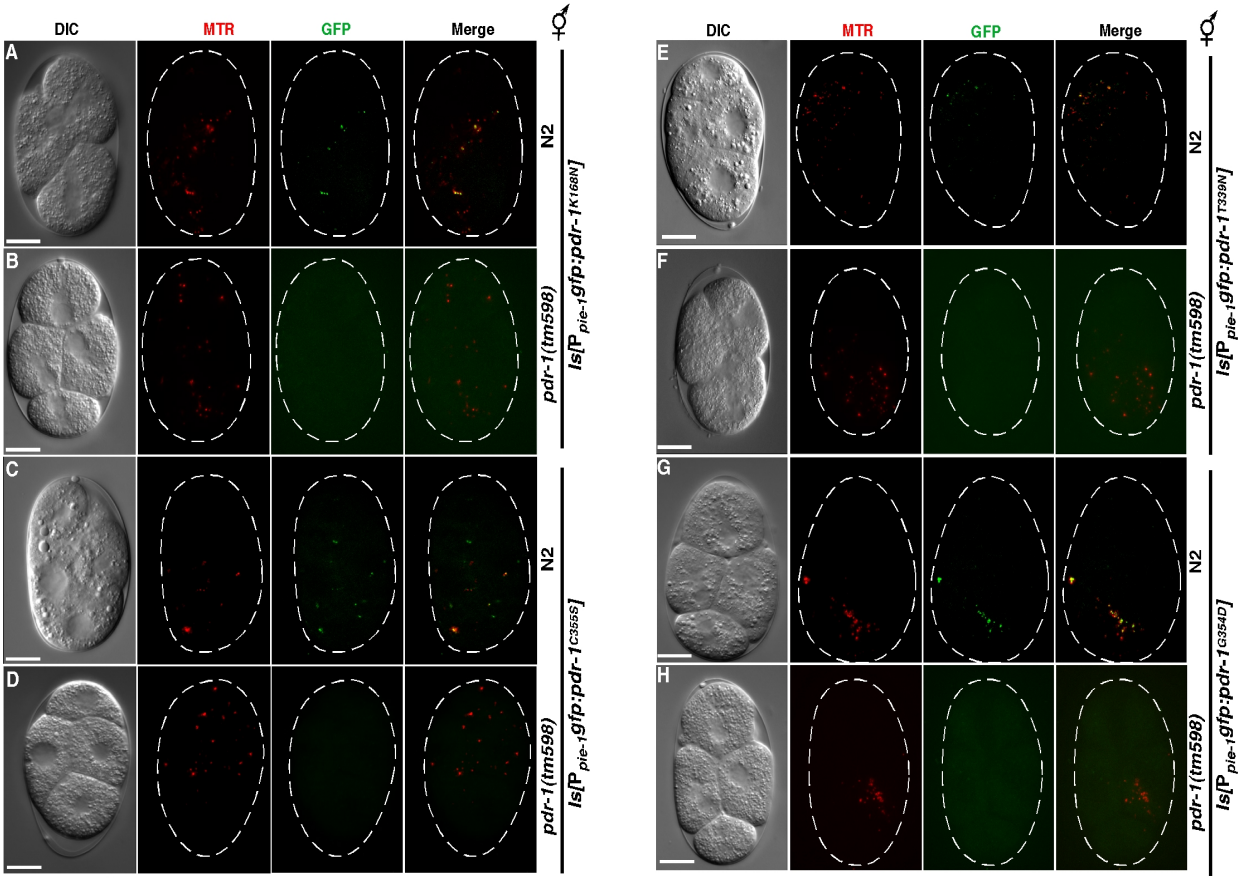

Fig. 3. 7. Localization patterns of different GFP::PDR-1 mutants in embryos with different maternal backgrounds. (**A** to **H**) GFP::PDR-1 fusions carrying the K168N mutation (A and B), the C355S mutation (C and D), the T339N mutation (E and F), and the G354D mutation (G and H) all translocated to paternal mitochondria in 4-cell embryos with an N2 maternal background, but failed to associate with paternal mitochondria in embryos with a *pdr-1(tm598)* maternal background. MTR stained N2 males were mated with N2 or *pdr-1(tm598)* hermaphrodites carrying the indicated transgene. All transgenes have a low-copy number and are integrated into the same *ben-1* locus, which is completely dispensable for *C. elegans* development and does not affect PME (see Materials and Methods). Scale bars represent 10 μm.

Interestingly, co-expression of both human Parkin and PINK1 in *C. elegans* using the same transgene expression system rescued the PME defect of the *pdr-1(tm598)* mutant, whereas expression of human Parkin alone did not rescue (Fig. 3.4I). Because human PINK1 kinase phosphorylates Parkin at its Serine 65 residue to activate the activity of Parkin *(167, 168)*, we tested whether expression of the human Parkin^{S65E} mutant, a phospho-mimic, could rescue the PME defect and found that expression of human Parkin^{S65E} largely bypassed the requirement for human PINK1 to rescue the PME defect (Fig. 3.4I). The findings that human Parkin and PINK1 cooperate to function in *C. elegans* as they do in humans to substitute for the function of PDR-1 indicate that the function and the acting mechanism of Parkin are highly conserved and that *C. elegans,* amenable to powerful genetic and reverse genetic analyses, can be used as a new animal model to understand and treat Parkinson's disease.

3.2.7 EM analysis reveals the specificity defect of autophagosome in *pdr-1* mutants.

To better understand how PDR-1 mediates autophagy of paternal mitochondria in *C. elegans*, we performed electron microscopy (EM) analysis. In N2 zygotes from mating of N2 males and hermaphrodites, a phagophore assembled and expanded over an individual paternal mitochondrion (Fig. 3.8A) to form a tightly enclosing autophagosome (Fig. 3.8B) *(177)*. In contrast, in *pdr-1(tm598)* zygotes from mating of *pdr-1(tm598)* males and hermaphrodites, autophagosomes often enclosed multiple degraded mitochondria and membranous compartments, including portions of endoplasmic reticulum (ER), which are recognized by membrane-bound ribosomes (Fig. 3.8, C to E, H, I). We performed electron tomography (ET) analysis to determine three-dimensional (3D) structures of autophagosomes and their cargos in *pdr-1(tm598)* embryos. As shown in Fig. 3.8E, one of the autophagosomes in a *pdr-1(tm598)* embryo contained two paternal mitochondria and a fragment of ER, which has never been observed in N2 embryos (Fig. 3.8, A and B) *(177, 183)*. The 3D model of this autophagosome

and a tomographic slice image showing its side view confirm that a fragment of ER is located inside the limiting autophagosome membranes (Fig. 3.8, F to H). Paternal mitochondria are readily distinguished from maternal mitochondria in cross-fertilized embryos due to their spherical morphology and unique dark aggregates in the matrix that form shortly after fertilization (Fig. 3.8, A to E) *(177, 183)*. In addition, the diameters of paternal mitochondria are also larger than the thickness of tubular maternal mitochondria *(177)*. Interestingly, we observed some autophagosome membranes enclosing not only paternal mitochondria, but also fragments of maternal mitochondria that are thinner and free of dark aggregates in *pdr-1(tm598)* embryos (Fig. 3.8I). In N2 embryos, maternal organelles are rarely enclosed in autophagosomes when they are actively removing paternal mitochondria (Fig. 3.8, A, B and J, and Fig. 3.9) *(177, 183)*. By contrast, 48% of autophagosomes in *pdr-1(tm598)* embryos contained pieces of ER, and sometimes, maternal mitochondria from the oocyte (Fig. 3.8J). This observation suggests that the autophagy machinery in *pdr-1(tm598)* embryos loses its ability to target only damaged paternal mitochondria and has become indiscriminate in removing both paternal mitochondria and maternal organelles in their vicinity. Because ER and mitochondria are the most abundant organelles in embryos, they are likely mistaken by autophagosomes with compromised cargo specificity in the *pdr-1(tm598)* mutant. The added burden to accommodate and degrade non-specific cargos and the inability to close autophagosomes (Fig. 3.5H) provide a mechanistic explanation for why PME is delayed in the *pdr-1* mutant.

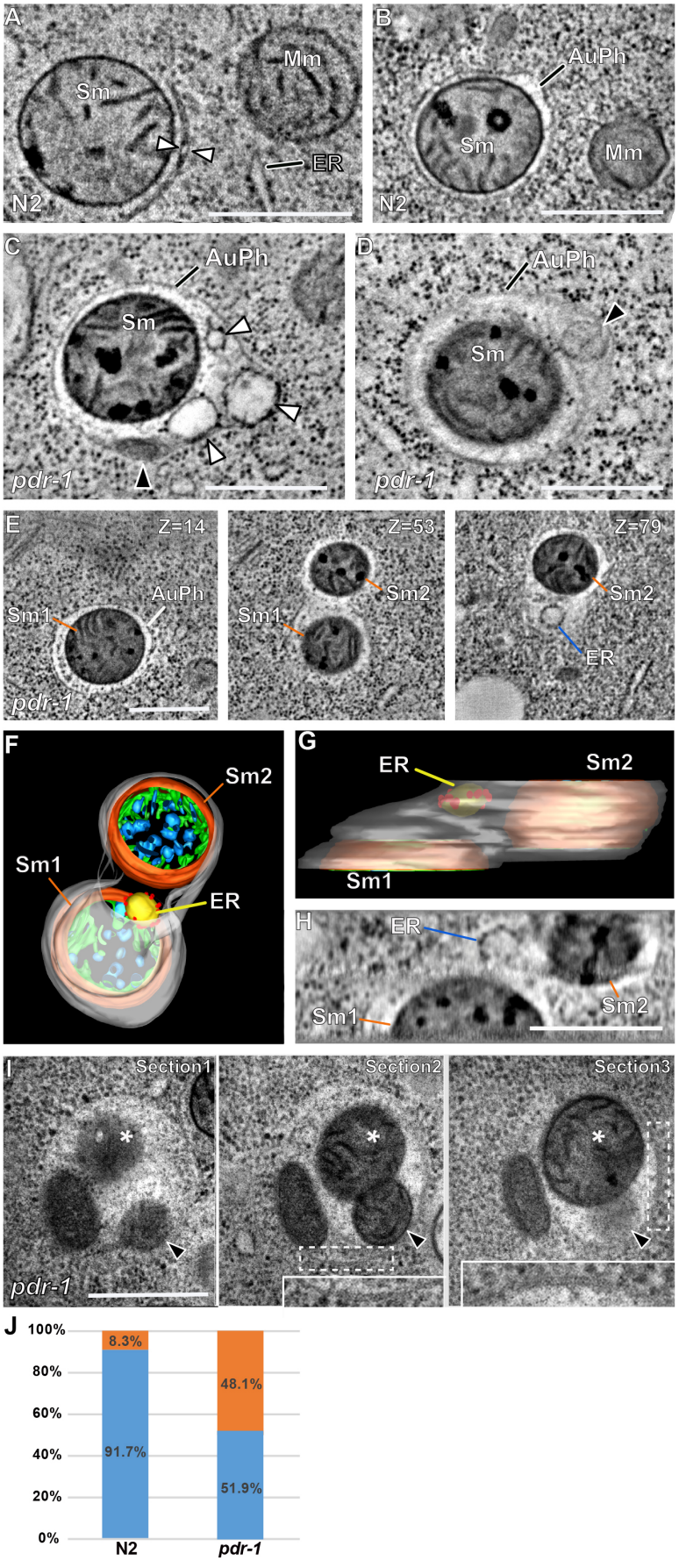
A
Mm
Sm
ER
N2
B
AuPh
Sm
Mm
N2
C
AuPh
Sm
pdr-1
D
AuPh
Sm
pdr-1
E
Z=14
AuPh
Sm1
pdr-1
Z=53
Sm2
Sm1
Z=79
Sm2
ER
F
Sm2
Sm1
ER
G
ER
Sm2
Sm1
H
ER
Sm1
Sm2
I
Section1
pdr-1
Section2
Section3
J
100%
80%
60%
40%
20%
0%
8.3%
91.7%
48.1%
51.9%
N2
pdr-1

Fig. 3. 8. Electron microscopy and tomography analyses of autophagosomes in N2 and *pdr-1(tm598)* embryos. (**A** and **B**) Electron tomographic slices of N2 embryos. Double membranes of a phagophore (arrowheads) are being assembled and expanding over a sperm mitochondrion (Sm)(A). Each autophagosome (AuPh) usually contains a single sperm mitochondrion in N2 embryos (B). Maternal mitochondria (Mm) from the oocyte have never been targeted by autophagosomes (*177*). (**C** and **D**) Electron tomographic slices of *pdr-1(tm598)* zygotes showing that autophagosomes contained multiple membranous compartments (arrowheads), some of which are identified to be ER because they have ribosomes on their surfaces (white arrowheads in C). (**E**) Sequential tomographic slice images of an autophagosome in a *pdr-1(tm598)* embryo. Slice numbers are indicated at the upper right corner. Two sperm mitochondria (Sm1 and Sm2) with dark aggregates and an ER fragment are present in the autophagosome. (**F** and **G**) Three-dimensional models of the autophagosome in (E). Red dots on the ER surface (yellow) are ribosomes. Dark aggregates are shown in blue, cristae in green, mitochondrial surface in orange, and AhPh membranes in grey. (**H**) Lateral view of the tomogram in (E) revealing locations of the two sperm mitochondria and the ER fragment in the autophagosome. (**I**) Three consecutive sections (120 nm) of a *pdr-1(tm598)* embryo. A fragment of a maternal mitochondrion (arrowhead) adjacent to a sperm mitochondrion (asterisk) is being encompassed by an autophagosome. The insets in the Section 2 and 3 panels show double membranes of the autophagosome marked with dashed rectangles in each panel. (**J**) Stacked column histogram showing autophagosomes containing extra membranous compartments (colored in orange) in N2 and *pdr-1(tm598*) embryos. 48% of autophagosomes from *pdr-1(tm598)* embryos contained other membranous entities in addition to the paternal mitochondrion, some of which are ER or maternal mitochondria. We occasionally observed unidentifiable extra membranes in autophagosomes in 8.3% N2 embryos (Fig. 3.9), but they did not appear to be pieces from maternal organelles. ER membranes and maternal mitochondria have not been detected in autophagosomes of N2 embryos (*177*). Scale bars indicate 500 nm.

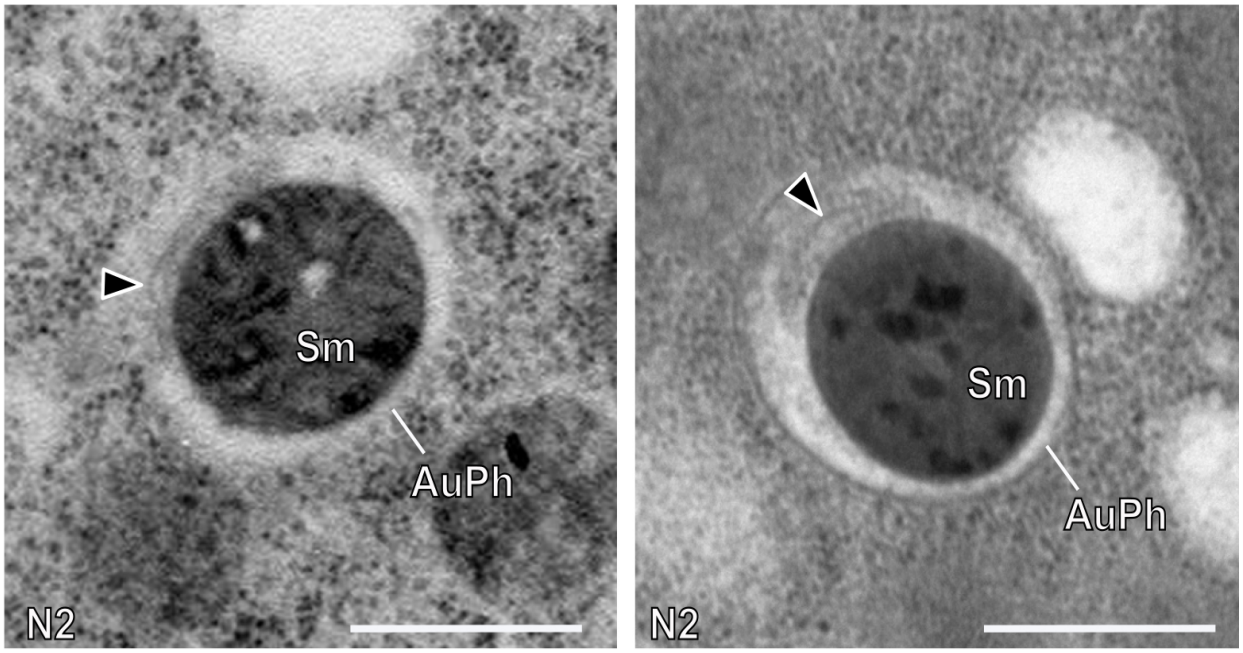

Fig. 3. 9. Examples of small membrane fragments seen in autophagosomes of N2 embryos. Each panel is a transmission electron micrograph showing an autophagosome (AuPh) containing a sperm mitochondrion (Sm) and extra membranes (arrowhead). They do not resemble fragments of ER or maternal mitochondria observed in autophagosomes of *pdr-1(tm598)* embryos shown in **Fig. 3. 8**. Scale bars indicate 500 nm.

3.2.8 Lethality is associated with nonspecific engulfment of maternal organelles.

We examined if inappropriate degradation of normal organelles by autophagosomes in the *pdr-1* mutant adversely affects the fitness or the viability of animals. Compared with N2 embryos that have a low lethality rate of 0.7%, *pdr-1(tm598)* embryos exhibit a significantly higher lethality rate of 2.9% (Fig. 3.10A, assays 1 and 2). The increased lethality in *pdr-1(tm598)* embryos is strongly suppressed by the low-copy P_{pie-1} *gfp::pdr-1* transgene (1.1%; Fig. 3.10A, assay 3), but not suppressed by the five low-copy P_{pie-1} *gfp::pdr-1* transgenes expressing PDR-1 mutants (Fig. 3.10A, assays 4-8). These results indicate that the increased lethality phenotype in *pdr-1(tm598)* embryos is specifically associated with reduced or loss of PDR-1 function. The increased embryonic death caused by loss of *pdr-1* could be due to delayed removal of damaged paternal mitochondria in embryos, or improper removal of normal organelles, such as ER and maternal mitochondria, or the combination of both. However, because loss of *cps-6* delays PME to a similar extent to that caused by loss of *pdr-1* (Fig. 3.5I, matings 1, 2, and 7), but does not cause increased embryonic lethality (Fig. 3.10B, assays 1 and 2), and because the *cps-6; pdr-1* double mutant, albeit having a stronger PME defect (Fig. 3.5I, matings 2 and 8), exhibits a comparable embryonic lethality rate to that of the *pdr-1* single mutant (Fig. 3.10B, assays 3 and 4), inappropriate removal of healthy organelles in the *pdr-1* mutant is likely the major cause of increased embryonic lethality.

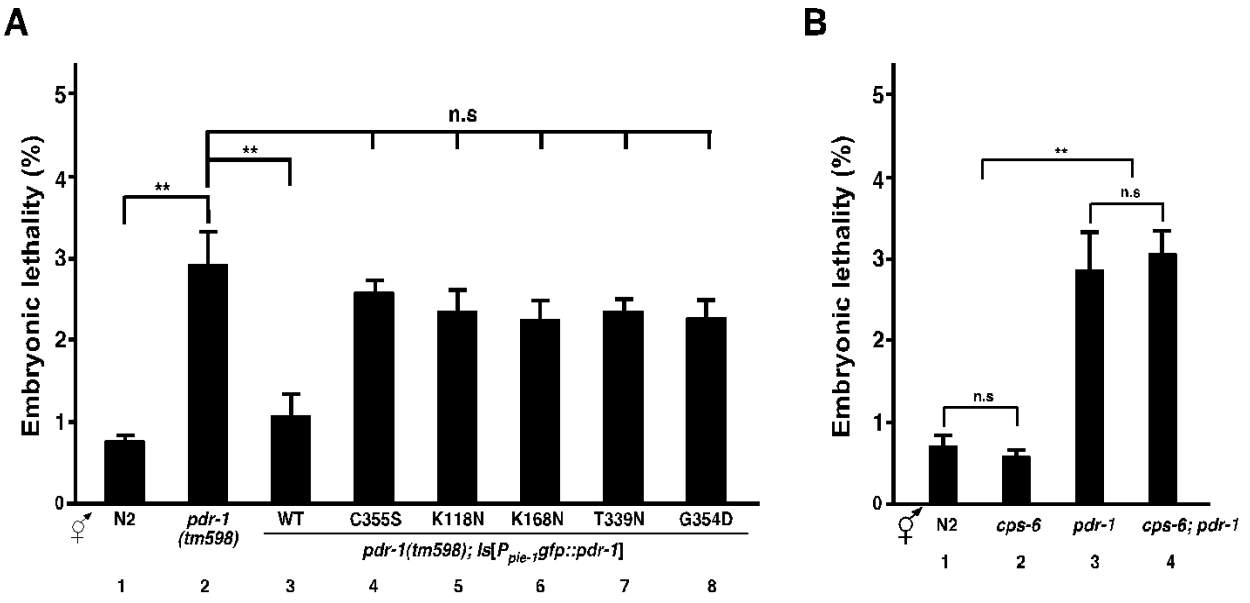

Fig. 3. 10. Loss of *pdr-1* causes increased embryonic lethality. (**A**) The embryonic lethality rate was scored in self-fertilized embryos of the indicated genotypes. Means ± SEM; n > 500 embryos per strain at 25°C. ** $P < 0.01$, using unpaired Student's *t*-test. (**B**) Loss of *cps-6* does not increase the lethality rate compared with N2 or *pdr-1(tm598*) embryos. *pdr-1* and *cps-6* alleles used are *tm598* and *tm3222*, respectively.

3.3 Discussion

A long-standing mystery in developmental biology is that mitochondria are inherited maternally in most animals *(109-111, 184)*. The autophagic-lysosomal pathway plays an important role in removing paternal mitochondria in *C. elegans* and *Drosophila* embryos *(34-36, 47, 177)*, but how paternal mitochondria are selectively degraded by the autophagy machinery remains poorly understood. In this study, we identify the *C. elegans* PDR-1 protein as the critical factor that flags paternal mitochondria for autophagic degradation. PDR-1 achieves this by specifically translocating to and concentrating on paternal mitochondria in fertilized eggs and then recruiting the autophagy machinery to paternal mitochondria. Consistent with these observations, loss of *pdr-1* results in impaired ability of phagophores to extend around and encapsulate paternal mitochondrion, and consequently, abnormal enclosure and degradation of normal maternal organelles, including ER and maternal mitochondria. The decreased autophagy specificity and ectopic removal of maternal organelles in the *pdr-1* mutant contribute to delayed PME and increased embryonic lethality. Importantly, expression of human Parkin and PINK1 in *C. elegans* fully rescues the PME defect of the *pdr-1* mutant and mutations at conserved residues of PDR-1 and Parkin that cause Parkinson's disease, also impair translocation of PDR-1 to paternal mitochondria and its activity in PME. These findings reveal the conserved function and mechanisms of Parkin in clearing damaged mitochondria and a previously unknown physiological role in PME. Interestingly, *Drosophila* Parkin appears to be dispensable for paternal mitochondrial destruction in fertilized eggs *(47)* and *C. elegans* PINK-1 seems to have a minor role in PME (Fig. 3.3). These observations suggest that additional E3 ubiquitin ligases and kinases could be involved in promoting efficient PME, as the mitochondrial ubiquitin ligase 1 (MUL1), an E3 ubiquitin ligase, has been shown to act in parallel to the Parkin/PINK1 pathway to maintain mitochondrial integrity in both *Drosophila* and mice *(185)*.

The prevalent model for Parkinson's disease is that Parkin deficiency results in failure to remove and thus accumulation of damaged mitochondria, which eventually leads to loss of neurons sensitive to the level of the healthy mitochondrial pool *(151, 154)*. Our study points to a new possibility that improper removal of healthy organelles such as ER and mitochondria in Parkin-deficient patients can exacerbate the damage caused by failure to remove damaged mitochondria in neurons or cells, facilitating the development of pathogenic outcomes. Our study also suggests that the *C. elegans* PME model could serve as an alternative experimental system to dissect the Parkin pathway and to treat Parkinson's disease.

3.4 Materials and methods

3.4.1 Strains

C. elegans strains were maintained at 20°C using standard methods (*144*). The alleles used for this study are: LGI, *cps-6(tm3222);* LGII, *rad-23(tm2595)*, *lgg-1(bp500), pink-1(tm6685);* LGIII, *pdr-1(tm598);* mtDNA, *uaDf5*. *smIs42* is an integrated transgene generated by gamma irradiation of animals carrying an extrachromosomal array containing P_{sur-5}*sur-5::gfp*. It was backcrossed four times with N2 animals before being used in this study.

3.4.2 Transgenic animals

Complex transgenic arrays were generated as previously described to promote expression of the transgenes in the germline and in early embryos (*180*). Briefly, *pdr-1(tm598)* animals were injected with 10 ng/µL of P_{sur-5}*sur-5::gfp* (transgenic marker), 10 ng/ µL pRF4 (transgenic marker), 100 ng/µL Sca I-digested N2 genomic DNA, and 2.5 ng/µL of P_{pie-1}*gfp::pdr-1* (wild-type, C355S, K118N, K168N, T339N, or G354D, respectively), or 2.5 ng/µL of P_{pie-1}*gfp::parkin* with P_{pie-1}*pink1*, P_{pie-1}*gfp::parkin,* or P_{pie-1}*gfp::parkin*^{S65E}.

3.4.3 Generation of low-copy integrated transgenes

Site-directed mutagenesis was used to insert the guide sequences into a Cas9/sgRNA (single guide RNA) expression vector (pDD162), which drives expression of both sgRNA and the Cas9 protein in the *C. elegans* germline (*186*). The *ben-1* locus was targeted for Cas9 cleavage using the guide sequence (AAGCAACTGCAGAGGAAGA) inserted into pDD162, which facilitates insertion of the single copy or low copy transgene at the *ben-1* locus using the methods described in detail (*179*). Briefly, *ben-1(tm234); vps-45(tm246)* animals were injected with the P_{pie-1}*gfp::pdr-1* construct (wild-type*,* C355S, K118N, K168N, T339N or G354D) at 60 ng/µL, *ben-1* and *vps-45* clones that can rescue the respective mutants at 60 ng/µL each, the

Cas9-sgRNA plasmid at 20 ng/µL, and transgenic markers P_{myo-2}DsRed at 20 ng/µL, and P_{myo-3}Venus at 60 ng/µL. Third generation (F3) transgenic animals were placed on nematode growth medium (NGM) plates containing 10 *µ*g/ml benzimidazole (Wako; approximately 50 animals/9-cm plate) and were cultured at 20°C for 7 to 10 days. F5 animals were placed on NGM agar plates (approximately 100 animals /9-cm plate) and cultured at 20°C for 3 days. During this positive (*vps-45)* and negative (*ben-1)* selection process, the animals carrying the integrated P_{pie-1}*gfp::pdr-1* and *vps-45* transgene without a complete *ben-1* rescuing fragment were selected. Surviving animals were singled out and examined by PCR for the presence of P_{pie-1}*gfp::pdr-1* and the *vps-45* rescuing fragment. The primer pair for *gfp::pdr-1* are: 5' ATGAGTAAAGGAGAAGAACTTTTCACTGG 3' and 5' CCAATGGTCCCATTGACACTC 3'. The primer pair for *vps-45*: 5' GGGCAAGGTGAATGTGGAAG 3' and 5' CTCCTGGAGCTCTTTCACCA 3'. Quantitative PCR analysis was then performed using purified genomic DNA from each integrated strain to determine the copy number of each integrated transgene, using the *ama-1* gene as an internal control. The primer pair for *pdr-1* are: 5' GGACGACAAGGGTGTGACTT 3' and 5' TCTGGACACTGGGATCTTCC 3'. The primer pair for *ama-1* are: 5' AGATGGACCTCACCGACAAC 3' and 5' CTGCAGATTACACGGAAGCA 3'. The copy number of each integrated P_{pie-1}*gfp::pdr-1* transgene is as follows: PDR-1^{WT} is 2, PDR-1^{C355S} is 6, PDR-1^{K118N} is 4, PDR-1^{K168N} is 14, PDR-1^{G354D} is 58, and PDR-1^{T339N} is 15.

3.4.4 MitoTracker Red (MTR) staining

1 mM MTR in dimethyl sulfoxide (DMSO) was diluted in M9 buffer (42.3 mM Na2HPO4, 22 mM KH2PO4, 8.6 mM NaCl, 18.7 mM NH4Cl) to a final concentration of 50 *µ*M before mixing with *E. coli* OP50 to treat *C. elegans* animals. L4 larval stage males were placed on the MTR/OP50 lawn for 12 hours and then cleaned up through three rounds of "bacterial shower", in which they were transferred to a fresh plate with unstained OP50 for 15 minutes each to remove

the MTR dye from their exteriors. Subsequently, MTR-stained males were mated with unstained young adult hermaphrodites for 8 hours before the mated hermaphrodites were dissected to obtain cross-fertilized embryos.

3.4.5 Immunostaining

Immunostaining of *C. elegans* embryos was performed as described previously (*187*), using an anti-LGG-1 mouse monoclonal antibody (1:100; provided by Hong Zhang, Institute of Biophysics, Beijing, China). Secondary antibodies used are FITC-conjugated goat anti-mouse antibody (1:100; Jackson ImmunoResearch laboratories, Inc.). Stained embryos were mounted on the slides with Vectashield Antifade Mounting Medium with DAPI.

3.4.6 Fluorescence imaging using widefield microscopy and Structured Illumination Microscopy (SIM)

Widefield fluorescent microscopy images were captured from the top to the bottom of the stained embryos using a Zeiss Axioplan 2 microscope equipped with a Cohu CCD camera and a SlideBook 5 software (Intelligent Imaging Innovations, Inc.). Z-stacks were then deconvolved and projected into one plane to depict all MTR-stained mitochondria from an embryo in a single image. SIM imaging is achieved by enlarging the Fouriet Domain of sample images about two folds with Nikon Structured Illumination Microscopy (N-SIM). Stained embryos were imaged with 488 nm and 561 nm channels (100 X, oil lens).

3.4.7 Quantification of colocalization or encapsulation of MTR-stained paternal mitochondria by autophagosomes

Using widefield fluorescent microscopy images, the colocalization ratio of MTR-stained paternal mitochondrial clusters with autophagosomes in fertilized eggs is determined as the

number of MTR-stained mitochondrial clusters that are associated with LGG-1 immunofluorescence signals divided by the total number of MTR-stained mitochondrial clusters. Using SIM images, the percentages of four classes of paternal mitochondria are determined: those fully encapsulated by autophagosomes (enclosed), those partially encapsulated (partially enclosed), those with nearby phagophore, and those that are not associated with any autophagosome or phagophores (isolated).

3.4.8 Quantification of colocalization ratio of GFP::PDR-1 with Paternal mitochondria

Using widefield fluorescent microscopy images, the colocalization ratio of maternal GFP::PDR-1 expressed from the integrated $P_{pie\text{-}1}$*gfp::pdr-1* transgene with MTR-stained paternal mitochondrial clusters in fertilized eggs is determined as the number of MTR-stained mitochondrial clusters that are associated with GFP::PDR-1 divided by the total number of MTR-stained mitochondrial clusters.

3.4.9 Quantification of paternal mitochondria in cross-fertilized embryos

The number of MTR fluorescent dots was scored from projected images of cross-fertilized embryos at the 64-cell stage derived from mating of MTR-stained males with unstained hermaphrodites and used as the relative mitochondrial number.

3.4.10 Embryonic lethality assays

The embryonic lethality assays were carried out at 25°C. Late L4 larvae were aged for 12 hours and then transferred to fresh plates to lay eggs for 6 hours before they were removed. The total number of embryos in the plates was then scored. After 24 hours, embryos that did not hatch were scored as dead embryos. Embryonic lethality rate was calculated as the number of dead embryos divided by the total number of embryos.

3.4.11 PCR analysis

Single cross-fertilized embryos at various developmental stages were dissected from mated hermaphrodites and analyzed by PCR. The primer pairs used to detect the *uaDf5* deletion are: P1, 5' GATTAGCACAAGCTTTATTGGATGG 3' and P2, 5' AAGATCTTAACA-TTCCGGCTGAGGC 3'.

3.4.12 Constructs

The full-length cDNA fragment encoding PDR-1 (wild-type or mutants), human Parkin (wild-type or S65E), or human PINK1 was subcloned into the pTE5 vector (*180*), which contains the promoter of the *pie-1* gene that drives gene expression in the germline and in early embryos in *C. elegans* and a GFP-coding region that allows construction of the GFP fusion.

3.4.13 Electron microscopy and electron tomography

Mated *C. elegans* hermaprodites were cryofixed by a HPM100 high-pressure freezer (Leica Microsystems, USA) and freeze-substituted in 2% osmium tetroxide in anhydrous acetone. After embedding epoxy resin, we performed ultramicrotomy, staining, and TEM imaging as described in Kang (2010)(*148*). Electron tomography analysis was carried out according to the protocol described previously (*188*). In brief, 250 nm thick sections were collected and tilt image series from 2 orthogonal axes were collected at 14500X from $+60^{o}$ to -60^{o} with 1.5 increments using a TF20 electron microscope (FEI, Hillsboroa, OR, USA). Tomograms were calculated using the Etomo module of the IMOD software package (Boulder Laboratory of 3D Electron Microscopy of the Cell, University of Colorado at Boulder). 3D models were generated with the 3dmod program in the same package.

Contribution statement: The electron microscopy data is done in collaboration with Dr. Byung-ho's group. The rest of the work is all done by myself.

Chapter 4

cei-1 regulates the pro-apoptotic function of CED-8 in *C. elegans*.

Apoptosis plays a pivot role in animal development. Abnormal apoptosis may result in severe pathological conditions, such as uncontrolled cell growth (cancer) that is caused by insufficient apoptosis and autoimmune diseases that are caused by excessive cell death. Therefore, deciphering the regulation and execution mechanisms of apoptosis makes it possible to treat those apoptosis-related diseases. Genetics studies in *C. elegans* have identified many components in the conserved apoptosis pathway. Here I will focus on the characterization of one poorly understood apoptotic protein in *C. elegans* called CED-8 (CEll Death abnormal). CED-8, a multi-pass transmembrane protein, is activated by the ced-3 cell death protease through proteolytic cleavage during apoptosis to promote programmed cell death. Activation of CED-8 also causes phosphatidyl-serine (PS) externalization during the embryonic development of *C. elegans*. However, it is unclear why CED-8 needs to be cleaved to gain its full pro-apoptotic function. We identified a CED-8-Interacting protein (CEI-1): A special form of hydroxyacyl-coenzyme A dehydrogenase encoded by the *cei-1* gene that localizes to plasma membrane and that suppresses the pro-apoptotic function of CED-8 in living cells through direct binding to the N-terminus of CED-8. During apoptosis, CED-3 cleaves CED-8 at the 21st amino acid (aspartic acid), which results in the relief of CED-8 from the CEI-1 suppression and thus promotes apoptosis. I also uncovered a *cis-acting* motif within the N-terminus of CED-8 that is responsible for the interaction between CED-8 and CEI-1. Disruption of this interaction by mutating this *cis-acting* motif not only results in constitutive activation of CED-8 independent of the caspase cleavage, but also causes an ectopic vesicle efflux phenotype in the living cells. My results thus provide important mechanistic insights into the activation of CED-8 during apoptosis.

4.1 Background

As a fundamental aspect of animal development and homeostasis, programmed cell death (apoptosis) plays an essential role in maintaining the physiological balance of cell numbers by opposing uncontrolled cell proliferation. Abnormal cell death results in severe outcomes (*189-191*). For example, insufficient cell death is usually associated with uncontrolled proliferation of the somatic cells, which causes tumors (*189-191*). During apoptosis, the cell collapses in a regimented fashion and is eventually engulfed by the phagocytes (*192*). *C. elegans* has been used as a genetics model to study the conserved core pathway that mediate programmed cell death. In the *C.elegans* hermaphrodite, 131 of the 1090 somatic cells generated during hermaphrodite development are invariantly destined to undergo apoptosis, (*193, 194*) which is driven by a conserved core apoptosis pathway. Lying at the heart of the apoptosis pathway is a special class of proteases, named “caspase”. Caspases cleaves after the aspartic acid residues of their substrates in cells that are programmed to die (*195, 196*). Upon activation in response to the physiological apoptotic stimuli, CED-3 cleaves a variety of substrates, which either inactivates proteins that are pivotal to maintain cellular homeostasis, or activates an arsenal of CED-3 substrates that execute different tasks in this suicide program (*197*).

One of the important aspects that are disturbed during apoptosis is plasma membrane phospholipid asymmetry. In normal cells, phospholipids are asymmetrically distributed in inner and outer leaflets of plasma membrane, with phosphatidylcholine (PC) and sphingomyelin (SM) predominantly in the outside leaflet, and phosphatidylserine (PS) and phosphatidylethanolamine (PE) in the inner leaflet of plasma membrane (*198*). During apoptosis, the membrane asymmetric distribution of PS could no longer be maintained (*199, 200*). PS residing in the inner leaflet of plasma membrane is flipped to the outer leaflet of plasma membrane, which serves as an “eat-me” signal to recruit phagocytes for engulfment (*201*), as well as disposal of the cell

corpse. In *C. elegans*, there are two engulfment pathways that utilize PS on the outer surface of the apoptotic cells to recruit phagocytes. The first pathway is comprised of: TTR-52, CED-1, CED-6, and CED-7, with TTR-52 serving as a bridging molecule to cross-link the PS ligand on the apoptotic cell and the CED-1 receptor on the phagocyte (*202, 203*). The second pathway consists of PSR-1 (PS Receptor-1), CED-2, CED-5, CED-10, and CED-12, with PSR-1 serving as a receptor for the PS ligand on the apoptotic cell (*202, 204-206*).

Previously, our laboratory has shown that CED-8 plays an important role in externalizing PS during programmed cell death (*207*). CED-8 was originally identified as a proapoptotic protein, because inactivation of *ced-8* causes a cell-death-delay phenotype (*208*). *ced-8* encodes a protein, witn eight transmembrane segments, which is homologous to the human XK transporter protein (*206, 207, 209*). In humans, patients that harbor mutations in the XK transporter protein suffer from McLeods syndromes (*209*). CED-8 in normal cells do not exhibit its pro-apoptotic function until it is activated by CED-3 caspase cleavage, which serves to function as one of the apoptotic execution events (*207*). The role of CED-8 in apoptosis is attributed to two aspects: first, CED-8 is important to regulate the kinetics of cell death (*208*); second, CED-8 promotes externalization of PS (*207*). How CED-3 caspase cleavage releases the pro-apoptotic function of CED-8 remains to be elucidated. Since the C-terminal cleavage product of CED-8 (21^{st} aa to the end) is fully functional in terms of both the kinetics and PS externalization, I hypothesized that the short N-terminus of CED-8 contains an inhibitory motif that keeps the full length CED-8 inactive before the cell is destined to die. This chapter of my dissertation summaries the findings on the mechanisms, by which the pro-apoptotic function of CED-8 is regulated via association with CEI-1 a hydroxyacyl-CoA dehydrogenase.

4.2 Experimental Results.

4.2.1 Alanine scanning in the N-terminus of CED-8

It has been shown previously that cleavage at the aspartic acid 21 of CED-8 leads to activation of the pro-apoptotic activity of CED-8 (*207*). In the complete loss-of-function *ced-8(n1891)* strain, programmed cell death occurs in a significantly delayed manner, as assayed by cell corpse numbers at different embryonic stages (*208*). Ectopic expression of wild-type CED-8 (CED-8^{WT}) or the activated form of CED-8 (acCED-8 or CED-$8^{\Delta 21}$, the truncated form from 21aa to the end) can rescue the cell corpse defect in *ced-8(n1891)* embryos *(207)*. The cleavage-resistant mutant, CED-8^{D21E}, however, failed to rescue the delay-of-cell-death phenotype in the *ced-8(n1891)* mutant *(210)* (Fig. 4.1D). The activation of CED-8 by CED-3 cleavage at Asp21 suggests that the 21 residue-long N-terminus of CED-8 plays an inhibitory role in suppressing the pro-apoptotic function of CED-8. Thus, I examined the N-terminus of the CED-8 to identify the minimal motif responsible for inhibition of CED-8 activity. I hypothesize that CED-8 will become constitutively active independent of the CED-3 cleavage event, if this putative inhibitory motif is altered. Mutations in the putative inhibitory motif, together with the CED-3 cleavage-resistant mutation CED-8^{D21E} will likely result in a functional CED-8 protein as acCED-8, the activated form of CED-8. To test this hypothesis, I performed alanine-scanning experiments by mutating every 2 or 3 amino acids in the N-terminus of the CED-8^{D21E} construct. When their rescue abilities are assessed in the *ced-8(n1891)* mutant, we found that substitutions of KSK (amino acid 7-9, KSK/AAA) or LLL(amino acid 10-12, LLL/AAA) with AAA partially rescued the cell death defect. Specifically, the reduced cell corpse defect at the bean/comma stage was rescued, while the increased cell corpse defect at the 4-fold stage was not (Fig. 4.1C). The rescue results indicate that the inhibitory motif likely includes KSKLLL (amino acid 7 to 12) in the N-terminus of CED-8. When comparing the cell corpse numbers in transgenic *ced-8(n1891)* embryos expressing these two CED-8 mutants with those expressing wild-type CED-8, there are approximately twelve cell corpses present at the 4-fold stage, which may have resulted from

ectopic cell death induced by these two CED-8 mutants (Fig. 4.1D). This gain-of-killing function in these two CED-8 mutants will be discussed in details in 4.2.3.

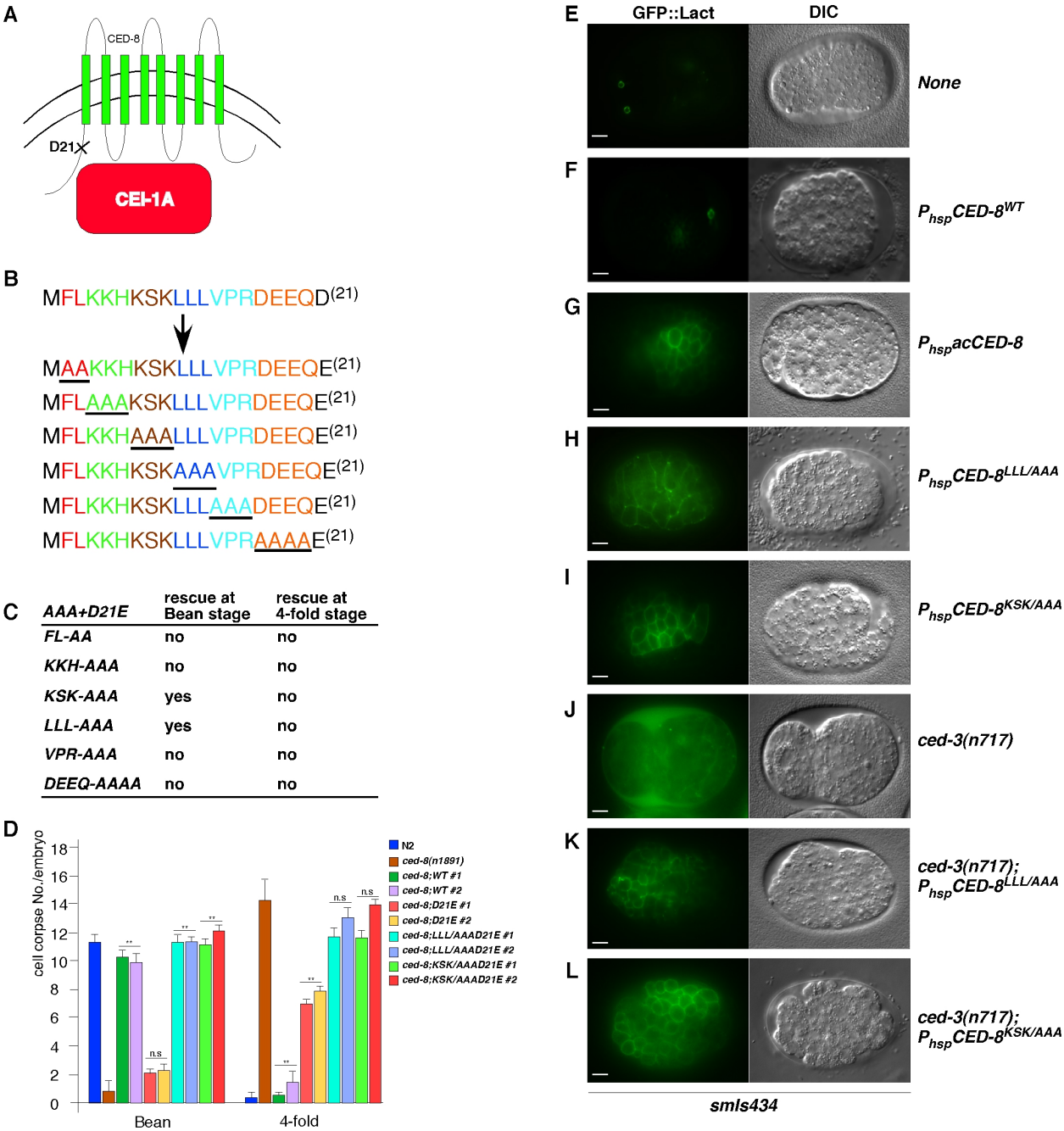

Fig. 4. 1. Identification of the inhibitory motif in the N-terminus of CED-8. (A) The hypothesized model of CEI-1-mediated suppression of the proapoptotic function of CED-8. **(B)** Design of the alanine scanning experiments spanning the N-terminal 21 amino acids of CED-8. **(C)** Summary of the rescue results of the alanine mutations. **(D)** Cell corpses scored in embryos with the indicated genotypes and embryonic stages. The average numbers of cell corpses ± SEM (n=15 embryos at each stage) are shown. ** $p<0.001$, * $0.001<p<0.01$ determined by

student t test. *ced-8(n1891)* is a complete loss-of-function allele. For each CED-8 mutant, two independent transgenic lines were generated. For example: "*ced-8;WT #1"* is the 1st transgenic strain generated by injecting the *ced-8(n1891)* strain with the $P_{hsp}CED\text{-}8^{WT}$ construct (*hsp*, heatshock promoter). **(E** to **L)** Expression of CED-$8^{LLL/AAA}$ or CED-$8^{KSK/AAA}$ induces ectopic PS exposure in all cells. *smIs434* is an integrated transgene (P_{hsp}*sGFP::Lact)* that can express the PS sensor, *sGFP::Lact* (a secreted GFP::Lactadherin fusion protein; Lactadherin is a protein that can specifically bind phospatidylserine(PS)) *(211, 212).* GFP::Lact and differential contrast interference (DIC) images of comma stage embryos from the following strains are shown: *smIs434* (E), *smIs434; ex[*$P_{hsp}CED\text{-}8^{WT}$*]* (F), *smIs434; ex[*P_{hsp}*acCED-8]* (G), *smIs434; ex[*$P_{hsp}CED\text{-}8^{LLL/AAA}$*]* (H), *smIs434; ex[*$P_{hsp}CED\text{-}8^{KSK/AAA}$*]* (I), *ced-3(n717); smIs434* (J), *ced-3(n717); smIs434; ex[*$P_{hsp}CED\text{-}8^{LLL/AAA}$*]* (K), *ced-3(n717); smIs434; ex[*$P_{hsp}CED\text{-}8^{KSK/AAA}$*]* (L). Heat-shock treatment was performed at 33°C for 45 min and embryos were examined after 2 hours recovery at 20 °C. Exposure time for each fluorescent image was identical (500 ms). Scale bars, 5 μm.

4.2.2 Ectopic PS flipping caused by the KSK/AAA or LLL/AAA mutations

One of the key functions of CED-8 in apoptosis is to flip PS to the surface of apoptotic cells. Moreover, overexpression of acCED-8, but not full length CED-8, can induce ectopic PS flipping in living cells of *C. elegans* embryos (*207*). I further interrogated the ability of those two inhibitory-motif mutants, CED-$8^{LLL/AAA}$ or CED-$8^{KSK/AAA}$, in disruption of PS asymmetry in living cells. To this purpose, I utilized a genetically encoded PS sensor, *smIs434*, (*211, 212*) which expresses a secreted GFP::Lact (GFP tagged Lactadherin with a secretion signal) that binds and labels the PS exposed on the surface of apoptotic cells. In *smIs434* embryos, the secreted GFP::Lact only labels the apoptotic cells with surface-exposed PS (*207*) (Fig. 4.1E). In contrast, global expression of acCED-8 under the control of a heat-shock promoter resulted in GFP::Lact labeling of all cells, including both living and apoptotic cells (*207*) (Fig. 4.1G). This suggests that acCED-8 can induce ectopic PS exposure on the surface of all cells. When the two CED-8 mutants, CED-$8^{LLL/AAA}$ or CED-$8^{KSK/AAA}$ are overexpressed under the control of the heat-shock promoter, all living cells displays surface-exposed PS in *smIs434* embryos. In comparison, overexpression of the full-length CED-8, CED-8^{WT}, in *smIs434* embryos, does not alter the staining pattern of GFP::Lactadherin, or cause ectopic PS exposure on the surface of all cells

(Fig. 4.1F). Specifically, overexpression of CED-8$^{KSK/AAA}$ induces in a similar PS staining pattern in living cells to that caused by overexpression of acCED-8 in living cells (Fig. 4.1G and I). Overexpression of CED-8$^{LLL/AAA}$ can also induce PS exposure on the surface of all cells. However, the pattern of GFP::Lact labeling is notably different, in that PS staining is unevenly distributed on cell surfaces, and there are PS-positive bright aggregates associated with the plasma membrane of the living cells (Fig. 4.1H). Those bright aggregates could be vesicles effluxes from the plasma membrane with PS on the outer leaflet (Fig. 4.2A and B). Our laboratory previously reported that CED-7 can efflux PS-containing vesicles from apoptotic cells to neighboring engulfing cells during apoptosis (*212*). I tested if the bright aggregate pattern of PS staining caused by CED-8$^{LLL/AAA}$ overexpression is mediated by CED-7. Compared with the *smIs434; ex[P$_{hsp}$CED-8$^{LLL/AAA}$]* embryos, the GFP::Lact staining pattern is not altered and still unevenly distributed on the surface of living cells in *ced-7(n2094); smIs434; ex[P$_{hsp}$CED-8$^{LLL/AAA}$]* embryos. This result indicates that this particular PS exposure phenotype, which is unique to CED-8$^{LLL/AAA}$, is independent of ced-7.

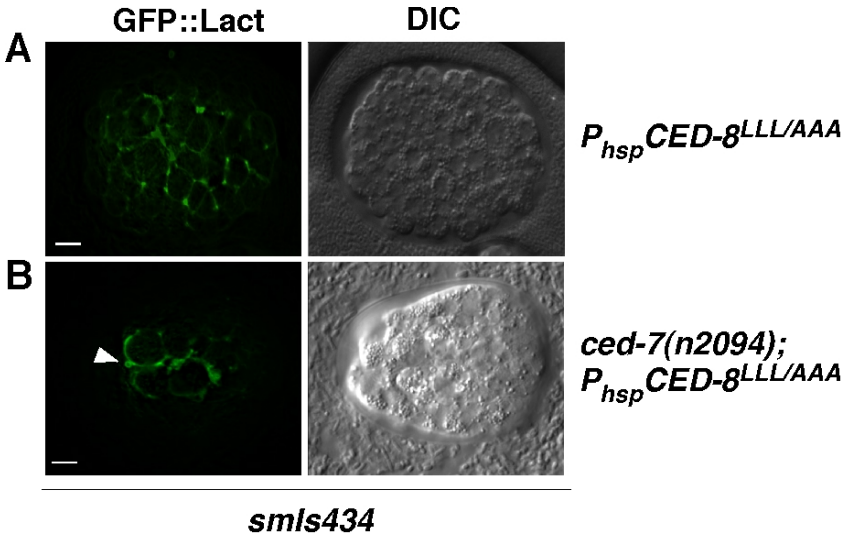

Fig. 4. 2. The PS positive vesicle efflux is not dependent on ced-7. GFP::Lact and differential contrast interference (DIC) images of comma stage embryos from the following strains are shown: *smIs434; ex[P$_{hsp}$CED-8$^{LLL/AAA}$]* (A) and *ced-7(n2094); smIs434; ex[P$_{hsp}$CED-8$^{LLL/AAA}$]* (B). The white arrow in (B) shows a typical extracellular vesicle that is associated with a living cell with ectopically exposed PS. Heat-shock treatment was performed at 33°C for 45 min

and embryos were examined after 2 h recovery at 20 °C. Exposure time for each fluorescent image was identical (500 ms). Scale bars, 5 μm.

To test if these ectopic PS flipping phenotypes in living cells induced by CED-8$^{KSK/AAA}$ or CED-8$^{LLL/AAA}$ are dependent on the activity of CED-3, I performed the same overexpression experiments in *ced-3(n717); smIs434 embryos*. CED-3 is crucial to apoptosis and no cell death occurs in *ced-3(n717)* embryos *(195, 196)*. Therefore in *ced-3(n717); smIs434 embryos,* the secreted GFP::Lactadherin accumulates in the cavity between the egg shell and the embryo, as no cells have PS on the surface (Fig. 4.1J). In *ced-3(n717); smIs434* embryos, overexpression of CED-8$^{LLL/AAA}$ or CED-8$^{KSK/AAA}$ still causes ectopic PS flipping in all living cells. These results suggest that the PS flipping abilities of the two CED-8 mutants with the mutated N-terminal inhibitory motif acts independently of CED-3.

4.2.3 Overexpression of CED-8$^{LLL/AAA}$ or CED-8$^{KSK/AAA}$ can induce ectopic cell death.

To further characterize the LLL/AAA and KSK/AAA mutations, I investigated the cell killing activity of these two CED-8 mutants. Ectopic death of the touch receptor neurons in *C. elegans* serves as a canonical assay to test toxicity of a given protein expressed under the control of the touch-cell-specific *mec-7* gene promoter (*213*). To assess their killing activity, CED-8$^{LLL/AAA}$ and CED-8$^{KSK/AAA}$ are overexpressed under the control of the *mec-7* promoter in a *bzIs8* strains. *bzIs8* is an integrated reporter line containing $P_{mec\text{-}4}GFP$ that labels the six touch neurons with GFP (mec-4 is also a touch-neuron-specific promoter) expression (*214*). The killing ability of CED-8 variants is assayed by scoring the missing rate of the two PLM neurons (Posterior Lateral Microtuble neurons) (*213*). CED-8^{WT} and acCED-8 are used as negative and positive controls. Through quantitating the death of this pair of PLM neurons, I observed a severe (around 70%) missing rate of PLMs when CED-8$^{LLL/AAA}$ or CED-8$^{KSK/AAA}$ are ectopically expressed in PLMs (Table 4.1). In contrast, overexpression of CED-8^{WT} causes little PLM

neuron missing (2%, Table 4.1). On the other hand, overexpression of acCED-8 causes a 34% PLM neuron-missing rate, suggesting that the activated form of CED-8 is able to induce cell death when ectopically expressed. The abnormally high killing ability associated with the two gain-of-function CED-8 mutants, CED-8$^{LLL/AAA}$ and CED-8$^{KSK/AAA}$, suggest mutations in the KSKLLL motif confer new and increased killing activity to CED-8 aside from the activity that mimics acCED-8. I generated an integrated transgene containing *P$_{mec-7}$CED-8$^{LLL/AAA}$*. The PLM killing rate in animals carrying the integrated transgene reached almost 100%, whereas the killing rate of the extrachromosomal transgenes is only around 70% (Table 4.1). The lower killing rate observed with the extrachromosomal transgene arrays is probably due to the mosaic presence of the transgene array. A significant proportion of transgenic positive animals, identified by transgenic marker (mCherry expression driven by *sur-5* promoter in the epithelial cells) may not have the DNA array in the PLM neurons, so that the killing rate is underestimated in strains with the extrachromosomal transgenic arrays.

I also tested if PLM killing caused by CED-8$^{LLL/AAA}$ overexpression is dependent on the activity of CED-3. In *ced-3(n717)* animals, the PLM-missing rates caused by overexpression of CED-8$^{LLL/AAA}$ and CED-8$^{KSK/AAA}$ decreased to around 40% in both cases (Table 4.1). These results indicate that the killing activity of CED-8$^{LLL/AAA}$ or CED-8$^{KSK/AAA}$ is partially dependent on the activity of the CED-3 caspase. This conclusion is also supported by the data using the integrated transgene containing P$_{mec-7}$CED-8$^{LLL/AAA}$. The PLM-missing rate decreased from 98% in *bzIs8; Is[P$_{mec-7}$CED-8$^{LLL/AAA}$]* animals to 46.6% in *ced-3(n717); bzIs8; Is[P$_{mec-7}$CED-8$^{LLL/AAA}$]* animals. Of note, ectopic PS flipping caused by CED-8$^{LLL/AAA}$ or CED-8$^{KSK/AAA}$ expression is independent of the CED-3 caspase activity. Thus, these two CED-8 mutants likely cause cell killing and PS externalization through different mechanisms.

genotype		missing PLM%
bzIs8		0%
bzIs8;Ex[P_{mec-7}CED-8^{WT}]		2%
bzIs8;Ex[P_{mec-7}acCED-8]		34%
bzIs8;Ex[P_{mec-7}CED-8$^{LLL/AAA}$]	L1	70.2%
	L2	68.6%
bzIs8;Ex[P_{mec-7}CED-8$^{KSK/AAA}$]	L1	79.9%
	L2	71.2%
ced-3(n717);bzIs8 *		0%
ced-3(n717);bzIs8;Ex[P_{mec-7}CED-8$^{LLL/AAA}$]	L1	38.5%
	L2	44.7%
ced-3(n717);bzIs8;Ex[P_{mec-7}CED-8$^{KSK/AAA}$]	L1	39.4%
	L2	37%
ced-2(n1994);bzIs8		0%
ced-2(n1994);bzIs8;Ex[P_{mec-7}CED-8$^{LLL/AAA}$]	L1	47.6%
	L2	55.2%
ced-2(n1994);bzIs8;Ex[P_{mec-7}CED-8$^{KSK/AAA}$]	L1	47.1%
	L2	56.7%
psr-1(tm469);bzIs8		0%
psr-1(tm469);bzIs8;Ex[P_{mec-7}CED-8$^{LLL/AAA}$]	L1	61.2%
	L2	57.3%
psr-1(tm469);bzIs8;Ex[P_{mec-7}CED-8$^{KSK/AAA}$]	L1	59.6%
	L2	57.6%
ced-7(n2094);bzIs8		0%
ced-7(n2094);bzIs8;Ex[P_{mec-7}CED-8$^{LLL/AAA}$]	L1	48.5%
	L2	43.2%

**ced-3(n717)* cause bzIs8 strain to express GFP marker in one or two extra neuron cells besides PLM neurons.

Table 4. 1. Ectopic cell death caused by overexpression of CED-8$^{LLL/AAA}$ or CED-8$^{KSK/AAA}$. *bzIs8* is used to facilitate the identification of the touch receptor neurons by labeling them with GFP. *bzIs8* is an integrated transgene that expresses GFP under the control mec-4 promoter. The percentage of PLM neuron death is determined in animals with the indicated genotypes. At least 300 L4 stage larvae from each strain were scored. Extra sister cells of PLMs can abnormally survive in *ced-3(n717)* animals. Those extra cells are supposed to undergo apoptosis immediately being born. *mec-4* promoter is also active in the one or two extra neurons cell due to their close relationship with PLMs.

4.2.4 Overexpression of CED-8$^{LLL/AAA}$ or CED-8$^{KSK/AAA}$ causes apoptosis but not necrosis.

Apoptosis and necrosis are two major forms of cell death (*213*). To determine the nature of cell death caused by overexpression of CED-8$^{LLL/AAA}$ or CED-8$^{KSK/AAA}$, I introduced the integrated transgene, *Is[P$_{mec-7}$CED-8$^{LLL/AAA}$]* into animals defective in *mec-6* or *clp-1*, both of which are crucial for necrosis (*215*). Strong loss-of-function mutations in *mec-6* or *clp-1* do not suppress the PLM death caused by overexpression of CED-8$^{LLL/AAA}$ or CED-8$^{KSK/AAA}$ (Table 4.2). In contrast, the PLM neuron missing rate is reduced to 46.6% in *ced-3(n717)* animals. These results suggest that the ectopic cell death induced by overexpression of CED-8$^{LLL/AAA}$ or CED-8$^{KSK/AAA}$ is apoptosis in nature.

4.2.5 Ectopic cell death caused by overexpression of CED-8$^{LLL/AAA}$ or CED-8$^{KSK/AAA}$ is partially suppressed by engulfment defects.

Timely removal of apoptotic cells or cell corpses through the phagocytosis process is important. Otherwise, lingering apoptotic cells may lyse and cause inflammation (*216*). In *C. elegans*, there are no dedicated phagocytes. Many cells can engulf adjacent cell corpse. Since externalized PS serves as an important “eat-me” signal to the nearby cells to trigger engulfment, abnormal exposure of PS on the surface of live cells could similarly signal to the neighboring cells and result in ectopic engulfment of the live cells (*211*). One possible mechanism underlying the loss of PLM neurons caused by CED-8$^{LLL/AAA}$ or CED-8$^{KSK/AAA}$ expression is that the PLM neurons with surface-exposed PS are treated as apoptotic cells and are removed by phagocytosis. To investigate this possibility, I scored the PLM-missing rate in strains defective in cell corpse engulfment (*211*). There are two partially redundant pathways that mediate engulfment of apoptotic cells: TTR-52, CED-1, CED-6, and CED-7 function in one pathway (1st pathway) (*202, 203*) and PSR-1 CED-2, CED-5, CED-10, and CED-12 act in the other (2nd pathway) (*203-206*). Both engulfment pathways can recognize PS exposed on the surface of

apoptotic cells. When the first pathway is blocked through inactivating CED-7, the PLM-missing rate caused by overexpression of CED-8$^{LLL/AAA}$ decreases to about 50% (Table 4.1). On the other hand, the PLM-missing rate caused by overexpression of CED-8$^{LLL/AAA}$ or CED-8$^{KSK/AAA}$ also decreased to about 50%, when CED-2 is inactivated (Table 4.1). However, when the PS receptor in the 2nd pathway, PSR-1, is mutated, a mild decrease in PLM-missing rate from 70% to around 60% was observed (Table 4.1). These results indicate that PSR-1 does not play a role as important as CED-2 in cell corpse engulfment and suggest that there is a second PS receptor that acts redundantly with PSR-1 in the second engulfment pathway. Overall, the decreases in PLM-missing rates in different engulfment-defective strains suggest that the ectopic engulfment of the PLM neurons contributes to the death of PLM neurons caused by overexpression of CED-8$^{LLL/AAA}$ or CED-8$^{KSK/AAA}$.

genotype	missing PLM%
Is[P_{mec-7}:ced-8$^{LLL/AAA}$];bzIs8	*98.1%*
clp-1(tm690);Is[P_{mec-7}:ced-8$^{LLL/AAA}$];bzIs8	*97.58%*
mec-6(e1342);Is[P_{mec-7}:ced-8$^{LLL/AAA}$];bzIs8	*98.13%*
**ced-3(n717);Is[P_{mec-7}:ced-8$^{LLL/AAA}$];bzIs8*	*46.6%*

**ced-3(n717)* cause bzIs8 strain to express GFP marker in one or two extra neuron cells besides PLM neurons.

Table 4. 2. Apoptotic nature of the cell death induced by overexpression of CED-8$^{LLL/AAA}$. The integrated transgene of CED-8$^{LLL/AAA}$ is used here. *bzIs8* is an interated transgene that expresses GFP under the control of *mec-4* promoter (a touch neuron cell specific promoter) and serves to facilitate the identification of the touch receptor neurons. The percentages of PLM neuron missing are determined in the indicated strains. In wildtype *C. elegans*, there is a pair of PLMs in the tail region posterior to the anus. Extra sister cells of PLMs can abnormally survive in *ced-3(n717)* animals. Those extra cells are supposed to undergo apoptosis immediately being born. The mec-4 promoter is also active in the one or two extra neurons cell due to their close relationship with PLMs.

4.2.6 *cei-1* is identified as a CED-8-interacting factor.

The KSKLLL motif within the N-terminus of CED-8 plays an inhibitory role in regulating the activity of CED-8. The mechanism by which this motif confers inhibition of CED-8 is unknown. One hypothesis is that a *trans-acting* factor is associated with CED-8 through the N-terminal KSKLLL motif. To identify CED-8-interacting proteins, we used a CED-8::GFP fusion protein to perform CED-8 co-immuno-precipitation (co-IP) experiments. By mass spectrometry analysis, *cei-1* (CED-8-interacting protein), defined by the open reading frame T08B2.7, was identified from a band that appears to be specific in the CED-8 co-IP sample. *cei-1* encodes a hydroxyacyl-CoA dehydrogenase, which is involved in beta-oxidation of fatty acids. Beta-oxidation of fatty acids usually occurs in mitochondria. There are three alternatively spliced forms encoded by *cei-1*. Consistent with a role in beta-oxidation, the B form (CEI-1B) is predicted to contain a mitochondria-targeting signal at its N-terminus. An online software, MitoProt II-v1.101 used to predict mitochondria-targeting proteins, suggests that CEI-1B localizes to mitochondria with a high probability (0.9905). The cleavage site after the mitochondria-targeting signal is predicted to be at Methionine 29. In contrast, the A form of CEI-1 (CEI-1A), which contains an additional 26-amino-acid sequence right before the CEI-1B sequence, is not predicted to localize to mitochondria with a probability of 0.5371. This additional 26-amino-acid sequence likely masks the mitochondria-target signal in CEI-1B (Fig. 4.3), and prevents CEI-1A from localizing to mitochondria. Thus, I hypothesized that CEI-1A is the one responsible for regulating the pro-apoptotic activity of CED-8.

Fig. 4. 3. A schematic representation of the gene *cei-1*. There are two alternative transcripts of *cei-1*, 'A' form and 'B' form. The 'A' form has 26 amino acids in its N terminus, which lack in 'B' form.

4.2.7 Different subcellular localization patterns of CEI-1A and CEI-1B

To verify the subcellular localization patterns of the two *cei-1* variants, I constructed plasmids that can express mCherry tagged CEI-1A and CEI-1B under the control of a heat-shock promoter. The mCherry-tagged CEI-1A is found to colocalize with GFP-tagged CED-8 on the plasma membrane in embryos (Fig. 4.4A). In contrast, the mCherry-tagged CEI-1B localizes to mitochondria (Fig. 4.4B). A *bona fide* mitochondria protein, CYN-1, is shown to colocalize with the mcherry::CEI-1B fusion protein (Fig. 4.4B). The differences in subcellular localization patterns between CEI-1A and CEI-1B indicate that they play different functions in distinct cellular compartments.

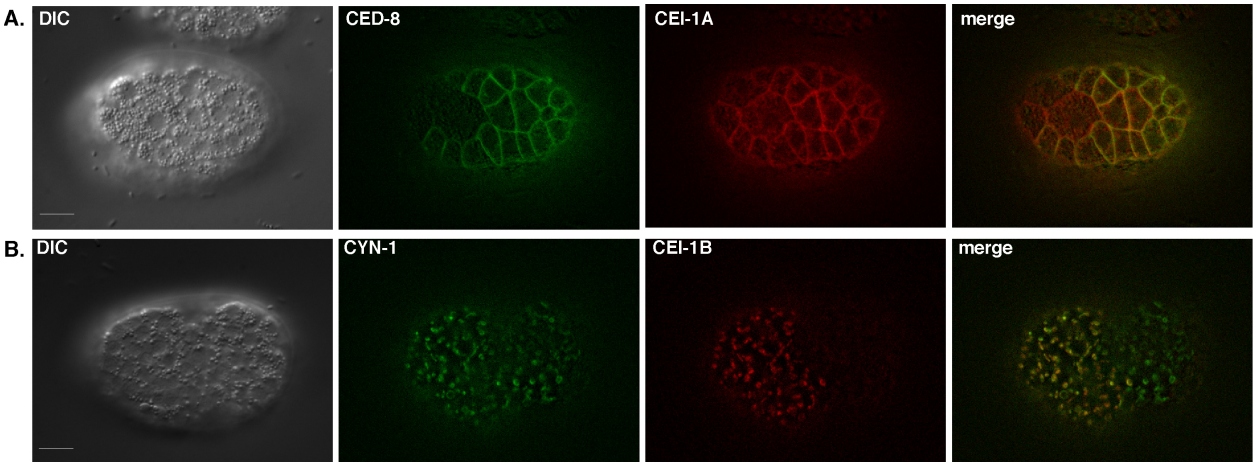

Fig. 4. 4. Differences in localization patterns between CEI-1A and CEI-1B. (A) Fluorescence and differential contrast interference (DIC) images are shown. *unc-76(e911)* worms were injected with 3 plasmids: P_{hsp}*mCherry::CEI-1A,* P_{ced-8}*CED-8:GFP, unc-76* rescuing plasmid that is used as the microinjection transgene marker. A comma stage embryo was imaged to visualize both CED-8::GFP (green) and mCherry::CEI-1A (red) expression patterns. **(B)** A comma stage embryo was imaged to visualize both CYN-1::GFP and mCherry::CEI-1B expression patterns. CYN-1 is a *bona fide* mitochondrial protein. *unc-76(e911)* worms are injected with 3 plasmids: P_{hsp}*mCherry::CEI-1B* (red), P_{sup-26}*CYN-1:GFP* (green), *unc-76* rescuing plasmid as the microinjection transgene marker. The *sup-26* promoter can drive protein expression globally in embryos. Exposure time for each fluorescent image was identical (500 ms). Scale bars, 5 *μ*m.

4.2.8 Plasma membrane localization of CEI-1A is dependent on the presence of CED-8.

Since no transmembrane domain is predicted based on the primary sequence of CEI-1A, the plasma membrane localization of CEI-1A may be dependent on its interaction with CED-8, which spans plasma membrane eight times (*207, 208*). In order to test this hypothesis, I expressed mCherry-tagged CEI-1A in the *ced-8(n1891)* mutant. In *ced-8(n1891)* embryos, the mCherry::CEI-1A fusion no longer associates with the plasma membrane and is diffuse in the cytosol (Fig. 4.5B). Furthermore, when I introduced the full-length CED-8 (CED-8^{WT}) back to the *ced-8(n1891)* strains, the plasma membrane localization of mCherry::CEI-1A is restored (Fig. 4.6C). In contrast, when acCED-8 that lacks the first 21 amino acids is introduced back into the *ced-8(n1891)* mutant, the mCherry::CEI-1A fusion still diffuses throughout the cytosol (Fig. 4.6D). Taking together, these results confirm that the plasma membrane localization of CEI-1A is dependent on its interaction with CED-8, which is a plasma membrane protein (*207, 208*). Particularly, the N-terminus of CED-8 likely provides the docking site for CEI-1A to interact with CED-8 and thus become associated with the plasma membrane. These results also suggest that CEI-1A may inhibit the pro-apoptotic function of CED-8 through direct physical association with the N-terminal inhibitory motif.

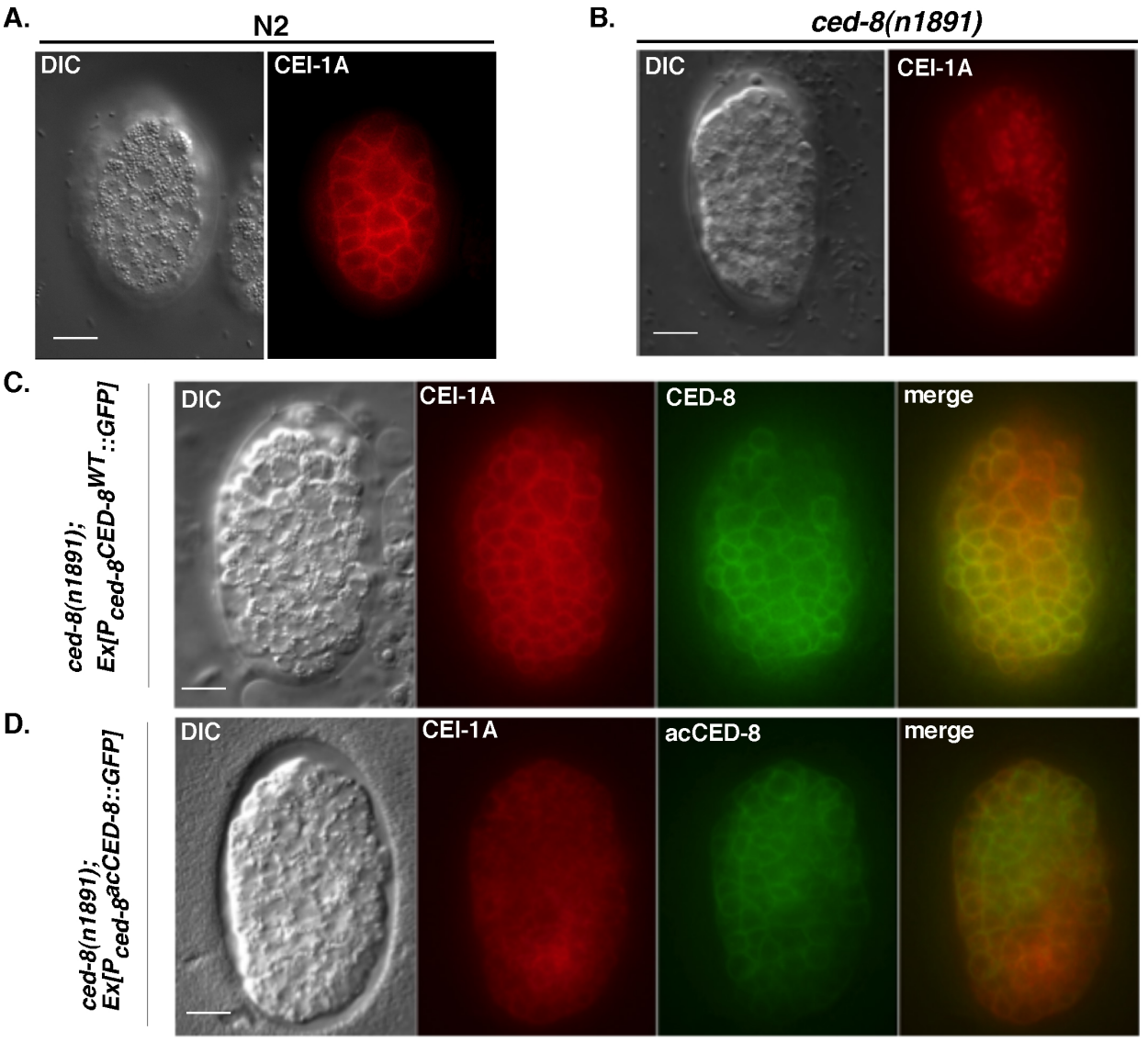

Fig. 4. 5. Plasma membrane localization of CEI-1A depends on CED-8. (A to **D)** Fluorescence and DIC images of comma stage embryos from the indicated strains are shown. mCherry::CEI-1A are shown in RED; GFP tagged CED-8 variants are shown in GREEN. (A) The same embryo in Fig. 4.4 A. *unc-76(e911)* worms are injected with 3 plasmids: P_{hsp}*mCherry::CEI-1A,* $P_{ced-8}CED\text{-}8^{WT}$*::GFP, unc-76* rescuing plasmid that is used as the transgene marker. This strain is considered to be wild-type regarding *ced-8*. (B) *unc-76(e911); ced-8(n1891)* worms are injected with 2 plasmids: P_{hsp}*mcherry::CEI-1A* and *unc-76* rescuing plasmid as the transgenic marker. *ced-8(n1891)* is a null allele. (C) *unc-76(e911); ced-8(n1891)* worms are injected with 3 plasmids: P_{hsp}*mcherry::CEI-1A,* $P_{ced-8}CED\text{-}8^{WT}$*::GFP* and *unc-76* rescuing plasmid that is used as the transgene marker. $P_{ced-8}CED\text{-}8^{WT}$*::GFP* expresses full-length CED-8 under the control of the *ced-8* promoter. (D) *unc-76(e911); ced-8(n1891)* worms are injected with 3 plasmids: P_{hsp}*mCherry::CEI-1A,* P_{ced-8}*acCED-8::GFP or called* P_{ced-8}*acCED-8::GFP* and *unc-76* rescuing plasmid used as the transgene marker. P_{ced-8}*acCED-8::GFP* expresses the activated form of CED-8 that lacks the first 21 amino acids under the control of the *ced-8* promoter. Exposure time for each fluorescent image was identical (500 ms). Scale bars, 5 μm.

4.2.9 Interaction between CEI-1 and CED-8 requires the N-terminus of CED-8.

I confirmed the binding between CEI-1 and CED-8 using a GST fusion protein pull-down assay. Both CEI-1 variants with GST tag are purified through glutathione (GSH) conjugated beads. Utilizing the *in vitro* transcription and translation system that is supplied with ^{35}S-Methionine, four CED-8 protein variants are synthesized and labeled with ^{35}S-Met: full length CED-8 (CED-8^{WT}), acCED-8 that lacks the first 21aa (acCED-8 or CED-8$^{\Delta 21}$), CED-8 containing the LLL to AAA mutation (CED-8$^{LLL/AAA}$), and CED-8 containing the KSK to AAA mutation (CED-8$^{KSK/AAA}$). In order to compare the binding affinity between CED-8^{WT} and CED-8$^{\Delta 21}$, I included an additional sample besides these four CED-8 variants, in which CED-8^{WT} and CED-8$^{\Delta 21}$ are mixed together in 1:1 ratio (Fig. 4.6B). The recombinant GST protein does not pull down any of the CED-8 variants (Fig. 4.6E). Both CEI-1A and CEI-1B bound CED-8^{WT} much better than CED-8$^{\Delta 21}$ (Fig. 4.6C, and D). In addition, there is no obvious decrease in binding affinity between CEI-1A/B and CED-8 when its N-terminal inhibitory motif is mutated (Fig. 4.6C, and D). Therefore, these *in vitro* binding data show that the N-terminus of CED-8 is crucial for the interaction between CED-8 and CEI-1. Specifically, lack of the 21aa N-terminus of CED-8 severely disrupts the binding affinity between CEI-1 and CED-8. Mutations in the inhibitory motif, LLL/AAA and KSK/AAA, however, do not obviously affect the binding affinity between CED-8 and CEI-1. These results indicate that an unknown mechanism, other than interfering with the binding to CEI-1, may account for the gain-of-function effect caused by two sets of CED-8 mutations, CED-8$^{LLL/AAA}$ and CED-8$^{KSK/AAA}$ as discussed in the subsections of 4.2.2, 4.2.3, 4.2.4 and 4.2.5.

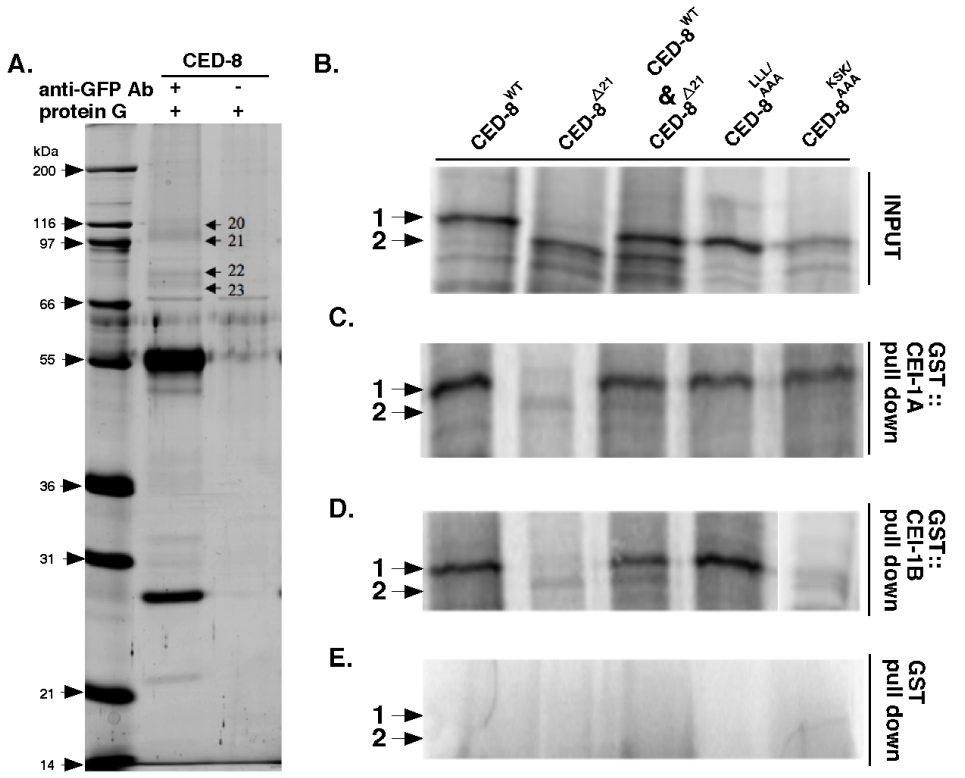

Fig. 4. 6. *In vitro* interaction between CEI-1 and CED-8 via its N-terminus region. (A) Silvering stained gel of the samples that immune-precipitate with CED-8::GFP fusion proteins. CEI-1 is identified from band 22 via mass spectrum. 48 peptides in band 22 that had been sequenced in the mass spectrum are specific to CEI-1. The molecular weight of CEI-1A is 84.8kDa, whereas CEI-1B that lacks the N-terminal 26 amino acids is 81.5kDa. **(B-E)** *In vitro* GST pull down assays show that CEI-1 interacts with CED-8. The molecular weight of CED-8^{WT} is 53.3kDa, whereas CED-$8^{\Delta 21}$ that lacks the first 21 amino acids is 50.7kDa. Arrow 1 indicates the band corresponding to, CED-8^{WT}, CED-$8^{LLL/AAA}$ and CED-$8^{KSK/AAA}$, all at 53.3kDa; arrow 2 indicates the band corresponding to CED-$8^{\Delta 21}$. Shown in B are five input samples of CED-8 variants: CED-8^{WT}, CED-$8^{\Delta 21}$, the mixture of CED-8^{WT} and CED-$8^{\Delta 21}$ in 1:1 ratio, CED-$8^{LLL/AAA}$, and CED-$8^{KSK/AAA}$. C shows the pull down results using the recombinant GST::CEI-1A fusion protein. D shows the pull down results using the recombinant GST::CEI-1B fusion protein. E shows the pull down results using the recombinant GST protein.

4.2.10 CEI-1 suppresses apoptosis through CED-8.

To verify the role of CEI-1 as an apoptosis suppressor, I counted the numbers of cell corpses during different embryonic stages when most apoptosis in *C. elegans* occurs. The cell corpse assay is a routine cell death assay in *C. elegans*. During *C. elegans* development, 131 of the 1090 somatic cells generated undergo apoptosis invariantly from animal to animal (*193*), the

majority of which occur in the embryonic development stages (*194*),. By scoring the cell corpse number at each embryonic stage in mutant embryos, genes that play various roles in apoptosis can be characterized. For example, mutations of genes that are responsible for apoptosis initiation or execution often cause reduction of cell corpses or delay of cell corpses appearnce (*214*). Mutations of genes that are involved in cell corpse engulfment usually cause increased cell corpse numbers in all embryonic stages, due to failure to remove cell corpses (*202*). Therefore, cell corpses accumulate in the engulfment-defect mutants. The cell corpse numbers normally increase, when a gene that suppresses cell death is defective.

To determine the role of CEI-1 in apoptosis, I counted cell corpses in embryos of the *cei-1(tm5740)* strain. *cei-1(tm5740)* is a deletion that removes a big segment of the *cei-1* coding region. Compared to the wild-type (N2) animals, the 2-fold stage *cei-1(tm5740)* embryos have significantly more cell corpses. There is no statistically increase in cell corpse numbers among all other embryonic stages. I also introduced *cei-1(tm5740)* into engulfment-defective backgrounds, which provide more sensitive backgrounds to detect the effect caused by mutating *cei-1*, because cell corpses persist longer. In *cei-1(tm5740); ced-7(n2094)* embryos, the cell corpse number increases at bean/comma, 2-fold, 2.5-fold stages. However, the cell corpse number of *cei-1(tm5740); ced-7(n2094)* decreases unexpectedly at 4-fold stage. Moreover, in *cei-1(tm5740); ced-2(n1994)* embryos, the cell corpse numbers increase at the bean, 3-fold and 4-fold stages. The cell corpse data observed in the engulfment-defective strains are consistent with CEI-1 acting as a suppressor of apoptosis.

In *ced-8(n1891)*, a delay-of-cell-corpse phenotype is observed. Expression of the wild-type CED-8 can rescue this delay-of-cell-corpse phenotype (Fig. 4.1D). However, expression of the cleavage-resistant mutant CED-8^{D21E} is unable to rescue the delay-of-cell-corpse phenotype (*207*) (Fig. 4.1D). This result indicates that CED-8 needs to be cleaved and released from the suppression mediated by the N-terminal inhibitory motif, in order to promote apoptosis. If the

sole function of the N-terminal inhibitory motif of CED-8 is to recruit CEI-1A, this N-terminal CED-3 cleavage will become dispensable in cells without CEI-1. To test this hypothesis, I introduced *cei-1(tm5740)* into the CED-8^{D21E} transgenic strain. The CED-8^{D21E} transgene became able to partially rescue the delay-of-cell-corpse phenotype caused by *ced-8(n1891)*, when CEI-1 is absent in embryos of *cei-1(tm5740); Is[*P_{ced-8}*CED-*8^{D21E}*]; ced-8(n1891)*. The cell corpse number at 4-fold stage is close to that of wild-type embryos, indicating complete rescue, whereas the cell corpse number at bean/comma stage slightly increases compared with that of *ced-8(n1891)* embryos, indicating partial rescue.

A more elegant experiment is performed in gene edited CED-8^{D21E} knock-in strain. The CED-8^{D21E} knock-in strain shows a delay-of-cell-death phenotype, very similar to that of the *ced-8(n1891)* strain. In *cei-1(tm5740); ced-8(smt236)* embryos (*smt236* is a CED-8^{D21E} gene edited allele), the phenotype of delay-of-cell-death is partially reversed. The cell death defect at the bean/comma stage was partially rescued, whereas the cell corpse defect at the 4-fold stage was almost completely rescued. Thus, these results confirm the role of CEI-1 as a CED-8 suppressor.

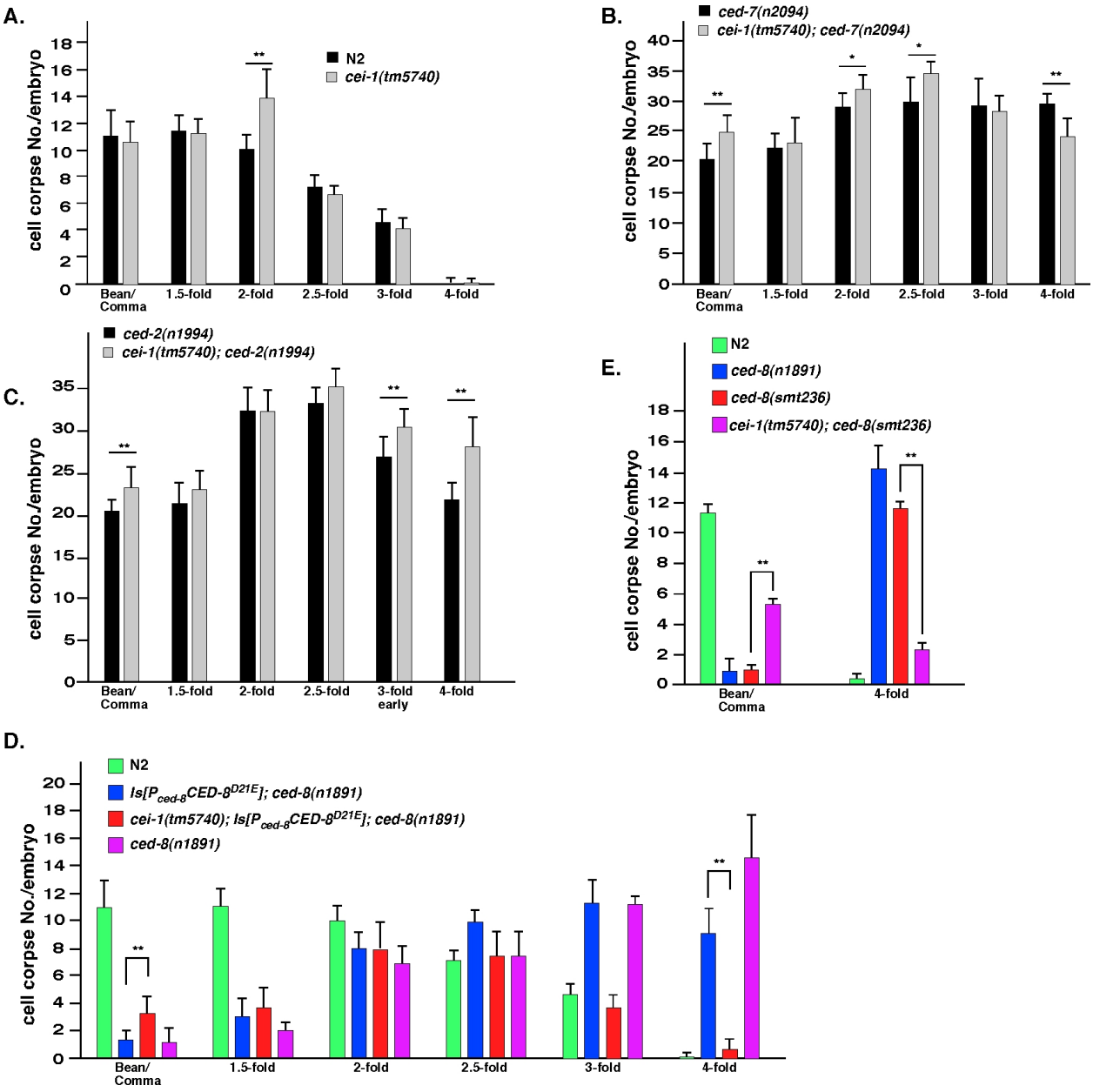

Fig. 4. 7. CEI-1 suppresses the pro-apoptotic function of CED-8. (A-E) Cell corpses are scored in embryos with the indicated genotypes and embryonic stages. The average number of cell corpses ± SD (standard deviation) are shown (n=15 embryos at each stage). ** $p<0.001$, * $0.001<p<0.01$ by student *t* test. *smt236* is the gene editing allele of *ced-8*, in which the endogenous *ced-8* gene contains a D21E substitution.

4.3 Discussion and Future Directions

Despite of decades of effort to elucidate the evolutionarily conserved pathway that regulates and mediates apoptosis, a significant number of those identified members from

genetic studies have not been characterized. *ced-8* ranks at the top of the list of previously uncharacterized factors. The *ced-8* mutant embryos display a delay-of-cell-death phenotype (*208*). However, little is known about the mechanism, by which *ced-8* executes its role in controlling the timing of programmed cell death (*208*). One possible scenario by which CED-8 regulates the kinetics of apoptosis is that CED-8 plays a positive feedback role in activating CED-3, the sole caspase in *C. elegans*. CED-8 is supposed to act downstream of CED-3 as one of its substrates (*207*). The positive feedback loop of CED-8 to further activate CED-3 theoretically can accelerate the process of programmed cell death, which is consistent with the prolonged or delayed apoptosis kinetics observed in *ced-8(n1891)*. However, there is no solid evidence to support the existence of this feedback loop mediated by CED-8. The data that shows the killing activity of CED-8$^{LLL/AAA}$ or CED-8$^{KSK/AAA}$ is partially dependent on CED-3, suggests, for the first time, existence of such a positive feedback loop from CED-8 to CED-3.

Another important function of CED-8 is to promote PS externalization during apoptosis (*207*). PS, as an important engulfment signal, need to be restricted in the inner leaflet of the plasma membrane in living cells (*198*). The maintenance of PS asymmetry is an energy-dependent process, which is mediated by the P4 ATPase, TAT-1/CHAT-1 complexes (*211*). During apoptosis, CED-8 is cleaved to promote the externalization of PS as well as other aspects of apoptosis via a poorly understood mechanism (*207*). In this chapter of my dissertation, I identified a KSKLLL motif within the N-terminal inhibitory domain of CED-8. Expression of CED-8 mutants containing mutations in this motif, CED-8$^{LLL/AAA}$ or CED-8$^{KSK/AAA}$, causes ectopic PS flipping even in cells that do not undergo apoptosis. Interestingly, the PS staining pattern induced by CED-8$^{KSK/AAA}$ is similar to that induced by CED-8$^{\Delta 21}$. However, the CED-8$^{LLL/AAA}$ induces a unique PS staining pattern, where living cells not only flip out PS, but also may efflux PS positive vesicles to the extracellular space. CED-8$^{LLL/AAA}$ or CED-8$^{KSK/AAA}$ has unanticipated strong cell killing activity, which is different from the activated CED-8 (CED-8$^{\Delta 21}$).

One future direction of this project is to fully characterize those two gain-of-function mutations that confer CED-8 such unique properties.

Another finding from this project is the identification of CEI-1A as a suppressor that associates with CED-8. The *cei-1* gene encodes two alternative transcriptional forms: 'A' form, which targets to the plasma membrane; 'B' form which targets to the mitochondria. This is an exemplary case where one gene can achieve differential functions through alternative splicing and targeting of the products to different subcellular compartments. CEI-1A binds specifically to the full-length CED-8, but not to the acCED-8, which is consistent with the role of CEI-1A in suppressing the pro-apoptotic function of CED-8 in living cells. Several important questions remain unanswered regarding this protein. Is the enzymatic activity of acetyl-CoA dehydrogenase associated with its regulation of CED-8? Furthermore, does CED-8 form a "barrel" structure that spans across the plasma membrane due to its eight transmembrane domains and that is typically seen with a lipid transporter? If so, CEI-1 could possibly block the CED-8 "barrel" from opening that faces the cytoplasm. The localization data suggest that the 'A' form, but not 'B' form of CEI-1 is related to CED-8 regulation. I will generate specific knock-in mutation to disrupt the CEI-1A form and keep CEI-1B unaffected by mutating the start codon of CEI-1A using the CRISPR/cas9 gene editing technique (*217*). The results summarized in this chapter do not completely decipher the mechanism, by which CED-8 is regulated. However, the identification of the *cis-acting* element and the *tran-sacting* factors makes numerous future characterizations possible.

4.4 Material and Methods

4.4.1 Strains and culture conditions

C. elegans strains were maintained using standard procedures (*218*). The following alleles were used in the genetic analyses: LGI, *cei-1(tm5740), mec-6(e1342), ;* LGIII, *ced-7(n2094), clp-1(tm690)*; LGIV, *ced-2(n1994), ced-3(n717), psr-1(tm469)*; LGV, *unc-76(e911)*; and LGX, *ced-8(n1891), ced-8(smt236), bzIs8, smIs434*. The chromosome information, where the integrated allele, *Is[P_{ced-8}CED-8^{D21E}] and Is[P_{mec-7}CED-$8^{LLL/AAA}$]* are on, is not known. *smIs434* is an integrated transgene generated by ultraviolet irradiation of animals carrying extrachromosomal arrays containing *P_{hsp}GFP::Lact* (*212*). They were backcrossed four times with wild-type animals before being used for genetic analyses. *bzIs8* carries a transgene of *P_{mec-4}GFP*, which only expresses in the six touch receptor neurons.

4.4.2 Transgenic animals

Transgenic animals were generated using standard protocols (*219*). *P_{hsp}CED-8^{WT}, P_{hsp}CED-8^{D21E}, P_{hsp}CED-$8^{LLL/AAA}$, P_{hsp}CED-$8^{KSK/AAA}$, P_{hsp}CED-$8^{FL/AA}$, P_{hsp}CED-$8^{KKH/AAA}$, P_{hsp}CED-$8^{VPR/AAA}$, and P_{hsp}CED-$8^{DEEQ/AAAA}$* were injected into *ced-8(n1891)* animals (at 5 ng/µl each) along with a *sur-5::mCherry* plasmid at (25 ng/µl) as a co-injection marker, which directs mCherry expression in all epithelial cells in most developmental stages (*220*). *P_{hsp}CED-8^{WT}, P_{hsp}CED-$8^{\Delta 21}$, P_{hsp}CED-$8^{LLL/AAA}$, and P_{hsp}CED-$8^{KSK/AAA}$* were injected into *smIs434* or *ced-3(n1891); smIs434* animals (at 25 ng/µl) along with a *sur-5::mCherry* plasmid (at 25 ng/µl) as a co-injection marker. *P_{hsp}CED-$8^{LLL/AAA}$* were injected into *ced-7(n2094); smIs434* animals (at 25 ng/µl) along with a *sur-5::mCherry* plasmid (at 25 ng/µl) as a co-injection marker. *P_{mec-7}CED-8^{WT}, P_{mec-7}CED-$8^{\Delta 21}$, P_{mec-7}CED-$8^{LLL/AAA}$, and P_{mec-7}CED-$8^{KSK/AAA}$* were injected into *bzIs8, or ced-3(n717); bzIs8, or ced-7(n2094); bzIs8, or ced-2(n1994); bzIs8, or psr-1(tm469); bzIs8* animals (at 25 ng/µl) along with a *sur-5::mCherry* and *rol-6* plasmid (each at 25 ng/µl) as a co-injection marker.

P_{hsp}*mCherry::CEI-1A* and P_{ced-8}*CED-8::GFP* were injected into *un-76(e911)* animals (at 25 ng/µl) along with an *unc-76* rescue plasmid (at 25 ng/µl) as a co-injection marker. P_{hsp}*mCherry::CEI-1B* and P_{sup-26}*CYN-1::GFP* were injected into *un-76(e911)* animals (at 25 ng/µl) along with an *unc-76* rescue plasmid (at 25 ng/µl) as a co-injection marker. *sup-26* promoter is a constitutive promoter that express protein globally throughout the embryos. P_{hsp}*mCherry::CEI-1A* were injected into *un-76(e911); ced-8(n1891)* animals at 25 ng/µl along with an unc-76 rescue plasmid (at 25 ng/µl) as a co-injection marker. P_{hsp}*mCherry::CEI-1A* and P_{ced-8}*CED-8*^{WT}*::GFP* or P_{ced-8}*CED-8*$^{\Delta 21}$*::GFP* were injected into *un-76(e911); ced-8(n1891)* animals (at 25 ng/µl) along with an *unc-76* rescue plasmid (at 25 ng/µl) as a co-injection marker. The *ced-8(smt236)* allele contains a D21E mutation in the endogenous locus of ced-8, which is done by CRISPR gene editing (*217*).

4.4.3 Quantification of cell corpses

The number of cell corpses in living embryos was scored using Nomarski optics (*84*).

4.4.4 Heat-shock treatment

Embryos with heatshock promoter transgenes were placed at 33°C for 45 min, followed by recovery at room temperature for 2 h.

4.4.5 Microscopy

For fluorescent microscopy, *C. elegans* embryos were mounted on agar pads and observed using × 100 optics on Axioplan 2 microscopes (Zeiss). Fluorescence and differential contrast interference images were captured using a charge-coupled device camera (PCO SensiCam) coupled with the Slidebook 5.0 software.

4.4.6 Molecular biology

In the alanine scanning experiments, the CED-8 mutations are introduced by PCR with CED-8 N-terminal sense primers that have corresponding mutations and a CED-8 antisense primer. The PCR constructs are subcloned into a vector that has a heat-shock promoter. To construct the plasmids used in the PLM neuron lethality assays, the corresponding CED-8 variants are PCRed and subcloned to the pPD52.102 with a *mec-7* promoter that is specific to touch receptor neurons. For CEI-1 constructs, the 'A' form and 'B' form genomic DNA are PCRed from a fosmid containing the CEI-1 gene before fusing with the mCherry coding fragment. The translational fusion of mCherry and CEI-1 are then subcloned to the vector with a heat-shock promoter.

4.4.7 Statistical analysis

P-values represent analysis from two-tailed Student's t-tests. **P<0.01; **P<0.001*.

4.4.8 TNT (*in vitro* transcription and translation) expression of CED-8

Briefly, CED-8 variants under the control of T7 promoter were synthesized and labeled with ^{35}S-methionine with TNT Transcription and Translation coupled system (Promega). The cruel products are used for GST pull down assay. The samples are resolved by 12% SDS-PAGE gel and are subjected to autoradiography.

4.4.9 GST Fusion Protein Pull-Down Assays

Purified GST-CEI-1 proteins or GST protein immobilized on Glutathione Sepharose beads (Pharmacia) were incubated with ^{35}S labeled CED-8 variants for 1-3 hr at 4°C in 500 μl binding buffer [150 mM NaCl, 10 mM HEPES (pH 7.6), 5 mM $MgCl_2$, 1 mM EDTA, 0.1% NP40, 1.0 mM DTT, 2.5 mg/ml BSA]. The resin was washed three times with 1 ml binding buffer and

one time with 1 ml binding buffer without BSA. The bound protein complexes were resolved on a 12% SDS polyacrylamide gel and subjected to autoradiography.

4.4.10 Quantification of posterior lateral microtubule neuron (PLM) Killing by CED-8 mutations

PLM neurons were scored in L4 larvae in the presence of the integrated transgene, *bzIs8*, using a Nomarski microscope equipped with epifluorescence (*210*).

Contribution statement: Dr. Ding Xue and I design the experiments in this chapter. Dr. Yong Shi performed the mass spectrum identification of CEI-1. I did all the rest of experiments in this chapter.

Chapter 5

Conclusions and Future Work

C. elegans is an established model organism used to study fundamental biological processes. The powerful genetic tools available in *C. elegans* provide feasible and simplified ways to decipher complex biological processes. *C. elegans* is particularly suitable to study highly conserved pathways (*218*). For example, programmed cell death, one of the most important aspects in animal development, is conserved in all multicellular organisms (*221, 222*). The nematode *C.elegans* has become an excellent animal model to study the apoptotic pathways. This transparent animal, in which all the cells have invariant life vs. death fates, allows for studies on programmed cell death at a single cell resolution in a way that no other systems can currently match.

Nowadays, novel technological innovations, such as gene editing (*223*) and deep sequencing (*224*), offer new opportunities to worm geneticists. Many phenomena or proteins that the scientific community was not previously able to characterize now become possible. Moreover, a substantial proportion of already known pathways or mechanisms can be revisited and reanalyzed in a more elegant and accurate fashion. Previously, many studies have been performed with multi-copy transgene methods. The high-copy number transgenes result in overexpression of proteins, the concentration of which may have been 1000 times of the physiological concentration. Free floating proteins at such a high concentration are able to interact non-specifically with other proteins besides their true binding partners, which often lead to false-positive results. Thus, the studies where high-copy transgene methods were used should be revisited by single-copy insertion or gene editing as a more accurate method to insure the validity and reproducibility of the work.

Our understanding of the mechanisms underlying programmed cell death benefits a lot

from the canonical forward genetic screenings for CEll Death abnormal (CED) mutants in *C. elegans (214, 218)*. Through these screens, the core pathways that are responsible for activation of apoptosis, execution of cell death, and engulfment of apoptotic cells are identified (Fig. 5. 1). In response to either extrinsic or intrinsic upstream apoptotic stimuli, *egl-1* is transcriptionally activated. After activation, EGL-1 inhibits the anti-apoptotic function of CED-9 (*225*) that serves to trap the pro-apoptotic factor CED-4 in its inactive form (*226*) and results in release of CED-4 from CED-9. Released CED-4 oligomerizes and assists in the activation of the inactive CED-3 zymogen (*221*). Activation of CED-3 then triggers an arsenal of killing machineries that execute specified tasks of the suicide program. The final destination for an apoptotic cell is to the phagocytes that can remove cell corpses through a process called engulfment. There are two parallel engulfment pathways in *C. elegans*. One pathway includes: *ced-1, ced-6, and ced-7*; while the second pathway consists of: *ced-2, ced-5, and ced-10 (201, 202)*. Both pathways utilize surface-exposed PS as the “eat-me” signal to recognize cell corpses. One of the major functions of CED-8 is to disrupt PS asymmetry maintained in the plasma membrane during apoptosis to cause PS externalization (*207*).

In chapter IV, I discussed the underlying mechanism, by which CED-8 is regulated. First of all, I identified an inhibitory motif within the N-terminus of CED-8. The two mutations of the inhibitory motif, LLL/AAA and KSK/AAA, exhibit unique properties that are different from the active form of CED-8, CED-8$^{\Delta 21}$. Second, an alternatively spliced form of the *cei-1* gene, (CED-8 Interaction protein) was found to associate with CED-8 and suppress its pro-apoptotic function in normal cells. My research in Chapter IV mainly deals with the regulatory events of CED-8. However, more studies are needed to focus on the downstream events of activated CED-8. This is crucial in order to uncover the mechanisms by which CED-8 promotes two aspects of cell death, the kinetics of apoptosis (*208*) and PS exposure (*207*). Studies on the mammalian homolog of CED-8, Xkr-8, have proposed that Xkr-8 itself is a scramblase that transports PS bi-

directionally between the two leaflets of plasma membrane (*227, 228*). However, this hypothesis has not yet been supported by an *in vitro* scramblase assay with purified recombinant proteins.

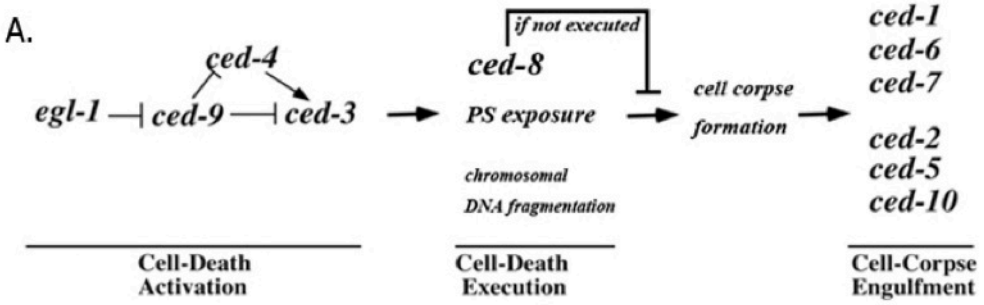

Fig. 5. 1. The apoptosis pathway in the nematode *Caenorhabditis elegans*. The CED (CEll Death abnormal) proteins are categorized into three sequential pathways that are involved in Cell-Death activation, Cell-Death Execution, and Cell-Corpse Engulfment.

In chapter II and III of my dissertation, another highly conserved developmental process, the paternal mitochondrial elimination (PME), is analyzed. PME guarantees the strict maternal inheritance pattern of mitochondria. In chapter II, a mitochondria nuclease, CPS-6, is identified as the DNase that promotes degradation of the paternal mitochondrial DNA and internal breakdown of paternal mitochondria (*14*). In chapter III, *pdr-1*, the *C. elegans* homolog of Parkin, was characterized under the context of PME. PME and apoptosis are similar in many ways. First, both processes involve nucleases to degrade nuclear and mitochondrial genomes, respectively. The most interesting part is that CPS-6 is involved in both processes. During apoptosis, CPS-6 residing within the intermembrane space of mitochondria is released to relocate into the nucleus where it promotes chromatin DNA fragmentation (*84*). While during PME, the CPS-6 in the paternal mitochondria relocates into the mitochondrial matrix and degrades the mitochondrial DNA. Thus, CPS-6 seems to be the specified nuclease involved in both suicide mechanisms. Moreover, both apoptotic cell corpses and paternal mitochondria are engulfed through membrane encapsulation. The apoptotic cell corpse is engulfed through the

process of phagocytosis, whereas the paternal mitochondria are engulfed by the autophagosome (*34, 35*). The complete degradation of engulfed apoptotic cell corpses and paternal mitochondria enclosed within autophagosomes is finished following the fusion between the phagosome or autophagosome and lysosomes (*34, 35, 229, 230*).

In chapter III, I characterized the conserved role of Parkin in regulating autophagy during the process of PME. In mammalian neurons, Parkin is important to maintain the quality of the mitochondria by removing unhealthy mitochondria via mitophagy (*84*). During PME, we found that paternal mitochondria lose their membrane potential immediately after fertilization (*14*). Parkin recognizes those depolarized paternal mitochondria and marks them for selective degradation via accurate expansion and enclosure of autophagosome membrane. Without Parkin, the autophagosomes nonspecifically engulf maternal organelles, which cause a delay of PME, as well as embryonic lethality, probably due to the loss of maternal healthy organelles. Parkin, mutations of which cause familial Parkinson's diseases, thus plays a conserved role in regulating autophagy that targets mitochondria as their cargos.

Overall, *C. elegans* provides us with an excellent system to study the conserved cellular pathways. Although genetic studies are powerful enough to find and verify the fundamental components of an uncharacterized pathway, its limitations lie in the ability to figure out the detailed biochemical mechanisms behind many biological processes. The future research pertaining to the Parkin project and the CED-8 project should be focused on the *in vitro* biochemical characterization. The major question that remains unanswered is how Parkin participates in PME via its E3 ubiquitination ligase activity. In the CED-8 project, characterization of the two gain-of-function mutations, CED-8$^{KSK/AAA}$ and CED-8$^{LLL/AAA}$, seems to provide the clues necessary to fully understand the mechanisms by which acCED-8 promotes cell death. As I continue my journey to uncover the great mystery of life, the ability to think like a geneticist will light my way.

Bibliography

1. L. Margulis, Origin of eukaryotic cells: evidence and research implications for a theory of the origin and evolution of microbial, plant, and animal cells on the Precambrian earth. (1970).

2. S. B. Vafai, V. K. Mootha, Mitochondrial disorders as windows into an ancient organelle. *Nature* **491**, 374 (2012).

3. N. Lane, W. Martin, The energetics of genome complexity. *Nature* **467**, 929 (2010).

4. X. Wang, The expanding role of mitochondria in apoptosis. *Genes & development* **15**, 2922 (2001).

5. E. Kayal *et al.*, Evolution of linear mitochondrial genomes in *medusozoan cnidarians*. *Genome Biology and Evolution* **4**, 1 (2012).

6. A. J. Bendich, DNA abandonment and the mechanisms of uniparental inheritance of mitochondria and chloroplasts. *Chromosome research* **21**, 287 (2013).

7. B. Lemire, Mitochondrial genetics. (2005).

8. D. J. Pagliarini *et al.*, A mitochondrial protein compendium elucidates complex I disease biology. *Cell* **134**, 112 (2008).

9. A. F. Huettner, M. Rabinowitz, Demonstration of the central body in the living cell. *Science* **78**, 367 (1933).

10. A. P. Mahowald, J. M. Strassheim, INTERCELLULAR MIGRATION OF CENTRIOLES IN THE GERMARIUM OF *DROSOPHILA MELANOGASTER* An Electron Microscopic Study. *The Journal of Cell Biology* **45**, 306 (1970).

11. A. Pimenta-Marques *et al.*, A mechanism for the elimination of the female gamete centrosome in *Drosophila melanogaster*. *Science*, aaf4866 0036 (2016).

12. S. Geisler *et al.*, PINK1/Parkin-mediated mitophagy is dependent on VDAC1 and p62/SQSTM1. *Nature cell biology* **12**, 119 (2010).

13. N. Matsuda *et al.*, PINK1 stabilized by mitochondrial depolarization recruits Parkin to damaged mitochondria and activates latent Parkin for mitophagy. *The Journal of cell biology* **189**, 211 (2010).

14. Q. Zhou *et al.*, Mitochondrial endonuclease G mediates breakdown of paternal mitochondria upon fertilization. *Science* **353**, 394 (2016).

15. B. Chance, G. R. Williams, A method for the localization of sites for oxidative phosphorylation. *Nature* **176**, 250 (1955).

16. C. R. Hackenbrock, B. Chazotte, S. S. Gupte, The random collision model and a critical assessment of diffusion and collision in mitochondrial electron transport. *Journal of bioenergetics and biomembranes* **18**, 331 (1986).

17. H. Schägger, K. Pfeiffer, The ratio of oxidative phosphorylation complexes I–V in bovine heart mitochondria and the composition of respiratory chain supercomplexes. *Journal of Biological Chemistry* **276**, 37861 (2001).

18. H. Schägger, G. von Jagow, Blue native electrophoresis for isolation of membrane protein complexes in enzymatically active form. *Analytical biochemistry* **199**, 223 (1991).

19. C.-M. Cruciat, S. Brunner, F. Baumann, W. Neupert, R. A. Stuart, The Cytochrome bc 1 and Cytochromec Oxidase Complexes Associate to Form a Single Supracomplex in Yeast Mitochondria. *Journal of Biological Chemistry* **275**, 18093 (2000).

20. X. Jiang *et al.*, A Small Molecule That Protects the Integrity of the Electron Transfer Chain Blocks the Mitochondrial Apoptotic Pathway. *Molecular Cell* **63**, 229 (2016).

21. X. Jiang, H. Jiang, Z. Shen, X. Wang, Activation of mitochondrial protease OMA1 by Bax and Bak promotes cytochrome c release during apoptosis. *Proceedings of the National Academy of Sciences* **111**, 14782 (2014).

22. Y. Wang *et al.*, Kinetics and specificity of paternal mitochondrial elimination in *Caenorhabditis elegans*. *Nature Communications* **7**, 12569 2041 (2016).

23. K. W. Osteryoung, Organelle fission. Crossing the evolutionary divide. *Plant physiology* **123**, 1213 (2000).

24. R. S. Williams, Mitochondrial gene expression in mammalian striated muscle. Evidence that variation in gene dosage is the major regulatory event. *Journal of Biological Chemistry* **261**, 12390 (1986).

25. R. S. Williams, S. Salmons, E. A. Newsholme, R. E. Kaufman, J. Mellor, Regulation of nuclear and mitochondrial gene expression by contractile activity in skeletal muscle. *Journal of Biological Chemistry* **261**, 376 (1986).

26. A. Chomyn, Mitochondrial genetic control of assembly and function of complex I in mammalian cells. *Journal of bioenergetics and biomembranes* **33**, 251 (2001).

27. Y. Bai, R. M. Shakeley, G. Attardi, Tight control of respiration by NADH dehydrogenase ND5 subunit gene expression in mouse mitochondria. *Molecular and cellular biology* **20**, 805 (2000).

28. J. I. Piruat, J. López-Barneo, Oxygen tension regulates mitochondrial DNA-encoded complex I gene expression. *Journal of Biological Chemistry* **280**, 42676 (2005).

29. C. M. Haynes, D. Ron, The mitochondrial UPR–protecting organelle protein homeostasis. *J Cell Sci* **123**, 3849 (2010).

30. N. Mizushima, T. Yoshimori, Y. Ohsumi, The role of Atg proteins in autophagosome formation. *Annual review of cell and developmental biology* **27**, 107 (2011).

31. Z. Xie, D. J. Klionsky, Autophagosome formation: core machinery and adaptations. *Nature cell biology* **9**, 1102 (2007).

32. M. Sato, K. Sato, Maternal inheritance of mitochondrial DNA: Degradation of paternal mitochondria by allogeneic organelle autophagy, allophagy. *Autophagy* **8**, 424 (2012).

33. S. Al Rawi *et al.*, Allophagy: a macroautophagic process degrading spermatozoid-inherited organelles. *Autophagy* **8**, 421 (2012).

34. S. Al Rawi *et al.*, Postfertilization autophagy of sperm organelles prevents paternal mitochondrial DNA transmission. *Science* **334**, 1144 (2011).

35. M. Sato, K. Sato, Degradation of paternal mitochondria by fertilization-triggered autophagy in *C. elegans* embryos. *Science* **334**, 1141 (2011).

36. Q. Zhou, H. Li, D. Xue, Elimination of paternal mitochondria through the lysosomal degradation pathway in *C. elegans*. *Cell research* **21**, 1662 (2011).

37. C. Hajjar, K. M. Sampuda, L. Boyd, Dual roles for ubiquitination in the processing of sperm organelles after fertilization. *BMC developmental biology* **14**, 1 1471 (2014).

38. M. Manil-Ségalen *et al.*, The *C. elegans* LC3 acts downstream of GABARAP to degrade autophagosomes by interacting with the HOPS subunit VPS39. *Developmental cell* **28**, 43 (2014).

39. A. Djeddi *et al.*, Sperm-inherited organelle clearance in *C. elegans* relies on LC3-dependent autophagosome targeting to the pericentrosomal area. *Development* **142**, 1705 (2015).

40. E. Shvets, A. Abada, H. Weidberg, Z. Elazar, Dissecting the involvement of LC3B and GATE-16 in p62 recruitment into autophagosomes. *Autophagy* **7**, 683 (2011).

41. F. Wu *et al.*, Structural basis of the differential function of the two *C. elegans* Atg8 homologs, LGG-1 and LGG-2, in autophagy. *Molecular cell* **60**, 914 (2015).

42. F. Wu, P. Wang, Y. Shen, N. N. Noda, H. Zhang, Small differences make a big impact: Structural insights into the differential function of the 2 Atg8 homologs in *C. elegans*. *Autophagy* **12**, 606 (2016).

43. K. T. Tokuyasu, Dynamics of spermiogenesis in *Drosophila melanogaster*. VI. Significance of “onion” nebenkern formation. *Journal of ultrastructure research* **53**, 93 (1975).

44. K. T. Tokuyasu, Dynamics of spermiogenesis in *Drosophila melanogaster*: III. Relation between axoneme and mitochondrial derivatives. *Experimental cell research* **84**, 239 (1974).

45. S. Z. DeLuca, P. H. O'Farrell, Barriers to male transmission of mitochondrial DNA in sperm development. *Developmental cell* **22**, 660 (2012).

46. J. N. Wolff, P. Sutovsky, J. W. O. Ballard, Mitochondrial DNA content of mature spermatozoa and oocytes in the genetic model *Drosophila*. *Cell and tissue research* **353**, 195 (2013).

47. Y. Politi *et al.*, Paternal mitochondrial destruction after fertilization is mediated by a common endocytic and autophagic pathway in *Drosophila*. *Developmental cell* **29**, 305 (2014).

48. Y.-X. Jin *et al.*, Autophagy and ubiquitin-mediated proteolysis may not be involved in the degradation of spermatozoon mitochondria in mouse and porcine early embryos. *Zygote* **24**, 31 (2016).

49. S.-M. Luo *et al.*, Unique insights into maternal mitochondrial inheritance in mice. *Proceedings of the National Academy of Sciences* **110**, 13038 (2013).

50. S.-M. Luo, Q.-Y. Sun, Autophagy is not involved in the degradation of sperm mitochondria after fertilization in mice. *Autophagy* **9**, 2156 (2013).

51. S.-M. Luo, H. Schatten, Q.-Y. Sun, Sperm mitochondria in reproduction: good or bad and where do they go? *Journal of Genetics and Genomics* **40**, 549 (2013).

52. W.-H. Song, Y.-J. Yi, M. Sutovsky, S. Meyers, P. Sutovsky, Autophagy and ubiquitin–proteasome system contribute to sperm mitophagy after mammalian fertilization. *Proceedings of the National Academy of Sciences* **113**, E5261 (2016).

53. P. Sutovsky *et al.*, Ubiquitinated sperm mitochondria, selective proteolysis, and the regulation of mitochondrial inheritance in mammalian embryos. *Biology of Reproduction* **63**, 582 (2000).

54. W. E. Thompson, J. Ramalho-Santos, P. Sutovsky, Ubiquitination of prohibitin in mammalian sperm mitochondria: possible roles in the regulation of mitochondrial inheritance and sperm quality control. *Biology of reproduction* **69**, 254 (2003).

55. J. R. Friedman *et al.*, ER tubules mark sites of mitochondrial division. *Science* **334**, 358 (2011).

56. S. C. Lewis, L. F. Uchiyama, J. Nunnari, ER-mitochondria contacts couple mtDNA synthesis with mitochondrial division in human cells. *Science* **353**, aaf5549 0036 (2016).

57. A. Santel *et al.*, Mitofusin-1 protein is a generally expressed mediator of mitochondrial fusion in mammalian cells. *Journal of cell science* **116**, 2763 (2003).

58. D. Otsuga *et al.*, The dynamin-related GTPase, Dnm1p, controls mitochondrial morphology in yeast. *The Journal of cell biology* **143**, 333 (1998).

59. E. Smirnova, L. Griparic, D.-L. Shurland, A. M. Van Der Bliek, Dynamin-related protein Drp1 is required for mitochondrial division in mammalian cells. *Molecular biology of the cell* **12**, 2245 (2001).

60. F. Legros, A. Lombès, P. Frachon, M. Rojo, Mitochondrial Fusion in Human Cells Is Efficient, Requires the Inner Membrane Potential, and Is Mediated by Mitofusins§V. (2002).

61. Y. Eura, N. Ishihara, S. Yokota, K. Mihara, Two mitofusin proteins, mammalian homologues of FZO, with distinct functions are both required for mitochondrial fusion. *Journal of Biochemistry* **134**, 333 (2003).

62. G. Twig *et al.*, Fission and selective fusion govern mitochondrial segregation and elimination by autophagy. *The EMBO journal* **27**, 433 (2008).

63. R. J. Youle, A. M. Van Der Bliek, Mitochondrial fission, fusion, and stress. *Science* **337**, 1062 (2012).

64. A. S. Rambold, B. Kostelecky, N. Elia, J. Lippincott-Schwartz, Tubular network formation protects mitochondria from autophagosomal degradation during nutrient starvation. *Proceedings of the National Academy of Sciences* **108**, 10190 (2011).

65. L. C. Gomes, G. Di Benedetto, L. Scorrano, During autophagy mitochondria elongate, are spared from degradation and sustain cell viability. *Nature cell biology* **13**, 589 (2011).

66. B. Levine, V. Deretic, Unveiling the roles of autophagy in innate and adaptive immunity. *Nature Reviews Immunology* **7**, 767 (2007).

67. D. Schmid, C. Münz, Innate and adaptive immunity through autophagy. *Immunity* **27**, 11 (2007).

68. I. Nakagawa *et al.*, Autophagy defends cells against invading group A *Streptococcus*. *Science* **306**, 1037 (2004).

69. R. M. Andrade, M. Wessendarp, M.-J. Gubbels, B. Striepen, C. S. Subauste, CD40 induces macrophage anti–*Toxoplasma gondii* activity by triggering autophagy-dependent fusion of pathogen-containing vacuoles and lysosomes. *The Journal of clinical investigation* **116**, 2366 (2006).

70. Y. M. Ling *et al.*, Vacuolar and plasma membrane stripping and autophagic elimination of *Toxoplasma gondii* in primed effector macrophages. *The Journal of experimental medicine* **203**, 2063 (2006).

71. S. B. Singh, A. S. Davis, G. A. Taylor, V. Deretic, Human IRGM induces autophagy to eliminate intracellular *mycobacteria*. *Science* **313**, 1438 (2006).

72. C. L. Birmingham, A. C. Smith, M. A. Bakowski, T. Yoshimori, J. H. Brumell, Autophagy controls *Salmonella* infection in response to damage to the *Salmonella*-containing vacuole. *Journal of Biological Chemistry* **281**, 11374 (2006).

73. C. Checroun, T. D. Wehrly, E. R. Fischer, S. F. Hayes, J. Celli, Autophagy-mediated reentry of *Francisella tularensis* into the endocytic compartment after cytoplasmic replication. *Proceedings of the National Academy of Sciences* **103**, 14578 (2006).

74. M. Djavaheri-Mergny *et al.*, NF-κB activation represses tumor necrosis factor-α-induced autophagy. *Journal of Biological Chemistry* **281**, 30373 (2006).

75. P. S. Manzanillo *et al.*, The ubiquitin ligase parkin mediates resistance to intracellular pathogens. *Nature* **501**, 512 (2013).

76. B. F. Py, M. M. Lipinski, J. Yuan, Autophagy limits *Listeria monocytogenes* intracellular growth in the early phase of primary infection. *Autophagy* **3**, 117 (2007).

77. K. A. Rich, C. Burkett, P. Webster, Cytoplasmic bacteria can be targets for autophagy. *Cellular microbiology* **5**, 455 (2003).

78. R. Scherz-Shouval *et al.*, Reactive oxygen species are essential for autophagy and specifically regulate the activity of Atg4. *The EMBO journal* **26**, 1749 (2007).

79. K. A. Rich, C. Burkett, P. Webster, Cytoplasmic bacteria can be targets for autophagy. *Cellular microbiology* **5**, 455 (2003).

80. M. Ogawa *et al.*, Escape of intracellular Shigella from autophagy. *Science* **307**, 727 (2005).

81. A. O. Amer, M. S. Swanson, Autophagy is an immediate macrophage response to *Legionella pneumophila*. *Cellular microbiology* **7**, 765 (2005).

82. J. Celli *et al.*, Brucella evades macrophage killing via VirB-dependent sustained interactions with the endoplasmic reticulum. *The Journal of experimental medicine* **198**, 545 (2003).

83. P. Sutovsky, T. C. McCauley, M. Sutovsky, B. N. Day, Early degradation of paternal mitochondria in domestic pig (*Sus scrofa*) is prevented by selective proteasomal inhibitors lactacystin and MG132. *Biology of Reproduction* **68**, 1793 (2003).

84. J. Parrish *et al.*, Mitochondrial endonuclease G is important for apoptosis in *C. elegans*. *Nature* **412**, 90 (2001).

85. L. Y. Li, X. Luo, X. Wang, Endonuclease G is an apoptotic DNase when released from mitochondria. *Nature* **412**, 95 (2001).

86. X. Wang, C. Yang, J. Chai, Y. Shi, D. Xue, Mechanisms of AIF-mediated apoptotic DNA degradation in *Caenorhabditis elegans*. *Science* **298**, 1587 (2002).

87. P. Widlak, W. T. Garrard, Discovery, regulation, and action of the major apoptotic nucleases DFF40/CAD and endonuclease G. *Journal of cellular biochemistry* **94**, 1078 (2005).

88. J. L. J. Lin *et al.*, Structural insights into apoptotic DNA degradation by CED-3 Protease Suppressor-6 (CPS-6) from *Caenorhabditis elegans*. *Journal of Biological Chemistry* **287**, 7110 (2012).

89. Y. Nishimura *et al.*, Active digestion of sperm mitochondrial DNA in single living sperm revealed by optical tweezers. *Proceedings of the National Academy of Sciences* **103**, 1382 (2006).

90. S. Kawano, R. W. Anderson, T. Nanba, T. Kuroiwa, Polymorphism and uniparental inheritance of mitochondrial DNA in *Physarum polycephalum*. *Microbiology* **133**, 3175 (1987).

91. Y. Moriyama, S. Kawano, Rapid, selective digestion of mitochondrial DNA in accordance with the matA hierarchy of multiallelic mating types in the mitochondrial inheritance of *Physarum polycephalum*. *Genetics* **164**, 963 (2003).

92. Y. Moriyama, T. Yamazaki, H. Nomura, N. Sasaki, S. Kawano, Early zygote-specific nuclease in mitochondria of the true slime mold *Physarum polycephalum*. *Current genetics* **48**, 334 (2005).

93. Y. Nishimura *et al.*, An mt+ gamete-specific nuclease that targets mt– chloroplasts during sexual reproduction in *C. reinhardtii*. *Genes & development* **16**, 1116 (2002).

94. R. Matsushima *et al.*, A conserved, Mg2+-dependent exonuclease degrades organelle DNA during *Arabidopsis* pollen development. *The Plant Cell* **23**, 1608 (2011).

95. M. Sato, K. Sato, Maternal inheritance of mitochondrial DNA by diverse mechanisms to eliminate paternal mitochondrial DNA. *Biochimica et Biophysica Acta (BBA)-Molecular Cell Research* **1833**, 1979 (2013).

96. M. Schwartz, J. Vissing, Paternal inheritance of mitochondrial DNA. *New England Journal of Medicine* **347**, 576 (2002).

97. A. J. Bendich, DNA abandonment and the mechanisms of uniparental inheritance of mitochondria and chloroplasts. *Chromosome research* **21**, 287 (2013).

98. Y. Kurihara *et al.*, Mitophagy plays an essential role in reducing mitochondrial production of reactive oxygen species and mutation of mitochondrial DNA by maintaining mitochondrial quantity and quality in yeast. *Journal of Biological Chemistry* **287**, 3265 (2012).

99. H. Kaneda *et al.*, Elimination of paternal mitochondrial DNA in intraspecific crosses during early mouse embryogenesis. *Proceedings of the National Academy of Sciences* **92**, 4542 (1995).

100. P. Sutovsky *et al.*, Development: ubiquitin tag for sperm mitochondria. *Nature* **402**, 371 (1999).

101. H. Shitara *et al.*, Selective and continuous elimination of mitochondria microinjected into mouse eggs from spermatids, but not from liver cells, occurs throughout embryogenesis. *Genetics* **156**, 1277 (2000).

102. J. A. Ross, D. K. Howe, A. Coleman-Hulbert, D. R. Denver, S. Estes, Paternal mitochondrial transmission in intra-species *Caenorhabditis briggsae* hybrids. *Molecular Biology and Evolution*, msw192 0737 (2016).

103. M. S. Sharpley *et al.*, Heteroplasmy of mouse mtDNA is genetically unstable and results in altered behavior and cognition. *Cell* **151**, 333 (2012).

104. K. T. Tokuyasu, W. J. Peacock, R. W. Hardy, Dynamics of spermiogenesis in *Drosophila melanogaster*. *Zeitschrift für Zellforschung und mikroskopische Anatomie* **127**, 492 (1972).

105. X. Wang, The expanding role of mitochondria in apoptosis. *Genes Dev* **15**, 2922 (Nov 15, 2001).

106. S. E. Calvo, V. K. Mootha, The mitochondrial proteome and human disease. *Annu Rev Genomics Hum Genet* **11**, 25 (2010).

107. D. C. Wallace, Mitochondrial DNA mutations in disease and aging. *Environ Mol Mutagen* **51**, 440 (Jun, 2010).

108. S. Dimauro, G. Davidzon, Mitochondrial DNA and disease. *Ann Med* **37**, 222 (2005).

109. C. W. Birky, Jr., Uniparental inheritance of mitochondrial and chloroplast genes: mechanisms and evolution. *Proc Natl Acad Sci U S A* **92**, 11331 (Dec 5, 1995).

110. D. C. Wallace, Why Do We Still Have a Maternally Inherited Mitochondrial DNA? Insights from Evolutionary Medicine. *Annual Review of Biochemistry* **76**, 781 (2007).

111. B. Levine, Z. Elazar, Development. Inheriting maternal mtDNA. *Science* **334**, 1069 (Nov 25, 2011).

112. P. Sutovsky *et al.*, Ubiquitinated Sperm Mitochondria, Selective Proteolysis, and the Regulation of Mitochondrial Inheritance in Mammalian Embryos. *Biology of Reproduction* **63**, 582 (August 1, 2000, 2000).

113. F. Ankel-Simons, J. M. Cummins, Misconceptions about mitochondria and mammalian fertilization: implications for theories on human evolution. *Proc Natl Acad Sci U S A* **93**, 13859 (Nov 26, 1996).

114. Y. Nishimura *et al.*, Active digestion of sperm mitochondrial DNA in single living sperm revealed by optical tweezers. *Proc Natl Acad Sci U S A* **103**, 1382 (Jan 31, 2006).

115. S. Al Rawi *et al.*, Postfertilization autophagy of sperm organelles prevents paternal mitochondrial DNA transmission. *Science* **334**, 1144 (Nov 25, 2011).

116. M. Sato, K. Sato, Degradation of paternal mitochondria by fertilization-triggered autophagy in *C. elegans* embryos. *Science* **334**, 1141 (Nov 25, 2011).

117. W. Y. Tsang, B. D. Lemire, Stable heteroplasmy but differential inheritance of a large mitochondrial DNA deletion in nematodes. *Biochemistry and Cell Biology* **80**, 645 (2002).

118. C. A. Hutchison, J. E. Newbold, S. S. Potter, M. H. Edgell, Maternal inheritance of mammalian mitochondrial DNA. *Nature* **251**, 536 (1974).

119. R. E. Giles, H. Blanc, H. M. Cann, D. C. Wallace, Maternal inheritance of human mitochondrial DNA. *Proc Natl Acad Sci U S A* **77**, 6715 (Nov, 1980).

120. J. Parrish *et al.*, Mitochondrial endonuclease G is important for apoptosis in *C. elegans*. *Nature* **412**, 90 (Jul 5, 2001).

121. L. Y. Li, X. Luo, X. Wang, Endonuclease G is an apoptotic DNase when released from mitochondria. *Nature* **412**, 95 (Jul 5, 2001).

122. J. L. Lin *et al.*, Structural insights into apoptotic DNA degradation by CED-3 protease suppressor-6 (CPS-6) from *Caenorhabditis elegans*. *J Biol Chem* **287**, 7110 (Mar 2, 2012).

123. T. Gu, S. Orita, M. Han, *Caenorhabditis elegans* SUR-5, a novel but conserved protein, negatively regulates LET-60 Ras activity during vulval induction. *Mol Cell Biol* **18**, 4556 (Aug, 1998).

124. D. R. Hsu, P. T. Chuang, B. J. Meyer, DPY-30, a nuclear protein essential early in embryogenesis for *Caenorhabditis elegans* dosage compensation. *Development* **121**, 3323 (Oct, 1995).

125. L. M. Loew, R. A. Tuft, W. Carrington, F. S. Fay, Imaging in five dimensions: time-dependent membrane potentials in individual mitochondria. *Biophys J* **65**, 2396 (Dec, 1993).

126. K. Jia, B. Levine, Autophagy and longevity: lessons from *C. elegans*. *Adv Exp Med Biol* **694**, 47 (2010).

127. Y. Tian *et al.*, *C. elegans* screen identifies autophagy genes specific to multicellular organisms. *Cell* **141**, 1042 (Jun 11, 2010).

128. K. Madura, Rad23 and Rpn10: perennial wallflowers join the melee. *Trends Biochem Sci* **29**, 637 (Dec, 2004).

129. M. W. Nachman, W. M. Brown, M. Stoneking, C. F. Aquadro, Nonneutral mitochondrial DNA variation in humans and chimpanzees. *Genetics* **142**, 953 (Mar, 1996).

130. J. M. Cummins, Fertilization and elimination of the paternal mitochondrial genome. *Human Reproduction* **15**, 92 (July 1, 2000, 2000).

131. M. S. Sharpley *et al.*, Heteroplasmy of mouse mtDNA is genetically unstable and results in altered behavior and cognition. *Cell* **151**, 333 (Oct 12, 2012).

132. B. Bowerman, C. A. Shelton, Cell polarity in the early *Caenorhabditis elegans* embryo. *Curr Opin Genet Dev* **9**, 390 (Aug, 1999).

133. G. Ashrafi, T. L. Schwarz, The pathways of mitophagy for quality control and clearance of mitochondria. *Cell Death Differ*, (Jun 29, 2012).

134. K. Wang, D. J. Klionsky, Mitochondria removal by autophagy. *Autophagy* **7**, 297 (Mar, 2011).

135. D. P. Narendra, R. J. Youle, Targeting mitochondrial dysfunction: role for PINK1 and Parkin in mitochondrial quality control. *Antioxid Redox Signal* **14**, 1929 (May 15, 2011).

136. B. Lemire, *Mitochondrial genetics*. T. C. e. R. Community, Ed., WormBook (2005).

137. C. McDermott-Roe *et al.*, Endonuclease G is a novel determinant of cardiac hypertrophy and mitochondrial function. *Nature* **478**, 114 (Oct 6, 2011).

138. S. Z. DeLuca, P. H. O'Farrell, Barriers to male transmission of mitochondrial DNA in sperm development. *Dev Cell* **22**, 660 (Mar 13, 2012).

139. B. Pakendorf, M. Stoneking, Mitochondrial DNA and Human Evolution. *Annual Review of Genomics and Human Genetics* **6**, 165 (2005).

140. J. P. Jenuth, A. C. Peterson, E. A. Shoubridge, Tissue-specific selection for different mtDNA genotypes in heteroplasmic mice. *Nat Genet* **16**, 93 (May, 1997).

141. N. Lane, Mitonuclear match: optimizing fitness and fertility over generations drives ageing within generations. *Bioessays* **33**, 860 (Nov, 2011).

142. D. J. Pagliarini *et al.*, A mitochondrial protein compendium elucidates complex I disease biology. *Cell* **134**, 112 (Jul 11, 2008).

143. T. A. Rosenquist, J. Kimble, Molecular cloning and transcript analysis of fem-3, a sex-determination gene in *Caenorhabditis elegans*. *Genes Dev* **2**, 606 (May, 1988).

144. S. Brenner, The genetics of *Caenorhabditis elegans*. *Genetics* **77**, 71 (May, 1974).

145. X. Wang, C. Yang, J. Chai, Y. Shi, D. Xue, Mechanisms of AIF-mediated apoptotic DNA degradation in *Caenorhabditis elegans*. *Science* **298**, 1587 (Nov 22, 2002).

146. X. Wang *et al.*, Cell Corpse Engulfment Mediated by *C. elegans* Phosphatidylserine Receptor Through CED-5 and CED-12. *Science* **302**, 1563 (November 28, 2003, 2003).

147. D. G. Breckenridge, B. H. Kang, D. Xue, Bcl-2 proteins EGL-1 and CED-9 do not regulate mitochondrial fission or fusion in *Caenorhabditis elegans*. *Curr Biol* **19**, 768 (May 12, 2009).

148. B. H. Kang, Electron microscopy and high-pressure freezing of Arabidopsis. *Methods Cell Biol* **96**, 259 (2010).

149. B. H. Kang, E. Nielsen, M. L. Preuss, D. Mastronarde, L. A. Staehelin, Electron tomography of RabA4b- and PI-4Kbeta1-labeled trans Golgi network compartments in Arabidopsis. *Traffic* **12**, 313 (Mar, 2011).

150. X. Wang *et al.*, *C. elegans* mitochondrial factor WAH-1 promotes phosphatidylserine externalization in apoptotic cells through phospholipid scramblase SCRM-1. *Nat Cell Biol* **9**, 541 (2007).

151. M. A. Lynch-Day, K. Mao, K. Wang, M. Zhao, D. J. Klionsky, The role of autophagy in Parkinson's disease. *Cold Spring Harb Perspect Med* **2**, a009357 (Apr, 2012).

152. T. Kitada *et al.*, Mutations in the parkin gene cause autosomal recessive juvenile parkinsonism. *Nature* **392**, 605 (Apr 9, 1998).

153. E. M. Valente *et al.*, Hereditary early-onset Parkinson's disease caused by mutations in PINK1. *Science* **304**, 1158 (May 21, 2004).

154. B. Bingol, M. Sheng, Mechanisms of mitophagy: PINK1, Parkin, USP30 and beyond. *Free Radic Biol Med*, (Apr 16, 2016).

155. J. Park *et al.*, Mitochondrial dysfunction in *Drosophila* PINK1 mutants is complemented by parkin. *Nature* **441**, 1157 (Jun 29, 2006).

156. I. E. Clark *et al.*, *Drosophila* pink1 is required for mitochondrial function and interacts genetically with parkin. *Nature* **441**, 1162 (Jun 29, 2006).

157. Y. Yang *et al.*, Mitochondrial pathology and muscle and dopaminergic neuron degeneration caused by inactivation of *Drosophila* Pink1 is rescued by Parkin. *Proc Natl Acad Sci U S A* **103**, 10793 (Jul 11, 2006).

158. M. Lazarou, S. M. Jin, L. A. Kane, R. J. Youle, Role of PINK1 binding to the TOM complex and alternate intracellular membranes in recruitment and activation of the E3 ligase Parkin. *Dev Cell* **22**, 320 (Feb 14, 2012).

159. E. Deas *et al.*, PINK1 cleavage at position A103 by the mitochondrial protease PARL. *Hum Mol Genet* **20**, 867 (Mar 1, 2011).

160. K. Yamano, R. J. Youle, PINK1 is degraded through the N-end rule pathway. *Autophagy* **9**, 1758 (Nov 1, 2013).

161. A. W. Greene *et al.*, Mitochondrial processing peptidase regulates PINK1 processing, import and Parkin recruitment. *EMBO Rep* **13**, 378 (Apr, 2012).

162. C. Meissner, H. Lorenz, A. Weihofen, D. J. Selkoe, M. K. Lemberg, The mitochondrial intramembrane protease PARL cleaves human Pink1 to regulate Pink1 trafficking. *J Neurochem* **117**, 856 (Jun, 2011).

163. S. Geisler *et al.*, PINK1/Parkin-mediated mitophagy is dependent on VDAC1 and p62/SQSTM1. *Nat Cell Biol* **12**, 119 (Feb, 2010).

164. N. Matsuda *et al.*, PINK1 stabilized by mitochondrial depolarization recruits Parkin to damaged mitochondria and activates latent Parkin for mitophagy. *The Journal of cell biology* **189**, 211 (2010).

165. D. P. Narendra *et al.*, PINK1 is selectively stabilized on impaired mitochondria to activate Parkin. *PLoS Biol* **8**, e1000298 (2010).

166. C. Vives-Bauza *et al.*, PINK1-dependent recruitment of Parkin to mitochondria in mitophagy. *Proc Natl Acad Sci U S A* **107**, 378 (Jan 5, 2010).

167. C. Kondapalli *et al.*, PINK1 is activated by mitochondrial membrane potential depolarization and stimulates Parkin E3 ligase activity by phosphorylating Serine 65. *Open Biol* **2**, 120080 (May, 2012).

168. K. Shiba-Fukushima *et al.*, PINK1-mediated phosphorylation of the Parkin ubiquitin-like domain primes mitochondrial translocation of Parkin and regulates mitophagy. *Sci Rep* **2**, 1002 (2012).

169. C. Zhang *et al.*, PINK1 triggers autocatalytic activation of Parkin to specify cell fate decisions. *Curr Biol* **24**, 1854 (Aug 18, 2014).

170. L. A. Kane *et al.*, PINK1 phosphorylates ubiquitin to activate Parkin E3 ubiquitin ligase activity. *J Cell Biol* **205**, 143 (Apr 28, 2014).

171. F. Koyano *et al.*, Ubiquitin is phosphorylated by PINK1 to activate parkin. *Nature* **510**, 162 (Jun 5, 2014).

172. A. Kazlauskaite *et al.*, Parkin is activated by PINK1-dependent phosphorylation of ubiquitin at Ser65. *Biochem J* **460**, 127 (May 15, 2014).

173. A. Ordureau *et al.*, Quantitative proteomics reveal a feedforward mechanism for mitochondrial PARKIN translocation and ubiquitin chain synthesis. *Mol Cell* **56**, 360 (Nov 6, 2014).

174. A. Ordureau *et al.*, Defining roles of PARKIN and ubiquitin phosphorylation by PINK1 in mitochondrial quality control using a ubiquitin replacement strategy. *Proc Natl Acad Sci U S A* **112**, 6637 (May 26, 2015).

175. A. Stolz, A. Ernst, I. Dikic, Cargo recognition and trafficking in selective autophagy. *Nat Cell Biol* **16**, 495 (Jun, 2014).

176. Y. C. Wong, E. L. Holzbaur, Optineurin is an autophagy receptor for damaged mitochondria in parkin-mediated mitophagy that is disrupted by an ALS-linked mutation. *Proc Natl Acad Sci U S A* **111**, E4439 (Oct 21, 2014).

177. Q. H. Zhou *et al.*, Mitochondrial endonuclease G mediates breakdown of paternal mitochondria upon fertilization. *Science* **353**, 394 (Jul 22, 2016).

178. K. Palikaras, E. Lionaki, N. Tavernarakis, Coordination of mitophagy and mitochondrial biogenesis during ageing in *C. elegans*. *Nature* **521**, 525 (May 28, 2015).

179. S. Yoshina, Y. Suehiro, E. Kage-Nakadai, S. Mitani, Locus-specific integration of extrachromosomal transgenes in *C. elegans* with the CRISPR/Cas9 system. *Biochemistry and Biophysics Reports* **5**, 70 (2016).

180. C. Tenenhaus, K. Subramaniam, M. A. Dunn, G. Seydoux, PIE-1 is a bifunctional protein that regulates maternal and zygotic gene expression in the embryonic germ line of *Caenorhabditis elegans*. *Genes Dev* **15**, 1031 (Apr 15, 2001).

181. J. F. Trempe *et al.*, Structure of parkin reveals mechanisms for ubiquitin ligase activation. *Science* **340**, 1451 (Jun 21, 2013).

182. N. Matsuda *et al.*, Diverse effects of pathogenic mutations of Parkin that catalyze multiple monoubiquitylation in vitro. *J Biol Chem* **281**, 3204 (Feb 10, 2006).

183. Y. Wang *et al.*, Kinetics and specificity of paternal mitochondrial elimination in *Caenorhabditis elegans*. *Nature Communications* **7**, DOI: 10.1038/ncomms12569 (2016).

184. M. Sato, K. Sato, Maternal inheritance of mitochondrial DNA by diverse mechanisms to eliminate paternal mitochondrial DNA. *Biochim Biophys Acta* **1833**, 1979 (Aug, 2013).

185. J. Yun *et al.*, MUL1 acts in parallel to the PINK1/parkin pathway in regulating mitofusin and compensates for loss of PINK1/parkin. *Elife* **3**, e01958 (2014).

186. D. J. Dickinson, J. D. Ward, D. J. Reiner, B. Goldstein, Engineering the *Caenorhabditis elegans* genome using Cas9-triggered homologous recombination. *Nat Methods* **10**, 1028 (Oct, 2013).

187. X. Wang *et al.*, *C. elegans* mitochondrial factor WAH-1 promotes phosphatidylserine externalization in apoptotic cells through phospholipid scramblase SCRM-1. *Nat Cell Biol* **9**, 541 (May, 2007).

188. K. Toyooka, B. H. Kang, Reconstructing plant cells in 3D by serial section electron tomography. *Methods Mol Biol* **1080**, 159 (2014).

189. K. Kuida *et al.*, Decreased apoptosis in the brain and premature lethality in CPP32-deficient mice. *Nature* **384**, 368 (1996).

190. K. Kuida *et al.*, Reduced apoptosis and cytochrome c–mediated caspase activation in mice lacking caspase 9. *Cell* **94**, 325 (1998).

191. E. E. Varfolomeev *et al.*, Targeted disruption of the mouse Caspase 8 gene ablates cell death induction by the TNF receptors, Fas/Apo1, and DR3 and is lethal prenatally. *Immunity* **9**, 267 (1998).

192. J. F. R. Kerr, A. H. Wyllie, A. R. Currie, Apoptosis: a basic biological phenomenon with wide-ranging implications in tissue kinetics. *British journal of cancer* **26**, 239 (1972).

193. J. E. Sulston, E. Schierenberg, J. G. White, J. N. Thomson, The embryonic cell lineage of the nematode *Caenorhabditis elegans*. *Developmental biology* **100**, 64 (1983).

194. J. E. Sulston, H. R. Horvitz, Post-embryonic cell lineages of the nematode, *Caenorhabditis elegans*. *Developmental biology* **56**, 110 (1977).

195. D. Xue, S. Shaham, H. R. Horvitz, The *Caenorhabditis elegans* cell-death protein CED-3 is a cysteine protease with substrate specificities similar to those of the human CPP32 protease. *Genes & Development* **10**, 1073 (1996).

196. J. Yuan, S. Shaham, S. Ledoux, H. M. Ellis, H. R. Horvitz, The *C. elegans* cell death gene ced-3 encodes a protein similar to mammalian interleukin-1β-converting enzyme. *Cell* **75**, 641 (1993).

197. X. Chen *et al.*, Regulation of CED-3 caspase localization and activation by *C. elegans* nuclear-membrane protein NPP-14. *Nature Structural & Molecular Biology 1545-9993*, (2016).

198. D. L. Daleke, Regulation of transbilayer plasma membrane phospholipid asymmetry. *Journal of lipid research* **44**, 233 (2003).

199. V. A. Fadok *et al.*, Exposure of phosphatidylserine on the surface of apoptotic lymphocytes triggers specific recognition and removal by macrophages. *The Journal of Immunology* **148**, 2207 (1992).

200. V. A. Fadok *et al.*, Different populations of macrophages use either the vitronectin receptor or the phosphatidylserine receptor to recognize and remove apoptotic cells. *The Journal of Immunology* **149**, 4029 (1992).

201. J. Savill, V. Fadok, Corpse clearance defines the meaning of cell death. *Nature* **407**, 784 (2000).

202. S. M. Pinto, M. O. Hengartner, Cleaning up the mess: cell corpse clearance in *Caenorhabditis elegans*. *Current opinion in cell biology* **24**, 881 (2012).

203. X. Wang *et al.*, *Caenorhabditis elegans* transthyretin-like protein TTR-52 mediates recognition of apoptotic cells by the CED-1 phagocyte receptor. *nature cell biology* **12**, 655 (2010).

204. H. Yang *et al.*, A lysine-rich motif in the phosphatidylserine receptor PSR-1 mediates recognition and removal of apoptotic cells. *Nature communications* **6**, (2015).

205. R. E. Ellis, D. M. Jacobson, H. R. Horvitz, Genes required for the engulfment of cell corpses during programmed cell death in *Caenorhabditis elegans*. *Genetics* **129**, 79 (1991).

206. P. W. Reddien, H. R. Horvitz, The engulfment process of programmed cell death in *Caenorhabditis elegans*. *Annu. Rev. Cell Dev. Biol.* **20**, 193 (2004).

207. Y.-Z. Chen, J. Mapes, E.-S. Lee, R. R. Skeen-Gaar, D. Xue, Caspase-mediated activation of *Caenorhabditis elegans* CED-8 promotes apoptosis and phosphatidylserine externalization. *Nature communications* **4**, (2013).

208. G. M. Stanfield, H. R. Horvitz, The ced-8 gene controls the timing of programmed cell deaths in *C. elegans*. *Molecular cell* **5**, 423 (2000).

209. M. Ho *et al.*, Isolation of the gene for McLeod syndrome that encodes a novel membrane transport protein. *Cell* **77**, 869 (1994).

210. X. Geng *et al.*, Inhibition of CED-3 zymogen activation and apoptosis in *Caenorhabditis elegans* by caspase homolog CSP-3. *Nature structural & molecular biology* **15**, 1094 (2008).

211. M. Darland-Ransom *et al.*, Role of C. elegans TAT-1 protein in maintaining plasma membrane phosphatidylserine asymmetry. *Science* **320**, 528 (2008).

212. J. Mapes *et al.*, CED-1, CED-7, and TTR-52 regulate surface phosphatidylserine expression on apoptotic and phagocytic cells. *Current Biology* **22**, 1267 (2012).

213. X. Geng *et al.*, Hepatitis B virus X protein targets the Bcl-2 protein CED-9 to induce intracellular Ca2+ increase and cell death in *Caenorhabditis elegans*. *Proceedings of the National Academy of Sciences* **109**, 18465 (2012).

214. S. Harbinder *et al.*, Genetically targeted cell disruption in *Caenorhabditis elegans*. *Proceedings of the National Academy of Sciences* **94**, 13128 (1997).

215. D. S. Chelur *et al.*, The mechanosensory protein MEC-6 is a subunit of the *C. elegans* touch-cell degenerin channel. *Nature* **420**, 669 (2002).

216. K. L. Rock, H. Kono, The inflammatory response to cell death. *Annual review of pathology* **3**, 99 (2008).

217. P. Zhao, Z. Zhang, H. Ke, Y. Yue, D. Xue, Oligonucleotide-based targeted gene editing in *C. elegans* via the CRISPR/Cas9 system. *Cell research* **24**, 247 (2014).

218. S. Brenner, The genetics of Caenorhabditis elegans. *Genetics* **77**, 71 (1974).

219. C. C. Mello, J. M. Kramer, D. Stinchcomb, V. Ambros, Efficient gene transfer in *C. elegans*: extrachromosomal maintenance and integration of transforming sequences. *The EMBO journal* **10**, 3959 (1991).

220. T. Gu, S. Orita, M. Han, *Caenorhabditis elegans* SUR-5, a novel but conserved protein, negatively regulates LET-60 Ras activity during vulval induction. *Molecular and Cellular Biology* **18**, 4556 (1998).

221. H. R. Horvitz, Genetic control of programmed cell death in the nematode *Caenorhabditis elegans*. *Cancer research* **59**, 1701s (1999).

222. D. L. Vaux, S. J. Korsmeyer, Cell death in development. *Cell* **96**, 245 (1999).

223. D. J. Dickinson, B. Goldstein, CRISPR-based methods for *Caenorhabditis elegans* genome engineering. *Genetics* **202**, 885 (2016).

224. S. Zuryn, S. Jarriault. (Taylor & Francis, 2013), vol. 2, pp. e25081 2162-4054.

225. M. O. Hengartner, H. R. Horvitz, *C. elegans* cell survival gene ced-9 encodes a functional homolog of the mammalian proto-oncogene bcl-2. *Cell* **76**, 665 (1994).

226. M. O. Hengartner, R. Ellis, R. Horvitz, *Caenorhabditis elegans* gene ced-9 protects cells from programmed cell death. (1992).

227. J. Suzuki, E. Imanishi, S. Nagata, Xkr8 phospholipid scrambling complex in apoptotic phosphatidylserine exposure. *Proceedings of the National Academy of Sciences*, 201610403 0027 (2016).

228. J. Suzuki, E. Imanishi, S. Nagata, Exposure of phosphatidylserine by Xk-related protein family members during apoptosis. *Journal of Biological Chemistry* **289**, 30257 (2014).

229. S. Cheng *et al.*, Autophagy genes coordinate with the class II PI/PtdIns 3-kinase PIKI-1 to regulate apoptotic cell clearance in *C. elegans*. *Autophagy* **9**, 2022 (2013).

230. M. Xu *et al.*, The lysosomal cathepsin protease CPL-1 plays a leading role in phagosomal degradation of apoptotic cells in *Caenorhabditis elegans*. *Molecular biology of the cell* **25**, 2071 (2014).

Appendix

Table 2. 1. Candidate genes that are predicted to encode mitochondrial proteins in *C. elegans.*

217 genes were identified as candidates that encode mitochondrial proteins and were subjected to the RNAi screen to identify mitochondria-specific genes important for PME. Human homologues of these candidate genes are indicted.

	Sequence	Name	Human Homologue
1	B0024.9	trx-2	cDNA FLJ55158, highly similar to Thioredoxin, mitochondrial
2	B0205.6	B0205.6	Isoform Mitochondrial of Cysteine desulfurase, mitochondrial
3	B0303.3	B0303.3	cDNA FLJ56214, highly similar to Trifunctional enzyme subunit beta, mitochondrial
4	B0334.4	B0334.4	Uncharacterized protein
5	B0334.5	B0334.5	Isoform 1 of UPF0551 protein C8orf38, mitochondrial
6	B0336.4a	rgs-5	A-kinase anchor protein 10, mitochondrial
7	B0361.5	psd-1	Isoform 1 of Phosphatidylserine decarboxylase proenzyme
8	B0432.2	djr-1.1	Protein DJ-1
9	B0432.4	misc-1	Mitochondrial 2-oxoglutarate/malate carrier protein
10	B0432.8	B0432.8	Isoform 1 of Putative deoxyribonuclease TATDN3
11	C01F1.2	sco-1	Protein SCO1 homolog, mitochondrial
12	C01G10.7	C01G10.7	Isoform 1 of Citrate lyase subunit beta-like protein, mitochondrial
13	C02F5.3	C02F5.3	Developmentally-regulated GTP-binding protein 2
14	C04E6.11	C04E6.11	Uncharacterized protein
15	C06G3.11	tin-9.1	Mitochondrial import inner membrane translocase subunit Tim9
16	C08A9.1	sod-3	superoxide dismutase [Mn], mitochondrial isoform A precursor
17	C08B6.8	C08B6.8	Isoform 1 of Oligoribonuclease, mitochondrial (Fragment)
18	C08F8.2b	C08F8.2	ATP-dependent RNA helicase SUPV3L1, mitochondrial
19	C09B8.7c	pak-1	Isoform 1 of Serine/threonine-protein kinase PAK 1
20	C10G11.5	pnk-1	cDNA FLJ56439, highly similar to Pantothenate kinase 4
21	C13B9.2	C13B9.2	Isoform 1 of Glycerate kinase
22	C14A4.2	dap-3	28S ribosomal protein S29, mitochondrial isoform 2
23	C16C10.1	C16C10.1	Solute carrier family 25 member 40
24	C16C10.11	har-1	Coiled-coil-helix-coiled-coil-helix domain-containing protein 10, mitochondrial
25	C18E3.5	C18E3.5	U5 small nuclear ribonucleoprotein 40 kDa protein
26	C18E9.6	tomm-40	Isoform 1 of Mitochondrial import receptor subunit TOM40 homolog
27	C23G10.2b	C23G10.2	Ribonuclease UK114
28	C24G6.8	C24G6.8	cDNA FLJ32471 fis, clone SKNMC2000322, highly similar to Peptidyl-tRNA hydrolase 2, mitochondrial
29	C26E6.12	C26E6.12	Isoform 1 of GTP-binding protein 10
30	C29E4.10	C29E4.10	Isoform 1 of Galactocerebrosidase
31	C29F3.1	ech-1	Trifunctional enzyme subunit alpha, mitochondrial
32	C30F12.2	C30F12.2	Lactation elevated protein 1
33	C30F12.7	idhg-2	Isocitrate dehydrogenase [NAD] subunit gamma, mitochondrial
34	C31E10.7	cytb-5.1	Isoform 1 of Cytochrome b5
35	C33A12.7	ethe-1	Protein ETHE1, mitochondrial
36	C33H5.19	tag-321	Transmembrane protein 65
37	C34B2.6	C34B2.6	Lon protease homolog
38	C34C12.8	C34C12.8	GrpE protein homolog 1, mitochondrial
39	C34E10.1	gop-3	Sorting and assembly machinery component 50 homolog
40	C34G6.4	pgp-2	Multidrug resistance protein 1
41	C35D10.4	coq-8	Isoform 3 of Chaperone activity of bc1 complex-like, mitochondrial
42	C35D10.5	C35D10.5	ubiquinol-cytochrome c reductase complex chaperone CBP3 homolog isoform c
43	C36A4.9	acs-19	acetyl-coenzyme A synthetase, cytoplasmic isoform 2
44	C39B5.6	C39B5.6	Probable glutamyl-tRNA(Gln) amidotransferase subunit B, mitochondrial
45	C39F7.4	rab-1	Isoform 1 of Ras-related protein Rab-1A
46	C41C4.10	sfxn-5	Sideroflexin-5
47	C41D11.8	cps-6	Endonuclease G, mitochondrial
48	C41G7.9	C41G7.9	Translocator protein
49	C42C1.10a	hpo-12	Mitochondrial thiamine pyrophosphate carrier
50	C43E11.4	tufm-2	elongation factor Tu, mitochondrial precursor
51	C43E11.7	ndx-7	Nucleoside diphosphate-linked moiety X motif 19, mitochondrial
52	C44B7.9	pmp-2	cDNA FLJ53353, highly similar to ATP-binding cassette sub-family D member 3
53	C45B11.1	pak-2	Isoform 1 of Serine/threonine-protein kinase PAK 4
54	C47E8.5	daf-21	Heat shock protein HSP 90-beta
55	C47G2.3	C47G2.3	Mitochondrial import inner membrane translocase subunit Tim22
56	C48D1.2	ced-3	Isoform 1 of Caspase-2
57	C49G7.11	djr-1.2	Protein DJ-1
58	C50F4.12	C50F4.12	Isoform 1 of mTERF domain-containing protein 1, mitochondrial
59	C50H11.1	acs-21	Isoform 1 of Acyl-CoA synthetase family member 3, mitochondrial
60	C52E12.2	unc-104	KIF1A variant protein
61	C54G10.4	C54G10.4	Mitochondrial carnitine/acylcarnitine carrier protein CACL
62	C54G4.8	cyc-1	Cytochrome c1, heme protein, mitochondrial
63	C56A3.6	C56A3.6	EF-hand domain-containing family member A2
64	C56G2.1	C56G2.1	Isoform 1 of A-kinase anchor protein 1, mitochondrial
65	D1037.3	ftn-2	Ferritin heavy chain
66	D1037.4	rab-8	Ras-related protein Rab-8B
67	D1046.3	D1046.3	S-adenosylmethionine mitochondrial carrier protein isoform a
68	D1054.15	tag-135	Isoform 2 of Pleiotropic regulator 1
69	D2013.5	eat-3	dynamin-like 120 kDa protein, mitochondrial isoform 8
70	D2023.6	D2023.6	Isoform 2 of Uncharacterized aarF domain-containing protein kinase 1
71	D2030.2	D2030.2	ATP-dependent Clp protease ATP-binding subunit clpX-like, mitochondrial
72	DH11.1	glna-2	Isoform 1 of Glutaminase kidney isoform, mitochondrial

73	DY3.1	tin-13	Mitochondrial import inner membrane translocase subunit Tim13
74	E04A4.4	hoe-1	Isoform 1 of Zinc phosphodiesterase ELAC protein 2
75	E04A4.5	E04A4.5	Mitochondrial import inner membrane translocase subunit Tim17-B
76	E04F6.2	E04F6.2	Isoform 2 of Parkin coregulated gene protein
77	EEED8.9	pink-1	Isoform 1 of Serine/threonine-protein kinase PINK1, mitochondrial
78	F01G4.6	F01G4.6	Isoform B of Phosphate carrier protein, mitochondrial
79	F09E5.15	prdx-2	Peroxiredoxin-2
80	F09E5.8	F09E5.8	Proline synthetase co-transcribed homolog (Bacterial), isoform CRA_b
81	F10D11.1	sod-2	superoxide dismutase [Mn], mitochondrial isoform A precursor
82	F13B9.8b	fis-2	Mitochondrial fission 1 protein
83	F13G3.7	F13G3.7	Solute carrier family 25 member 44
84	F14F4.3	mrp-5	Multidrug resistance-associated protein 5
85	F15A4.11	tag-281	Transmembrane protein C9orf46
86	F15D3.6	F15D3.6	Protein slowmo homolog 2
87	F15D3.7	F15D3.7	Mitochondrial import inner membrane translocase subunit Tim23
88	F17E5.2	F17E5.2	Isoform 2 of Calcium-binding mitochondrial carrier protein SCaMC-2
89	F20D1.9	F20D1.9	Mitochondrial glutamate carrier 2
90	F20D6.11	F20D6.11	Isoform 3 of Apoptosis-inducing factor 3
91	F21C3.3	hint-1	Histidine triad nucleotide-binding protein 1
92	F23H11.9	crls-1	Isoform 1 of Cardiolipin synthase
93	F23H12.1	snb-2	Uncharacterized protein
94	F23H12.2	tomm-20	Mitochondrial import receptor subunit TOM20 homolog
95	F25H2.5	ndk-1	Isoform 1 of Nucleoside diphosphate kinase B
96	F25H9.7	F25H9.7	Protein ACN9 homolog, mitochondrial
97	F26H11.5	exl-1	Uncharacterized protein
98	F26H9.6	rab-5	Ras-related protein Rab-5B
99	F28C10.3	F28C10.3	Ribosomal protein S6 kinase alpha-3
100	F28C6.8	F28C6.8	Isoform 1 of Protein-tyrosine phosphatase mitochondrial 1
101	F29C12.4	F29C12.4	Isoform 1 of Elongation factor G, mitochondrial
102	F29C4.6	tut-1	Cytoplasmic tRNA 2-thiolation protein 1
103	F30A10.5	stl-1	Stomatin-like protein 2
104	F31D4.3	fkb-6	Peptidyl-prolyl cis-trans isomerase FKBP4
105	F32A7.4	F32A7.4	Isoform 1 of Methyltransferase-like protein 17, mitochondrial
106	F32D1.3	F32D1.3	Transmembrane and TPR repeat-containing protein 2
107	F32H2.5	fasn-1	Fatty acid synthase
108	F33A8.6	F33A8.6	Integrin-linked kinase-associated serine/threonine phosphatase 2C
109	F36H1.2	tag-144	Uncharacterized protein
110	F38B2.1	ifa-1	Isoform C of Prelamin-A/C
111	F38B6.6	F38B6.6	Isoform 3 of Transmembrane and TPR repeat-containing protein 4
112	F39B2.11	mtx-1	Isoform 1 of Metaxin-1
113	F39B2.7	F39B2.7	Isoform 2 of tRNA modification GTPase GTPBP3, mitochondrial
114	F43G9.3	F43G9.3	Solute carrier family 25 member 42
115	F44E2.6	F44E2.6	Similar to Methionine-R-sulfoxide reductase B2, mitochondrial precursor
116	F44E7.4b	F44E7.4	Insulin-degrading enzyme
117	F44E7.9	F44E7.9	Isoform 2 of Uncharacterized protein C20orf24
118	F45G2.8	F45G2.8	Mitochondrial import inner membrane translocase subunit TIM16
119	F45G2.9	F45G2.9	Putative ribosomal RNA methyltransferase 2
120	F46B6.6a	F46B6.6	Translation initiation factor IF-2, mitochondrial
121	F46E10.1	acs-1	cDNA FLJ51819, weakly similar to Long-chain-fatty-acid--CoA ligase
122	F46G10.3	sir-2.3	NAD-dependent ADP-ribosyltransferase sirtuin-4
123	F46G10.7	sir-2.2	NAD-dependent ADP-ribosyltransferase sirtuin-4
124	F46G11.1	F46G11.1	Isoform 1 of Twinkle protein, mitochondrial
125	F46H5.3	F46H5.3	Creatine kinase M-type
126	F49E8.5	dif-1	Mitochondrial carnitine/acylcarnitine carrier protein
127	F52C9.3	F52C9.3	cDNA FLJ59963, highly similar to Homo sapiens multiple substrate lipid kinase (MULK), mRNA
128	F52F12.1	"oct-1"	Isoform 1 of Solute carrier family 22 member 5
129	F52F12.7	F52F12.7	Uncharacterized protein
130	F52H3.2	F52H3.2	Isoform 5 of Protein MTO1 homolog, mitochondrial
131	F53A3.7	F53A3.7	DNL-type zinc finger protein
132	F53F10.3	F53F10.3	Brain protein 44
133	F53F10.4	unc-108	Ras-related protein Rab-2A
134	F53G12.1	rab-11.1	cDNA FLJ61136, highly similar to Ras-related protein Rab-11A
135	F54B3.3	atad-3	Isoform 2 of ATPase family AAA domain-containing protein 3A
136	F54C9.6	bcs-1	Mitochondrial chaperone BCS1
137	F55C5.5	tsfm-1	Isoform 2 of Elongation factor Ts, mitochondrial
138	F56A11.5	F56A11.5	Isoform 1 of MOSC domain-containing protein 1, mitochondrial
139	F56B3.11a	F56B3.11	TIM21-like protein, mitochondrial
140	F56C11.3	F56C11.3	Isoform 1 of FAD-linked sulfhydryl oxidase ALR
141	F56E3.3	klp-4	Isoform 3 of Kinesin-like protein KIF13A
142	F56H1.6	rad-8	Isoform 1 of Reticulon-4-interacting protein 1, mitochondrial
143	F58G11.1	letm-1	Isoform 1 of LETM1 and EF-hand domain-containing protein 1, mitochondrial
144	F59A2.3	cri-3	Complement component 1 Q subcomponent-binding protein, mitochondrial
145	F59C6.12	F59C6.12	Isoform 1 of UPF0598 protein C8orf82
146	F59G1.7	frh-1	Isoform 1 of Frataxin, mitochondrial
147	H06I04.2	sft-1	Isoform 1 of Surfeit locus protein 1
148	H13N06.4a	suox-1	Sulfite oxidase, mitochondrial
149	H14A12.2a	fum-1	Isoform Mitochondrial of Fumarate hydratase, mitochondrial
150	H24K24.4	H24K24.4	Isoform 1 of tRNA (uracil-5-)-methyltransferase homolog A (Fragment)
151	H32C10.1	H32C10.1	Isoform 1 of Cat eye syndrome critical region protein 5
152	K01C8.7a	K01C8.7	Mitochondrial folate transporter/carrier
153	K01H12.2	ant-1.3	ADP/ATP translocase 1

154	K02B2.3	mcu-1	Isoform 3 of Calcium uniporter protein, mitochondrial
155	K02D10.1	K02D10.1	protein NipSnap homolog 1 isoform 2
156	K02F3.2	K02F3.2	Calcium-binding mitochondrial carrier protein Aralar1
157	K04D7.2	mspn-1	Isoform 1 of ATPase family AAA domain-containing protein 1
158	K05C4.7	K05C4.7	Armadillo repeat-containing protein 1
159	K07A1.12	lin-53	Isoform 2 of Histone-binding protein RBBP4
160	K07B1.3	ucp-4	Mitochondrial uncoupling protein 4
161	K08F11.5	K08F11.5	Isoform 1 of Mitochondrial Rho GTPase 1
162	K09A9.2	rab-14	Ras-related protein Rab-14
163	K09E4.3	K09E4.3	Isoform 1 of Probable methyltransferase C20orf7, mitochondrial
164	K09H11.1	K09H11.1	Isoform 1 of Acyl-CoA dehydrogenase family member 10
165	K11G12.5	K11G12.5	Isoform 1 of Mitochondrial dicarboxylate carrier
166	K11H12.1	K11H12.1	BolA-like protein 1
167	K11H12.8a	K11H12.8	cDNA FLJ59630, highly similar to Growth hormone-inducible transmembrane protein
168	K11H3.1	gpdh-2	Glycerol-3-phosphate dehydrogenase [NAD+], cytoplasmic
169	K11H3.3	K11H3.3	Tricarboxylate transport protein, mitochondrial
170	M01E5.2	M01E5.2	GTP-binding protein 5
171	M01F1.3	M01F1.3	Lipoyl synthase, mitochondrial
172	M03C11.5	ymel-1	Isoform 2 of ATP-dependent zinc metalloprotease YME1L1
173	M05B5.4	M05B5.4	Group XV phospholipase A2
174	M88.7	M88.7	CDGSH iron-sulfur domain-containing protein 3, mitochondrial
175	R02F2.9	R02F2.9	Peptidyl-tRNA hydrolase ICT1, mitochondrial
176	R05G6.7	R05G6.7	Isoform 1 of Voltage-dependent anion-selective channel protein 2
177	R06C1.2	fdps-1	farnesyl pyrophosphate synthase isoform b
178	R07B1.12	glo-1	Ras-related protein Rab-32
179	R07E5.13	R07E5.13	Brain protein 44-like protein
180	R07H5.3	nuaf-3	Isoform a of NADH dehydrogenase [ubiquinone] 1 alpha subcomplex assembly factor 3
181	R107.2	R107.2	cDNA FLJ61130
182	R10E4.5	nth-1	Endonuclease III-like protein 1
183	R10H10.1	lpd-8	Isoform 1 of NFU1 iron-sulfur cluster scaffold homolog, mitochondrial
184	R10H10.6	R10H10.6	cDNA, FLJ96841
185	R11A8.4	sir-2.1	NAD-dependent deacetylase sirtuin-1
186	R11A8.5	R11A8.5	Prostaglandin E synthase 2
187	R11D1.1	R11D1.1	Isoform 1 of DDB1- and CUL4-associated factor 5
188	R11F4.1	R11F4.1	Isoform 1 of Glycerol kinase
189	R144.13	R144.13	Coenzyme Q-binding protein COQ10 homolog B, mitochondrial
190	R151.7	R151.7	Uncharacterized protein
191	R53.5	R53.5	UPF0765 protein C10orf58
192	R74.4	dnj-16	25 kDa protein
193	T01B11.2a	T01B11.2	Isoform 1 of Alanine--glyoxylate aminotransferase 2-like 1
194	T01B11.4	ant-1.4	ADP/ATP translocase 1
195	T02D1.5	pmp-4	ATP-binding cassette sub-family D member 2
196	T03F1.7	T03F1.7	Dimethyladenosine transferase 1, mitochondrial
197	T04F8.1	sfxn-1.5	Sideroflexin-1
198	T05E11.3	T05E11.3	Endoplasmin
199	T05G5.5	T05G5.5	Isoform 1 of Dephospho-CoA kinase domain-containing protein
200	T07D4.3	rha-1	ATP-dependent RNA helicase A
201	T08B2.7	T08B2.7	Trifunctional enzyme subunit alpha, mitochondrial
202	T09B4.9	T09B4.9	Mitochondrial import inner membrane translocase subunit TIM44
203	T09F3.2	T09F3.2	Solute carrier family 25 member 33
204	T10B11.1	pcbd-1	Pterin-4-alpha-carbinolamine dehydratase
205	T10B11.2	T10B11.2	Ceramide kinase
206	T10B5.5	cct-7	T-complex protein 1 subunit eta
207	T10E9.7a	nuo-2	NADH dehydrogenase [ubiquinone] iron-sulfur protein 3, mitochondrial
208	T10F2.2	T10F2.2	Mitochondrial ornithine transporter 1
209	T10H9.4	snb-1	cDNA FLJ61298, highly similar to Vesicle-associated membrane protein 1
210	T13C5.8	mtp-18	Isoform 1 of Mitochondrial fission process protein 1
211	T14G11.3	immt-1	Uncharacterized protein
212	T18D3.9	T18D3.9	Protein Mpv17
213	T19B4.4	dnj-21	DnaJ homolog subfamily C member 15
214	T20B3.1	T20B3.1	Peroxisomal carnitine O-octanoyltransferase
215	T20D3.11	clec-30	C-type LECtin
216	T20D3.5b	T20D3.5	Mitochondrial carrier triple repeat protein 1
217	T20G5.10	T20G5.10	Isoform 1 of Biogenesis of lysosome-related organelles complex 1 subunit 1